Author:
Barnard, Katie E

Title:
Dissecting the Role of the PARylation Stress Response During Tissue Repair and Inflammation in Drosophila

Author:
Barnard, Katie E

Title:
Dissecting the Role of the PARylation Stress Response During Tissue Repair and Inflammation in Drosophila

Dissecting the Role of the PARylation Stress Response During Tissue Repair and Inflammation in *Drosophila*

Katie Barnard

University of Bristol

MSc by Research in Biochemistry

Supervisor: Dr Helen Weavers

A dissertation submitted to the University of Bristol in accordance with the requirements for award of the degree of MSc by Research in the Faculty of Life Sciences.

School of Biochemistry

Submitted January 2023

Word count: 24856

Abstract

In response to injury, tissues (such as the skin) must quickly repair themselves in order to restore barrier integrity. Tissue repair is normally accompanied by a rapid inflammatory response, whereby innate immune cells are recruited to the damaged tissue, where they release toxic mediators (e.g. reactive oxygen species, ROS) to combat invading pathogens and avoid infection. However, these reactive molecules can also significantly damage the host tissue (including subcellular components such as DNA). Therefore, injured tissues upregulate protective pathways to combat this collateral damage. Whilst some of these wound-induced pathways have now been identified, many more stress responses are likely to be involved. Poly(ADP-ribosyl)ation (PARylation) is a well-known stress response to radiation-induced DNA damage that is mediated by Poly(ADP-ribose) polymerase 1 (PARP1). Recent studies on PARP1 hyperactivation have highlighted a negative role for PARylation in the healing process of chronic wounds, however little is known about the role of PARP1 in acute wounds. This study aims to characterise the role of PARylation during wound re-epithelialisation and inflammation using the genetically tractable and translucent *Drosophila* embryo. We show that PARylation significantly increased following epithelial wounding. Moreover, inhibition of this PARylation response (by RNAi-induced *parp* knockdown) significantly reduced the rate of wound closure and impaired the formation of the contractile actin cable at the wound edge that normally aids wound contraction. Conversely, knock-down of poly(ADP-ribose) glycohydrolase (PARG), which reverses PARylation, caused a defective wound closure phenotype. Wound-induced inflammation was also impacted by *parp* knockdown with decreased hemocyte migration to the wound and increased corpse uptake. Taken together, the results of this study highlight a key role for Parp in tissue repair following wounding and suggest that efficient repair requires fine-tuning of the PARylation response. Future work should focus on understanding the underlying molecular mechanism(s), including identification of the targets of PARP1 activity.

Dedication and Acknowledgements

I would like to thank Dr Helen Weavers for her instruction throughout this project, as well as all necessary experimental laboratory and statistical analysis training. I am extremely grateful for her guidance and for making this project possible. I would also like to thank all of the Weavers' lab group for their support with special mention to Dr Giuliana Clemente for her expertise in the field of embryonic wounding and to Jack Holcombe for training me how to form laser-induced wounds in *Drosophila* embryos and complete protein extractions.

I would also like to thank Wolfson Bioimaging Facility for the use of their confocal microscope which made *in vivo* live imaging possible and to Dr Dominic Alibhai for training me how to use the microscope and the associated software.

Author’s Declaration

I declare that the work in this dissertation was carried out in accordance with the requirements of the University's *Regulations and Code of Practice for Research Degree Programmes* and that it has not been submitted for any other academic award. Except where indicated by specific reference in the text, the work is the candidate's own work. Work done in collaboration with, or with the assistance of, others, is indicated as such. Any views expressed in the dissertation are those of the author.

SIGNED:  DATE: 03/01/2023

Contents

List of Abbreviations

AO	Acridine orange
ARH3	ADP-ribosyl hydrolase
ART	ADP-ribosyl transferase
BSA	Bovine serum albumin
BRCT	BRCA1 C-terminus
DDR	DNA damage response
DSB	Double strand break
JNK	Jun N-terminal kinase
Keap1	Kelch-like ECH-associated protein 1
NF-κB	Nuclear factor kappa B
NLS	Nuclear localisation sequence
NRF2	Nuclear factor-erythroid factor 2-related factor 2
PAR	Poly-ADP-ribose
PARG	Poly-ADP-ribose glycohydrolase
PARP	Poly-ADP-ribose polymerase
PBM	PAR binding motif
PBS	Phosphate buffered saline
PBZ	PAR-bind zinc finger
PTM	Post-translational modification
TPA	Tetradecanoyl phorbol acetate
TRE	TPA response element
TX	Triton-X
UAS	Upstream activating sequence
XRCC1	X-ray cross-complimenting repair protein 1
ZnF	Zinc finger subdomain

List of Figures

List of Tables

Chapter 1 Introduction

1.1 Acute Wound Healing

The skin's epithelial barrier serves as a physical barrier between the internal and external environments, with the goal of limiting damage to the host from harmful stimuli. Therefore, any damage to the skin must be rapidly and efficiently repaired to restore barrier integrity and to maintain homeostasis (Eming et al., 2014).

Wound healing (of tissues like the skin) is a highly complex process, involving many different cell types. The healing process of an acute epithelial mammalian wound can generally be summarised in four key (and overlapping) stages: i) haemostasis (temporary sealing of the wound), ii) inflammation, iii) cellular proliferation of the epithelium and iv) remodelling of the tissue architecture (Raziyeva et al., 2021). Under ideal conditions, wounding immediately activates the haemostasis cascade, a protective mechanism mediated by platelets to prevent excessive blood loss (Raziyeva et al., 2021). The latter stages of the cascade cleave fibrinogen to fibrin via the action of thrombin, to produce a cross-linked fibrin clot that seals and protects the wound (Vilar et al., 2020). Formation of the fibrin plug is a temporary measure to protect the open wound and to act as a scaffold for other repair factors (Eming et al., 2014). This is rapidly succeeded by the inflammatory stages of healing, wherein innate immune cells such as neutrophils and macrophages infiltrate the wound site (Laurens et al., 2006).

Inflammation involves the recruitment of both cells of the innate, and to a lesser extent, the adaptive immune system, to clear away any debris and destroy any cells that have the potential to cause infection such as invading pathogens (Weavers & Martin, 2020). Inflammation is characterised by the upregulation of various inflammatory regulators, including IL-1β, IL-6 and TNFα (El-Hamoly et al., 2014). Innate immune cells together with damaged epithelial cells surrounding the wound release various reactive oxygen species (ROS), including superoxide and hydrogen peroxide, to help combat any pathogens that may be present, and thus preventing infection (Raziyeva et al., 2021). In the following days, the 'proliferative stage' begins to restore the skin's barrier integrity through a process termed 're-epithelialisation' which requires the remodelling of mammalian granulation tissue (Aragona et al., 2017). Keratinocytes, fibroblasts and anti-inflammatory macrophages (of the 'M2' phenotype) all play central roles in re-epithelialisation (Raziyeva et al., 2021). The final stage of wound healing is the 'remodelling phase' which can take years to fully resolve. During this stage granulation tissue is replaced with scar tissue and any remaining immune cells are removed, either by returning to the dermis to continue their established roles or through direct removal via apoptosis (Raziyeva et al., 2021).

Re-epithelialisation itself is a key part of the healing process as this culminates in permanent sealing of the wound to protect the host from the external environment. The mechanisms underlying re-epithelialisation have been the focus of many studies over past decades, involving various model organisms. Recent seminal work using live-imaging studies in murine skin has demonstrated that the epithelial tissue encompassing the wound is divided into zones; the leading edge (nearest to the wound) comprises migratory (non-proliferative) cells whilst further back actively dividing cells make up the proliferation zone (Aragona et al., 2017). These were previously thought of as two separate areas, however, thanks to advances in imaging techniques, it has become clear that these areas overlap with a central epithelial region exhibiting both migration and proliferation behaviours (Park et al., 2017) as observed in mammalian cells. Epithelial cell migration begins within minutes of wound formation and has been recognised for decades (Radice, 1980). There are variations in the extent of migration that takes place within the murine epidermis, both within the epithelial plane (from the proliferation zone to the wound centre) and also across the various layers of the skin (suprabasal, basal and dermis) (Park et al., 2017). During the first day post-wounding (in the murine epithelium), levels of cell migration are highest at the leading edge with a decreasing gradient moving away, towards the proliferation zone. Basal cells also show the highest levels of migration which decreases with increasing levels of differentiation (Park et al., 2017). Cells undergoing active migration become elongated and are angled towards the wound centre whereas those several rows back appear more compacted and cuboidal in shape, likely due to increased density (Aragona et al., 2017). Migration and proliferation appear to contribute to two thirds of the wound healing process, with wound contraction aiding in the final third (Aragona et al., 2017). Some studies have suggested that wounding induces rapid asymmetric division of stem cells within the proliferation zone, giving rise to self-renewing progenitors that can migrate towards the wound centre to aid in re-epithelialisation (Aragona et al., 2017).

Defects within the wound healing process can lead to the development of chronic, non-healing wounds that lack structural and functional integrity (Eming et al., 2014). Chronic wounds can develop in the healing process of almost any wound, but there are many underlying human medical conditions, such as diabetes mellitus or ischemia (often in combination), that can increase an individual's risk (Raziyeva et al., 2021). Infection is also a major contributing factor in chronic wound development. Although most if not all wounds are likely to have low levels of infection, inflammation and epidermal derived anti-microbial peptides (AMPs) can normally work together to keep this at a tolerable level (Eming et al., 2014). This, however, is not the case for chronic wounds; instead, these wounds exhibit prolonged, unresolved inflammation due to competing pro- and anti-inflammatory signals and therefore have disrupted healing capacities (Eming et al., 2014). Excessive ROS and oxidative stress are also a key feature in chronic non-healing wounds (see Introduction section 1.2).

In fact, many different factors work alongside one another and contribute to the development of a chronic wound. For example, diabetic foot ulcers (in humans) exhibit excessive expression of pro-inflammatory cytokines (TNF-α) which in turn promotes macrophage polarisation towards the pro-inflammatory M1 phenotype (Raziyeva et al., 2021). Proteases can also become dysregulated in chronic wounds; one example is matrix metalloproteinases (MMPs). MMPs are secreted by innate immune cells and play a role in the healing process (at low concentrations). Neutrophils secrete a variety of MMPs including MMP-8 and -9, both of which are upregulated in chronic diabetic foot ulcers (Nguyen et al., 2018). MMP-8 is beneficial to the repair process by aiding in the repair of damaged collagen and the ECM. MMP-9, on the other hand, is detrimental and further promotes the pro-inflammatory environment (Nguyen et al., 2018). Taken together, these factors lead to the development of a non-healing wound that does not follow the established stages of healing and instead can take many months or even years to heal without clinical intervention.

Chronic wounds not only have a severe negative impact on a patient's quality of life, but they also place a significant burden on healthcare services. The NHS spends approximately £8.3 billion per year on wound treatment (2017/18), with £5.6 billion of that total being allocated to the treatment of non-healing wounds (Guest et al., 2020). A randomised study of 3000 patients was conducted to assess the frequency and impact of non-healing wounds, in this study 30% of the 3000 patients experienced a non-healing wound which did not resolve during the one-year study period (Guest et al., 2020). As expected, the impact of managing these wounds was significantly greater on the healthcare service compared to those that did heal appropriately. The average cost of treatment for a healthy wound was £1500 but this rose to £3700 if the wound did not heal (Guest et al., 2020). The data obtained in this study highlights the desperate need for improving the prognosis and treatment of chronic wounds. To this end, the molecular and cellular mechanisms underpinning normal (acute) wound healing need to be better understood. as well as uncovering where the key issues arise that promote the formation of chronic wounds. Therapeutics could then be developed to either drive the mechanisms behind healthy healing processes or to block the pathways responsible for the formation of chronic wounds.

1.2 Role of Reactive Oxygen Species (ROS) and Oxidative Stress in Wound Healing

As mentioned above, a key role of inflammation is to prevent pathogenic infection, one method of which is the production of reactive oxygen species (ROS) by inflammatory cells (Li et al., 2021). ROS are oxygen-containing molecules that have gained electrons and become reduced to form highly reactive, unstable radicals (Dunnill et al., 2017). The most commonly studied ROS include superoxide radicals, hydroxyl radicals and singlet oxygen (Irrera et al., 2017). Immediately following injury, ROS are produced in immune cells and damaged epithelia by both NADPH oxidases and

mitochondria (Niethammer et al., 2009) during a process known as the ‘respiratory burst’ which acts as a first line of host defence against invading pathogens (Nguyen et al., 2017) and prevents infections at the wound site. NADPH oxidase is the driving force behind the conversion of molecular oxygen to superoxide radicals (auf dem Keller et al., 2006). The importance of NADPH oxidases is demonstrated by chronic granulomatous disease (CGD), an inherited immunodeficiency caused by defective NADPH oxidase in phagocytic cells (Seger, 2008); individuals affected by CGD experience frequent infections since their bodies are unable to activate the respiratory burst. In CGD patients, although phagocytes are able to engulf the pathogen, they are then unable to break it down via ROS production, resulting in granuloma formation (Seger, 2008). CGD highlights the importance of possessing functional NADPH oxidase and ROS production.

Within the wound environment, low concentrations of ROS are beneficial in tissue repair and act as secondary messenger signals to both promote the recruitment of leukocytes to the wound margin (Niethammer et al., 2009) and to stimulate angiogenesis (Dunnill et al., 2017). Many other processes require ROS for proper function such as protein phosphorylation and cellular differentiation (Pizzino et al., 2017). However, unregulated levels of ROS can be detrimental to the repair process, with potential to cause damage to the host. As previously mentioned, ROS are highly reactive molecules that are not only capable of destroying pathogens but also damaging healthy tissue (Weavers et al., 2019) since ROS are indiscriminate in their actions between invading pathogens and the host tissue. Oxidative stress is defined as an imbalance between the production of ROS and detoxification/ removal by antioxidants (Irrera et al., 2017). Excessive ROS accumulation can damage otherwise healthy DNA, proteins and lipid membranes (Mehta et al., 2018) and can damage DNA via the formation of bulky lesions; one such example is the hydroxylation of deoxyguanosine residues at carbon position 8 by singlet oxygen to produce 8-hydroxydeoxyguanosine (8-OHdG) lesions (Kuchino et al., 1987). Elevated levels of 8-OHdG can be used as a marker of oxidative stress (Pizzino et al., 2017). Consequently, sustained high ROS concentrations and high levels of oxidative stress can be detrimental to host tissue (Sumioka et al., 2021) – indeed oxidative stress is a key factor in the pathogenesis of chronic non-healing wounds.

1.3 Cytoprotection to Mitigate Collateral Damage to the Repairing Tissue

Mammalian cells and tissues, including injured tissues, have developed a variety of systems to help deal with and counter high oxidative stress levels to prevent unnecessary damage (Thorpe et al., 2004). Cells can employ a range of cytoprotective mechanisms to mitigate oxidative damage, either by direct protection (neutralisation) through the action of antioxidants, as well as by upregulation of other protective factors that repair ROS-induced damage (Mehta et al., 2018). A key cytoprotective factor that has been implicated in wound healing is the transcription factor nuclear factor-erythroid 2-related factor 2 (Nrf2). Nrf2 is often thought of as the master regulator of the antioxidant response

within mammalian tissues, the key function is to prevent unnecessary ROS-induced damage to the host (Soares & Ribeiro, 2015). Nrf2 activity is regulated at a post-translational level by Kelch-like ECH-associated protein 1 (Keap1) (Hiebert & Werner, 2019). Under conditions of homeostasis (where levels of oxidative stress are low meaning minimal cytoprotection is required), Keap1 binds and retains Nrf2 within the cytosol ensuring only minimal levels of Nrf2-driven transcription can take place (Hiebert & Werner, 2019). The presence of ROS destabilises this Nrf2-Keap1 interaction, via the formation of a disulphide bond that interrupts the tertiary structure of Keap1 (Soares & Ribeiro, 2015), resulting in translocation of Nrf2 to the nucleus where Nrf2 is able to bind antioxidant response elements (AREs) within the promoter region of DNA to upregulate the production of cytoprotective genes and proteins (Ke et al., 2021).

Nrf2 was first investigated as a potential cytoprotective factor during wound healing in a murine study (Braun et al., 2002) that compared control and Nrf2-knockout mice. Although the overall rate of murine wound closure was not significantly impaired by Nrf2 knock-out, expression of key wound genes was disrupted and the inflammatory response was prolonged (Braun et al., 2002). However, it was thought that compensatory upregulation of related antioxidant systems (e.g. Nrf3) could be masking a repair defect. Indeed, more recent work using mouse and *Drosophila* models has highlighted a crucial role for antioxidants following wound repair. Glutathione is the most abundant of the cellular antioxidants and has been shown to play a central role in wound repair via cytoprotection (Telorack et al., 2016); without glutathione, tissues exhibit increased apoptosis and impaired healing capacity that cannot be rescued by Nrf2 activation. Intriguingly, however, sustained high levels of Nrf2 activation can lead to fibroblast senescence and may also increase the risk of cancer (Hiebert et al., 2018).

Moreover, recent studies in *Drosophila* (which have the advantage of possessing less genetic redundancy) have uncovered a complex cytoprotective ‘resilience’ network that is activated upon wounding, to protect the damaged tissues from ROS-induced oxidative damage (Weavers et al., 2019). This network involves cross-communication between the transcription factor Nrf2, JNK and calcium signalling, and the DNA repair factor Gadd45 to drive efficient wound repair (Weavers et al., 2019). The presence of ROS activates the Nrf2 cytoprotective pathway and this upregulates the downstream expression of antioxidants. Since Gadd45 is involved in the DNA damage response (DDR), it is likely that it plays a key role in repairing the ROS-induced damage following wounding. Indeed knocking down Nrf2 and Gadd45 simultaneously impairs wound repair more significantly than singular knockdowns, suggesting a key role in protecting the repairing tissue in *Drosophila* (Weavers et al., 2019).

Since the epithelial barrier (skin) is constantly exposed to ROS-inducing insults in the form of ultraviolet (UV) irradiation, chemicals etc. (Telorack et al., 2016), perhaps high levels of cytoprotective molecules/pathways are active within the epithelium, even in unwounded conditions. These levels might be elevated further following additional insult (e.g. wounding). Consistent with this, murine studies have highlighted a key role for Nrf2 in the protection of the epithelium against UV-induced ROS damage (Schäfer et al., 2012).

Although a growing number of cytoprotective pathways are being implicated in ensuring efficient tissue repair following damage, we envision that there are many more yet to be uncovered.

1.4 The PARP Family and the Enzymatic Structure of PARP1

Since oxidative stress is associated with ROS-induced damage to DNA, cytoprotection (particularly during wound healing) is likely to require DNA damage repair. Indeed, poly(ADP-ribosyl)ation, more commonly known as PARylation, is a reversible post-translational modification (PTM) involved in the response to DNA damage that the Weavers lab recently showed to be upregulated following wounding (Weavers et al., 2019). PARylation is also particularly elevated in chronic wounds, including human wounds (Bodnár et al., 2018). The family of enzymes responsible for catalysing PARylation are poly(ADP-ribose) polymerases, or PARPs. The mechanism of action of PARPs involves the transfer of ADP-ribose units from NAD^+ to a target protein, causing the protein to become MARylated (addition of one ADP-ribose unit) or PARylated (addition of two or more units) (see schematic in Figure 1).

There are currently 17 recognised members of the PARP family with various roles including but not limited to, DNA damage repair, chromatin remodelling, cell cycle regulation and mRNA stability (Brady et al., 2018). These 17 family members have been classified further into different groups depending on their enzymatic role (Zaja et al., 2013). PARPs 1-6 are able to carry out PARylation due to conserved glutamate resides whereas PARPs 7, 8, 10-12, and 14-16 can only facilitate MARylation (addition of one ADP-ribose unit) (Zaja et al., 2013). PARP1 and 2 are recruited to both single-strand (SSBs) and double-strand breaks (DSBs) within damaged DNA (Azarm & Smith, 2020). PARP5 and PARP6 (sometimes referred to as PARP5b) are more commonly known as tankyrase-1 and –2, respectively. Tankyrases are capable of carrying out PARylation as well as a variety of other key roles such as maintenance of telomeres, involvement in mitosis and cell signalling pathways; for example, PARylation of target proteins by tankyrases marks proteins for ubiquitination and subsequent degradation, influencing biochemical pathways (Langelier et al., 2019). In contrast to PARP1 and 2, PARylation by tankyrases results in the formation of much shorter, unbranched chains of approximately 20 PAR units in length (Azarm & Smith, 2020).

PARP1 was first discovered in 1963 in nuclear extracts from hen liver as an unknown enzyme activated by nicotinamide mononucleotides (NMN), and dependent on DNA (Chambon et al., 1963). In the past five decades, our understanding of PARP1 has greatly improved through many studies but there still remains plenty to be uncovered. DNA damage repair was the first noted role for PARP1 (Satoh & Lindahl, 1992), however, since then a variety of other roles have been elucidated, implicating the enzyme as a more general response to cytotoxic stress. PARP1 is the most well-studied of all of the PARP enzymes in terms of both structure and function, and is the most abundant following genotoxic stress, producing 90% of cellular PAR (Ke et al., 2019).

The 116-kDa PARP1 protein comprises 3 functional domains: the N-terminal binding domain, the central automodification domain, and the C-terminal catalytic domain. The N-terminal binding domain contains three zinc-finger (ZnF) subdomains and the nuclear localisation sequence (NLS) (Rajiah & Skepper, 2014). Following recognition of DNA damage, all three zinc-fingers are in contact with DNA. ZnF1 and ZnF2 directly facilitate PARP1 binding to sites of DNA damage whereas ZnF3 regulates enzymatic activity (Krüger et al., 2020). The NLS is located between ZnF2 and ZnF3, and is closely followed by a caspase-3 cleavage site involved in the initiation of apoptosis (Ke et al., 2019). During apoptosis PARP1 undergoes cleavage by caspase-3 and caspase-7 to produce two fragments of 24kDa and 89kDa (Erener et al., 2012). The 24kDa fragment contains the first two zinc fingers so is able to bind DNA but is enzymatically inactive; the 89kDa fragment on the other hand comprises both the automodification and the catalytic domain, allowing this fragment to retain basal levels of activity (Germain et al., 1999).

There are two key types of PARylation: trans-PARylation and auto-PARylation. Trans-PARylation is the addition of ADP-ribose units to other target proteins/acceptors such as histones, which are the second most abundant PARylated protein following PARP1 (Rudolph et al., 2021). Histone PARylation Factor 1 (HPF1) works together with PARP1 to promote the PARylation of histones, (Rudolph et al., 2021). HPF1 interacts with the catalytic domain of PARP1, causing two important changes, firstly promoting trans-PARylation over auto-PARylation, and secondly promoting addition of PAR units to serine residues rather than glutamate (most common site of PARylation) (Langelier et al., 2019). Auto-PARylation is a form of automodification in which the PARP enzyme, particularly PARP1, itself becomes PARylated in response to genotoxic stress (Zaja et al., 2013). PARP1 contains a central automodification domain that comprises various amino acid acceptors that function alongside the BRCT subdomain for auto-PARylation (Luo & Kraus, 2012). Three key sites of automodification have been uncovered for PARP1: Asp-387, Glu-488, and Glu-491 (Tao et al., 2009).

The C-terminal catalytic domain contains the WGR (Trp-Gly-Arg) motif that facilitates nucleic acid binding, the ADP-ribosyl transferase (ART) fold, and the helical domain. All 17 members of the PARP family have an ART fold within this domain, hence why they are often referred to as ARTD enzymes due to shared homology with the diphtheria toxin ART fold (Langelier et al., 2019). The other regions differ between the PARP family members to provide unique functions (Langelier et al., 2018). The helical domain of PARPs binds NAD^+ subunits for PARylation at the active site (Banerjee et al., 2019). As previously mentioned, PARPs act by transferring ADP-ribose units to a target protein using NAD^+ as a substrate (Figure 1). A covalent ester bond is formed between the ADP-ribose unit and a carboxyl group on the target protein at specific amino acids, normally glutamate, aspartate or serine (Páhi et al., 2020), nicotinamide is also released as a by-product. PAR units can be attached in straight chains, but additional PAR units can be added to PAR chains at 2'-1' ribose-ribose bonds to form branched polymers (Páhi et al., 2020). These polymers (straight or branched) can extend up to 200 PAR units in length (Azarm & Smith, 2020). The hydroxyl (-OH) group of ADP-ribose acts as the acceptor for additional PAR units and branching can take place every 5-20 residues at 2"-OH on PARP1 (Rudolph et al., 2021).

When inactive and not bound to DNA, PARP1 adopts a folded configuration in which helices form at specific sections (Langelier et al., 2019), blocking NAD^+ from accessing the active site. This forms a selective steric block and acts a method of autoinhibition to keep basal levels of PARylation low, preventing excessive consumption of NAD^+. Upon detection of DNA strand breaks ZnF1, ZnF3 and WGR organise around the site resulting in allosteric destabilisation of the helical domain (Azarm & Smith, 2020). PARP1 undergoes a conformational change to an unfolded configuration (Langelier et al., 2012), allowing access to the helical domain, and increasing levels of PARP1 activity by 1000-fold (Langelier et al., 2018).

Poly(ADP-ribose) glycohydrolase (PARG) reverses the PARylation modification by hydrolysing PAR units from the target protein (Figure 1). PARG is responsible for dynamic catabolism of PAR units, meaning that under normal homeostatic conditions the majority of PAR units have a half-life of below six minutes (Zaja et al., 2013). This can be increased to seven hours for an extremely large/branched polymer, or reduced to 40 seconds during high levels of DNA damage (Alvarez-Gonzalez & Althaus, 1989). PARG cleaves terminal ribose units from the polymer by hydrolysing the *O*-glycosidic bond (Páhi et al., 2020). ADP-ribosyl hydrolase (ARH3) is a 39-kDa protein also capable of hydrolysing PAR units but with a lower specificity compared to PARG (Páhi et al., 2020).

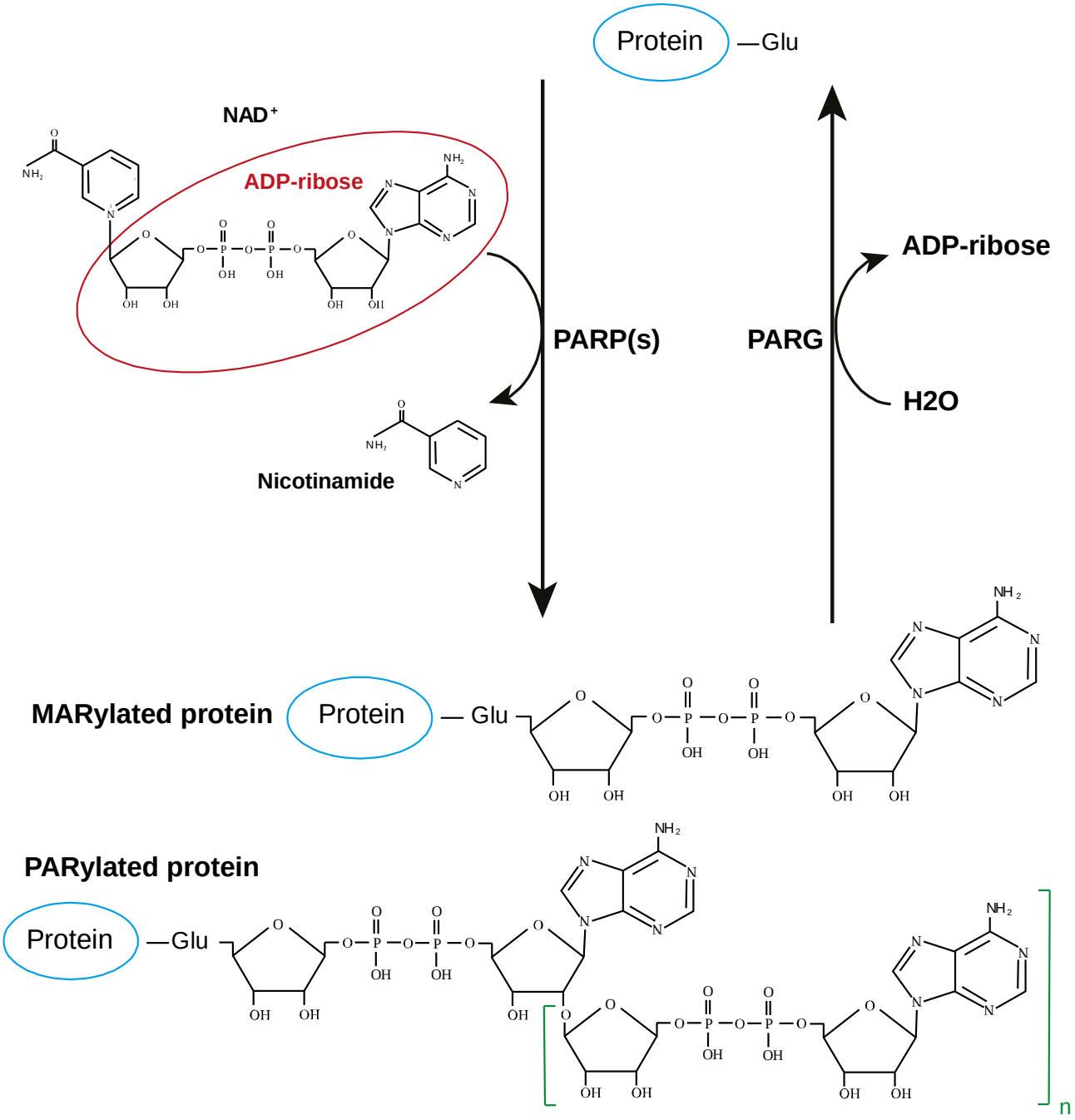

Figure 1: **Schematic of the chemical reaction behind PARylation.** PARylation is a reversible post-translational modification carried out by poly(ADP-ribose) polymerases (PARPs) and poly(ADP-glycohydrolase (PARG). PARP enzymes facilitate the transfer of an ADP-ribose unit from NAD^+ to the target protein, resulting in the release of a nicotinamide unit. MARylated proteins have only one bound ADP-ribose unit whereas PARylated proteins have two or more (as represented by 'n') bound units. PARG acts to remove ADP-ribose units via a hydrolysation reaction.

1.5 Cellular Functions of the PARylation Stress Response

Many cellular proteins possess specialised motifs that facilitate recognition of and interaction with PAR units on target proteins. The first motif to be discovered was the PAR binding motif (PBM), a motif comprising of only eight amino acids with a high specificity for recognising and binding PAR units (Zaja et al., 2013). As previously mentioned, PARP1 plays a key role in the DNA damage repair

response. One of the central enzymes in controlling DNA repair is the X-ray repair cross-complementing gene 1 (XRCC1) (Zhen & Yu, 2019), which contains a PBM within its BRCA1 C-terminus (BRCT) domain. These BRCT domains recognise and bind the ADP-ribosyl unit (Azarm & Smith, 2020) within PARylated PARP1 (Pleschke et al., 2000). Since auto-PARylation of PARP1 is stimulated by genotoxic stress (Zaja et al., 2013), this results in the formation of a PARP1-XRCC1 complex at the site of damage (Pleschke et al., 2000). XRCC1 is then able to recruit other repair proteins, leading to the formation of a large protein complex and consequent repair of the DNA damage (Zhen & Yu, 2019). Another method for interacting with PAR is through PAR-binding zinc fingers (PBZs) that are around 30 amino acids in length and can recognise/bind either monomers of ADP-ribose or the ribose-ribose bond within PAR units (Azarm & Smith, 2020).

Following DNA damage, PARP1 localises to the cell nucleus where the enzyme is able to carry out either auto- or trans-PARylation of DNA damage response (DDR)-associated proteins (including of PARP1 itself). In some circumstances, the DNA damage may be too severe for the repair mechanisms to correct, in which case the cell must undergo some form of cell death. Under these conditions, PARP1 levels are abnormally high due to excessive levels of DNA damage resulting in hyper-activation of PARP1 and PAR accumulation (Zhou et al., 2021). Free PAR units, most commonly generated via PARG action, are then translocated out of the nucleus and in to the cytoplasm (Mashimo et al., 2022) where they act as a 'death messenger' (Ke et al., 2019). These free PAR units signal for the cell to undergo a form of PARP1-dependent, caspase-independent cell death process known as parthanatos (Zhou et al., 2021). Since PARylation requires the consumption of NAD^+ units, such over-activation of PARP1 can drain the NAD^+ pool, as is seen following excessive levels of DNA damage, where up to 80% of the NAD^+ pool can be drained within a matter of minutes (Zhou et al., 2021). NAD^+ is also required in the production of ATP for metabolic use by the body; without ATP, cells cannot carry out their normal functions, in turn leading to the depletion of energetic substrates (Ke et al., 2019). This could have potential implications when PARylation is activated in stressed tissues, including at wounds as the depletion of NAD^+ and ATP could hinder tissue repair. The combination of PARP1 hyperactivation, PAR accumulation and NAD^+/ATP depletion (causing mitochondrial depolarization) can result in the translocation of apoptosis inducing factor (AIF) out of the mitochondria (Zhou et al., 2021). In the cytoplasm AIF is able to interact with other pro-death factors (such as macrophage migration inhibitory factor, MIF) to form the AIF/MIF complex that is then translocated into the nucleus, allowing cleavage of DNA strands and ultimately cell death (Zhou et al., 2021).

As well as its classical role in DNA repair, PARP1 has multiple additional roles within the cell, one common example is chromatin remodeling as PAR units carry a strong negative charge, causing DNA repulsion and chromatin decondensation (Ciccarone et al., 2017). PARP1 can also play a role

in transcriptional regulation by directly binding to DNA poly-nucleosomes (triggered by the absence of NAD^+) and preventing transcription (Kraus, 2008); in these scenarios PARP1 is later released once NAD^+ levels have recovered and transcription is allowed to resume (Kraus, 2008). PARP1 has also been implicated within the process of membrane repair and may aid endocytosis of repair proteins (Mashimo et al., 2022).

1.6 The Emerging Role of PARP1 and PARylation in Chronic Wounds

As previously mentioned, complications in the wound healing process can lead to the development of chronic, non-healing wounds. These wounds have unresolved, high levels of inflammation and subsequently high levels of ROS and oxidative stress causing damage to proteins, lipids and DNA (Bodnár et al., 2018). In these situations, the high levels of oxidative and genotoxic stress could potentially result in the activation (and upregulation) of PARP1. Indeed, a handful of recent studies have confirmed that PARP1 is hyperactivated in chronic wounds using a number of mammalian models (Banerjee et al., 2019). For example, murine models have been used to explore the role of PARP hyperactivation in ischemic and diabetic wounds, since PARP is known to be hyperactivated in both conditions (Zhou et al., 2017). In diabetic/ischemic mice only ~40% of wounds healed, however addition of a PARP inhibitor (PJ-34) caused the proportion of healing wounds to increase to approximately 70% (Zhou et al., 2017). These data suggest that PARylation is detrimental in chronic wounds. It is tempting to speculate that in normal acute wounds, PARP1 might be activated, perform its required role and then PAR subunits would undergo degradation via the action of PARG. Whereas in chronic wounds, due to the unresolved inflammation, the production of PARP1 and subsequent autoPARylation might continue to lead to hyperactivation of PARP1 (Banerjee et al., 2019). This could further promote a positive feedback loop of inflammation, as PARP1 is known to promote the expression of pro-inflammatory mediators such as IL-6 and TNF-α via the action of nuclear factor kappa B (NF-κB) (El-Hamoly et al., 2014). Indeed, in another study wild-type mice were wounded via a skin incision and some mice were treated with one of two common PARP inhibitors, 3-aminobenzamide (3-AB) and PJ-34 (in the form of a cream), to assess the impact on wound closure (El-Hamoly et al., 2014). PARP inhibition reduced the expression of pro-inflammatory regulators, most notably TNF-α, and helped in the restoration of cellular energy levels by limiting excessive NAD+ consumption, subsequently improving the rate of wound closure (El-Hamoly et al., 2014). Similar results were observed in a murine study of third-degree burn healing which used Olaparib as the PARP inhibitor; levels of pro-inflammatory mediators were decreased, and the overall rate of wound healing improved compared to controls (Ahmed et al., 2018).

Human wounds have also been analysed to explore key differences between acute and chronic wounds and have revealed a striking difference in levels of PARP1 accumulation and subsequent PARylation. Wound fluid was sampled from human volunteers from both healing (acute) and non-

healing (chronic) wounds (Bodnár et al., 2018) and significant changes were detected in the antioxidant profile between the different wound environments; chronic wounds showed an increase in TNF-α (inflammatory cytokine), IL-8 (involved in granulocyte recruitment), and VEGF (required for vascularisation) (Bodnár et al., 2018) compared to healing acute wounds. This increase in pro-inflammatory mediators is likely to correlate with increased levels of ROS, confirmed by an increase in protein carbonylation in chronic wounds indicating higher levels of protein oxidation. Immunohistochemistry was also used to detect PARP1 and PARylation in ulcer biopsies; strong, positive staining for PARP1 was detected in the chronic venous ulcers, particularly at the wound edge, whereas samples of healthy unwounded skin showed little staining. Taken together, these data show that human chronic wounds have elevated levels of inflammation, ROS, oxidative stress and hyper-PARylation (Bodnár et al., 2018). Nevertheless, whether PARylation plays beneficial roles in acute wound repair, such as for promoting DNA damage repair, remains immensely under-explored.

1.7 *Drosophila melanogaster* as a Valuable Model Organism

This study uses *Drosophila melanogaster* as the chosen experimental model organism due to their optical translucency, high levels of genetic tractability and the vast availability of transgenic stocks. *Drosophila* are optically translucent during both the embryonic and pupal stages of development, making them a desirable tool for live imaging (Weavers & Wood, 2016). *Drosophila* also have relatively short life cycles, going from freshly laid embryo to adult fly in only 10 days allowing for genetics to be altered and tracked across multiple generations in a relatively short time frame. Another desirable characteristic of *Drosophila* is that many of the genes involved in human health and disease have homologs within the *Drosophila* genome but there is far less genetic redundancy (and thus less compensation) within *Drosophila*. *Drosophila* also only have four pairs of chromosomes, simplifying genetic crosses.

Another powerful experimental tool is that *Drosophila* can be used for targeted gene expression, enabling knockdown of a specific gene in a particular tissue by employing the Gal4/upstream activating sequence (UAS) system (Brand & Perrimon, 1993). Gal4 is a transcriptional activator found in yeast (*Saccharomyces cerevisiae*) that drives galactose-induced gene expression (Elliot & Brand, 2008). The Gal4 activator functions by dimerising and binding to specific DNA sequences called upstream activating sequences (UAS) via zinc finger domains (Elliot & Brand, 2008). This yeast system has been exploited for targeted genetic manipulation in a variety of lab models to stimulate tissue-specific expression. *Drosophila* was the first model that was utilised to exploit the Gal4/UAS bipartite system, allowing geneticists to drive ectopic expression of any target gene (Brand & Perrimon, 1993). Brand and Perrimon (1993) designed a vector to drive expression of a target gene, this vector contained a tandem array of five optimized Gal4 binding sites (UAS sites) which

can be followed by the target gene of interest. In practise, to use the GAL4-UAS system, *Drosophila* fly stocks are mated with each parent stock containing one half of the system (see Figure 2). One parent will possess the coding sequence for Gal4 which is driven by a cell/tissue specific promoter; the other parent will possess the UAS construct followed by the target gene e.g. a gene to be over-expressed or an RNAi construct to permit tissue specific gene knockdown (Elliot & Brand, 2008). Due to the bipartite system, otherwise lethal transgenic combinations can be created as neither parental line will be able to express the gene, allowing these organisms to properly develop. Only the F_1 progeny with both required halves, the Gal4 activator and the UAS responder that is then able to transcribe and subsequently express the transgene in a tissue-specific manner (Elliot & Brand, 2008). This is an excellent genetic tool as it allows knockdown or overexpression of a gene in a specific cell or tissue type, to better understand the key function. Expression levels can be altered by manipulating the availability of UAS sites or by altering the number of both driver and responders (Busson & Pret, 2007).

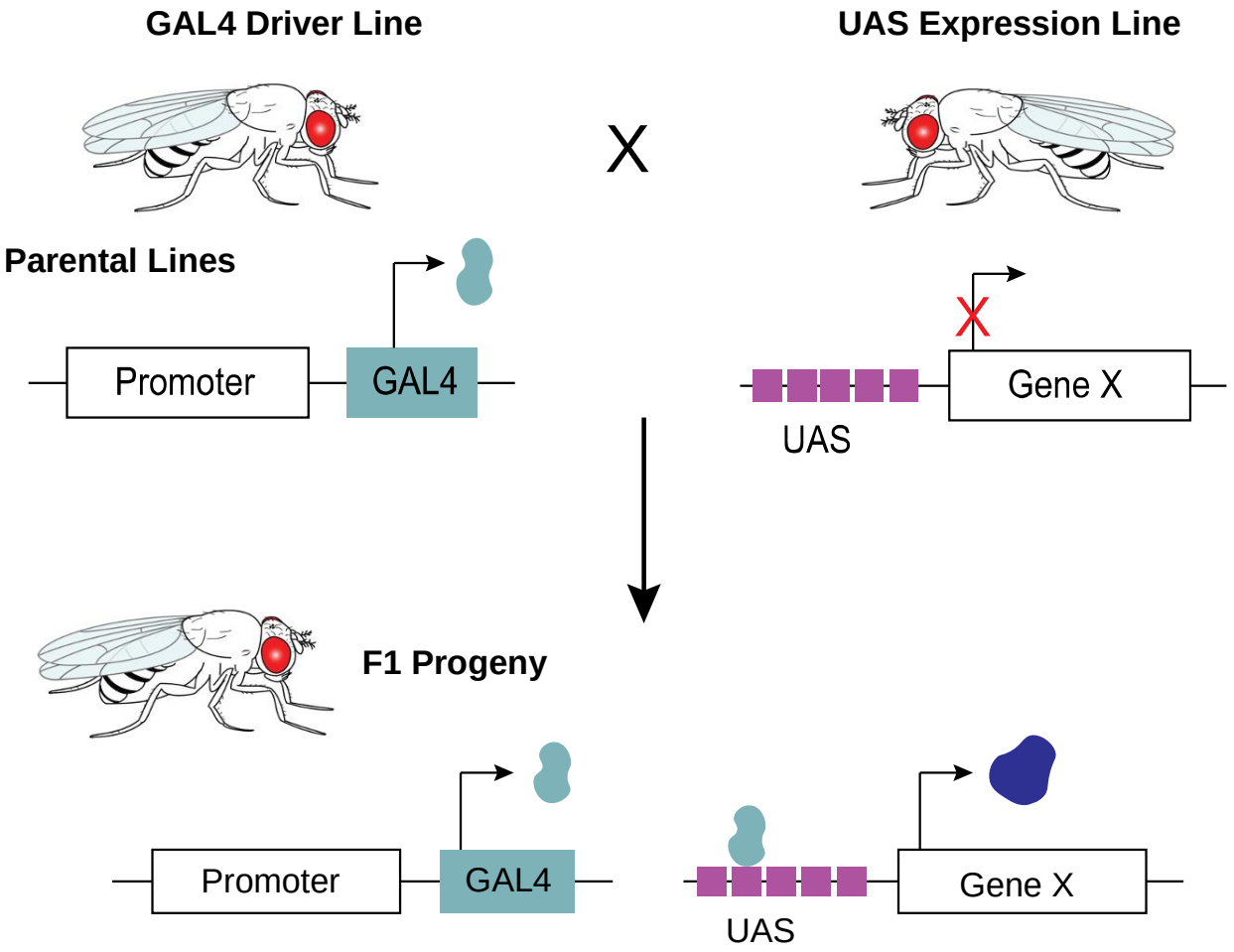

FIgure 2:* Schematic representation of the Gal4/UAS system in *Drosophila melanogaster. Parental lines each encode one part of the system, either the Gal4 driver or the upstream activating sequence (UAS) conjugated to the gene of interest (gene X). Only the F1 progeny is able to express gene X as the transcribed Gal4 protein binds to the UAS, activating gene X transcription.

1.8 Using *Drosophila melanogaster* to Study Wound Repair and Inflammation

Drosophila have been used as a model organism for many years and have greatly aided our understanding of many aspects of developmental biology as well as wound repair and inflammation (Letsou & Bohmann, 2005). Due to their genetic tractability and optical translucency, *Drosophila* are a particularly valuable model in which to explore the molecular mechanisms underlying tissue repair. One of the key features of the wound healing process that *Drosophila* has helped elucidate is the formation of the contractile actin cable during re-epithelialisation that works to draw the wound closed. This process was actually first observed in the chick embryo (Martin & Lewis, 1992) and has since been recorded in many other embryonic wounds (Rothenberg & Fernandez-Gonzalez, 2019), including mouse, *Drosophila melanogaster* (Wood et al., 2002) and zebrafish (Richardson et al., 2016), suggesting a conserved mechanism of action. Although the chick model was traditionally a valuable tool for understanding the basics of wound repair, including the presence of an actin cable, these experiments were conducted on fixed tissue (Martin & Lewis, 1992).

In recent years, advancements in live imaging have allowed researchers to use *in vivo* models, such as *Drosophila*, to track wound closure mechanisms in real time (Ducuing & Vincent, 2016). Transgenic *Drosophila* stocks allow for labelling of key features, for example using GFP-tagged actin to visualise actin accumulation and cable formation over the period of wound closure. Following wounding, a single row of cells within the epidermis forms a thick actin cable at the leading edge of the wound with five times the actin concentration of other surrounding cells (Martin & Lewis, 1992). The cytoskeleton of cells adjacent to the wound becomes polarised, resulting in the formation of a supracellular cable composed mainly of actin and myosin (Rothenberg & Fernandez-Gonzalez, 2019). This is known as the actomyosin purse string, or more commonly the actin cable, which works alongside various other cytoskeletal proteins such as microtubules to draw the embryonic wound closed (Rothenberg & Fernandez-Gonzalez, 2019). The cable that is formed is a dynamic structure, able to move and contract as the embryo heals aiding in efficient wound closure and maintaining a taut wound edge. *Drosophila* mutants lacking an actin cable had irregular shaped wounds with jagged edges (Ducuing & Vincent, 2016).

Another actin-based mechanism in embryonic wound healing that has involved *Drosophila*-based research is the formation of actin-containing filopodia and lamellipodia (Wood et al., 2002). The production of these structures is mediated via Rho-GTPases, namely Cdc42, and is upregulated in the latter stages of embryonic wound closure. *Drosophila* embryos in particular exhibit four key stages of epithelial wound repair: wound expansion, coalescence (actin cable begins to form), contraction (majority of wound closure), and finally contraction (Abreu-Blanco et al., 2012). Both the actin cable and actin protrusions are involved in efficient wound closure but at different stages of epithelial repair. Knocking down either one of these processes does not prevent wound closure,

however, this does cause a significantly slower rate of closure. The actin cable is generated during the coalescence stage along with other forms of cellular machinery required for repair, the cable then acts as a purse string during contraction to rapidly reduce the area of the wound (Abreu-Blanco et al., 2012). Apical protrusions are visible during the contraction stage but play a far more crucial role during later stages of closure to repair the remaining opening of the wound, to 'knit together' the opposite sides (Abreu-Blanco et al., 2012). *Drosophila* mutants lacking Zasp52 (protein central to actin cable formation) exhibited a 20% decrease in the rate of closure compared to wild-type controls (Ducuing & Vincent, 2016).

Drosophila embryos and pupae are the most common lifecycle stages used within wound healing research since these are translucent, providing considerable benefit for live imaging. However, larvae have also been developed for use in wound healing assays to explore the impact of genetic manipulation on repair rate (Galko & Krasnow, 2004). One such study analysed the genetic impact of Yorkie (Yki), a transcriptional co-activator involved in regulation of cellular proliferation and apoptosis (Tsai et al., 2017). Larval wounds do not heal via cellular proliferation (Galko & Krasnow, 2004), instead directed cell migration promotes closure (Tsai et al., 2017). This study uncovered a role for Yki in epidermal repair in larvae that does not involve proliferation and instead regulates polymerisation of actin (Tsai et al., 2017). The basics of wound healing have been studied extensively in many model organisms, however the tissue mechanics behind the healing process are not yet well understood. *Drosophila* imaginal wing discs have been used to study the role of tissue mechanics, specifically epithelial cell junctions surrounding the wound site (Tetley et al., 2019). Alongside formation of the actin cable post wound formation, epithelial cells also undergo intercalation at the wound edge to aid in the healing process and the timing of this event correlates with that of most rapid wound closure. This study highlighted a key role for epithelial interaction, and that blocking this process impairs the healing capacity (Tetley et al., 2019).

Inflammation plays a central role in the process of wound healing across all species. It is therefore not surprising that *Drosophila* embryos and pupae have been used in many scientific studies to help elucidate the behaviour of immune cells. The mechanism of macrophage recruitment during inflammation is highly conserved across many different species. *Drosophila* have far fewer immune cell lineages, unlike the many observed in mammals, and predominantly contain macrophage-like cells (known as hemocytes in *Drosophila*) across all stages of development (Weavers & Wood, 2016). Nevertheless, *Drosophila* embryos have been used as valuable *in vivo* models of inflammation to explore the mechanisms regulating macrophage (hemocyte) recruitment to laser-induced wounds within the epithelium. For example, dynamic live-imaging revealed an important role for small GTPases in hemocyte migration; hemocytes displayed significant defects in their wound recruitment following the knockdown of small GTPases (such as Rho, Cdc42 and Rac) in *Drosophila*

embryos (Stramer et al., 2005). Macrophages have long been known to engulf pathogens and apoptotic corpses, however, another *Drosophila* study showed that corpse engulfment during embryonic development may 'prime' the innate immune system, a process that had traditionally been associated with the adaptive immune system. Macrophage priming is induced by JNK signalling downstream of corpse uptake resulting in cellular memory that allows the macrophages to respond more rapidly following wounding or infection (Weavers et al., 2016). Nevertheless, wound-induced macrophage infiltration also involves ROS production to prevent infection, however, this can be detrimental to the healing process as ROS may induce oxidative damage to the cell. As previously mentioned, *Drosophila* (and other species) have developed cytoprotective mechanisms to help counter this damage (Weavers et al., 2019). Wounding triggers activation of a cytoprotective network comprising the transcription factor Nrf2, the JNK cascade, calcium and Gadd45 which work to protect and repair DNA (Weavers et al., 2019).

Since PARP is also a key protein in the DNA damage response, there is potential for PARylation to be implicated in some capacity in the mechanism of wound cytoprotection. *Drosophila* only have one PARP gene, *parp*, which encodes three isoforms: dParp-I, dParp-II, and dParp-e (Miwa et al., 2020). Each of these are transcribed via differential splicing and varying the start site of transcription (Miwa et al., 2020). Some isoforms are expressed across the whole lifecycle whereas some are only expressed during specific developmental stages (Tulin & Spradling, 2003). The isoform of interest for this study is dParp-I due to the similarity in both structure and function to mammalian PARP1 (Tulin & Spradling, 2003) and the fact that dParp-I is the only enzymatically active PARP isoform in *Drosophila*. The other fly Parp isoforms are unable to carry out PARylation as dParp-II lacks the central automodification domain, and dParp-e lacks the C-terminal catalytic domain (Ishak et al., 2016). *Drosophila* also express one *parg* gene (dParg) on the X-chromosome (Hanai et al., 2004) to allow for the production of PARG and subsequent degradation of PAR. However, *Drosophila* lack ARH3 that is present in mammals and other species to work alongside PARG to break down PAR units (Ghosh et al., 2018). Therefore, it is likely that *Drosophila* depend entirely on the *parg* gene to prevent PARP1 hyperactivation. *parg* has been implicated in the function of the nervous system, as knocking down *parg* has been shown to induce neurodegeneration in adult flies impairing limb development and causing issues with flying (Hanai et al., 2004). Nevertheless, the role of PARP and PARylation in wound repair and inflammation has not yet been studied in *Drosophila.*

1.9 Project Aims

The key aims of this study are to explore the role of PARylation following wounding in *Drosophila* using a combination of genetic manipulation, live confocal imaging, and immunostaining. As

mentioned above, I will be using *Drosophila* embryos as their optical translucency allows for live timelapse imaging and their diverse genetic capabilities allows for targeted genetic knockdown of *parp* or *parg*, the genes of interest. Specifically, I aim to:

1. **Assess the role of the PARylation stress response** in the repairing epithelium in terms of the rate of wound closure and the effect on subcellular behaviours (including the leading-edge actin cable).

2. **Assess the role of PARylation in relation to innate inflammatory immune cells (*Drosophila* hemocytes)**. I plan to investigate whether PARP is required for *Drosophila* immune cell behaviour, firstly during 'normal' homeostatic patrolling in unwounded embryos, and secondly during their inflammatory migration to wounds.

Chapter 2 Materials and Methods

2.1 *Drosophila* Husbandry and Stock Keeping

Fly stocks were maintained according to standard protocols (Greenspan, 1997). Stocks were stored at 18^{o}C, and genetic crosses carried out at 25^{o}C unless otherwise stated. The following *Drosophila* stocks were obtained from Bloomington *Drosophila* Stock Centre (Indiana University) using the listed ID numbers, unless otherwise stated; wild-type *w67* (ID: 6599)*, daughterless-gal4* (ubiquitously expressed gal4 driver) (ID: 31775)*, UAS-GFP-Moesin* (ID: 31775)*, Ecad-GFP* (Kyoto ID: 109007)*, serpent-Gal4 (*hemocyte specific driver) (Brückner et al., 2004)*, UAS-GFP* (ID: 5431)*, crq-gal4 (*hemocyte specific driver) (ID: 25041)*, UAS-redstinger* (nuclear RFP*)* (ID: 8547)*, Tre-GFP* (JNK activity reporter) (Chatterjee & Bohmann, 2012)*, UAS-moe-mcherry* (ID: 35521), *UAS-parp RNAi* (ID: 57265), *UAS-parp RNAi* (ID: 34888) (Zhang et al., 2019), *UAS-parg RNAi* (ID: 61333), *ubiEcad-GFP* (ID:60584) (Oda et al., 1998), *srpH2A3mch* (gift from Daria Siekhaus), *srp-mchCyto* (gift from Daria Siekhaus)

2.2 Staging *Drosophila* Embryos

Embryos were collected from overnight apple juice plates by rinsing the plate with distilled water and using a paintbrush to gently dislodge them, the embryos were collected in an egg basket. The egg baskets were submerged in 50% bleach (sodium hypochlorite) (VWR International) for 2 minutes to remove the outer chorion membrane, the dechorionated embryos were then thoroughly rinsed with distilled water to prevent any chemical damage. Midgut morphology was the main identifier to ensure the appropriate developmental stages of *Drosophila* embryos were selected for experiments. The midgut undergoes a variety of morphological changes as the embryo develops, starting as a 'sphere' (~stage 13) and gradually decondensing to form segments (~stage 15) until the full convoluted system forms (stage 17). *Drosophila* midguts are visible under the UV light of the fluorescent microscope, if the stock used has ubiquitously expressed actin, then the appropriate fluorescent filter can also be used (e.g. the 488nm filter for GFP conjugated actin). For figure 13 (exploring the role of the JNK pathway), the GFP filter was used to confirm appropriate developmental stage since the fluorescence disperses across the embryo over the course of development. Hemocytes can also be used in the process of staging embryos, hemocytes migrate through the *Drosophila* embryo during embryonic development, originating from the anterior head mesoderm (Weavers & Wood, 2016) (Figure 3A & B). The hemocytes then follow a well-defined route at specific embryonic stages, beginning in the head mesoderm (stage 10) and first migrating along the anterior-posterior axis (stage 12/13) followed by lateral migration to form three distinct ventral row (stage 14/15) until evenly distributed across the whole embryo (stage 17) (Tepass et al., 1994).

2.3 Wounding *Drosophila* Embryos

Embryos of the appropriate developmental stage (e.g. stage 14/15) and with the correct transgenes (e.g. fluorophores) were selected using a Leica fluorescent stereoscope (as described above). These embryos were mounted on a glass slide with double-sided scotch tape in 10S Voltalef oil (VWR) (Figure 3C). A nitrogen-pumped Micropoint ablation laser (Andor Technologies) at 435nm (Weavers et al., 2019) was used to induce wounds in the epithelium of *Drosophila* embryos using a 63X oil immersion lens (Figure 3D).

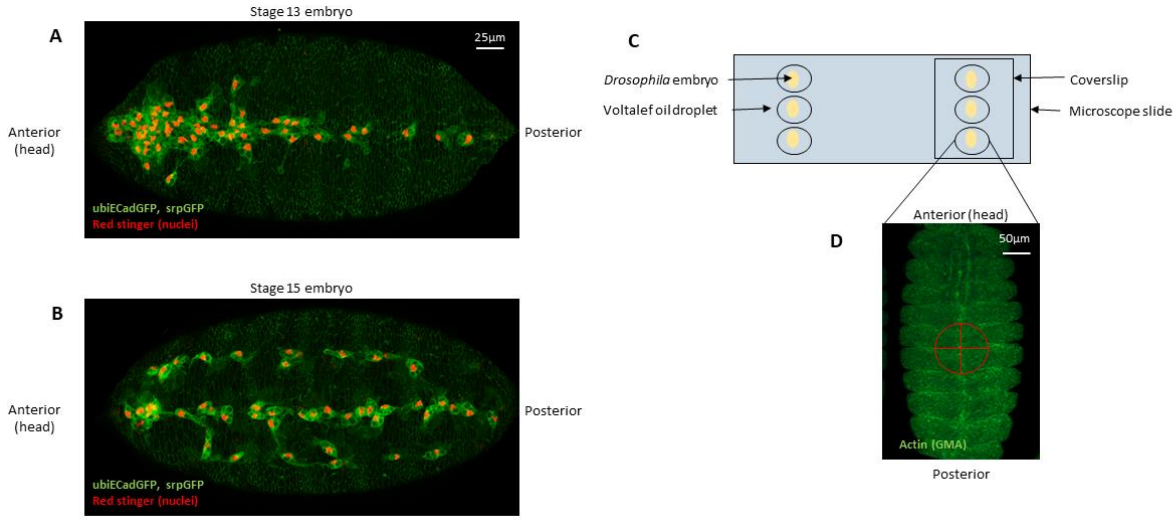

Figure 3: **Method of wounding and selecting appropriately staged embryos.** (A & B) Stage 13 (A) and stage 15 (B) unwounded *ubiECadGFP, srp>GFP; srpH2A3mch x w67* embryos showing hemocyte dispersion away from the head at the anterior end of the embryo (stage 13). (C) Schematic showing method of mounting *Drosophila* embryos for embryo selection and wounding. (D) Fluorescent microscope image of a *Drosophila* embryo mounted in an anterior to posterior orientation ready for wounding, red crosshair demonstrating where a wound would be induced via laser ablation.

2.4 Fixing Unwounded *Drosophila* Embryos

Embryos were collected from overnight apple juice plates, dechorionated using 50% bleach and rinsed using distilled water. The dechorionated embryos were fixed in a 1:1 mixture of heptane and 4% paraformaldehyde (PFA) diluted in 1x phosphate buffered saline (PBS) for 20 minutes on the rotor. The purpose of the heptane is to allow the fix (PFA) to penetrate the hydrophobic vitelline membrane by puncturing holes in the membrane. The PFA was discarded, and the fixed embryos were vigorously shaken in a 1:1 mixture of heptane and methanol for 30 seconds to fully dissolve the remainder of the vitelline membrane. The embryos were then rinsed three times in methanol before storage in methanol at -20^{o}C.

2.5 Fixing Wounded *Drosophila* Embryos

The appropriately staged embryos were selected, mounted, and wounded as described above in section 2.2.1. The wounded embryos were stored at 25^{o}C for 20 minutes to allow for the wound to

begin the healing process and form the actin cable; before transfer from the glass slide to an Eppendorf containing the 1:1 heptane:methanol mixture. These embryos then followed the same procedure as the unwounded embryos with the exception of devitillinisation. The fixed wounded embryos were transferred to a glass slide with double-sided scotch tape with a drop of PBS to prevent dehydration. A tungsten needle was used to remove the vitelline membrane by hand rather than the chemical (methanol-based) method described above. The devitellinised embryos were collected from the slide using a glass pipette, rinsed in methanol, and stored at -20^{o}C.

2.6 Immunostaining Fixed Embryos

Immunostaining was carried out on fixed embryos, both wounded and unwounded, after using the fixing methods described above. The following primary antibodies were used: anti-polyADP ribose (anti-PAR) (10H, mouse, Abcam, 1:200), anti-GFP (goat, Abcam, 1:200) and anti-pH2AvD (rabbit, Gene Tex, 1:300) (DNA damage reporter). The methanol was removed from the fixed embryos and the embryos were rehydrated and blocked using a mixture of 1x PBS, 0.3% Triton-X detergent and 0.5% bovine serum albumin (BSA) (PBS-TX-BSA solution) for a total of one hour at room temperature. The primary antibodies were diluted to the appropriate concentrations (described above) in PBS-TX-BSA solution and were added to the embryos before overnight incubation at 4^{o}C. Negative controls were treated in the same manner with the exception that anti-PAR primary was not added to the embryos. The following day the primary antibody solution was removed, and the embryos were blocked for a total of 30 minutes in PBS-TX-BSA solution. An additional blocking stage using horse serum (Invitrogen, 1:50) diluted in PBS-TX-BSA was then carried out for another 30 minutes. The primary anti-PAR antibody was amplified using biotinylated anti-mouse (horse, Vector Lab, 1:200) for one hour before 30 minutes of blocking with PBS-TX-BSA. The following secondary antibodies were used, Streptavidin-conjugated fluorophore Cy5 (Jackson Immuno Research, 1:200), anti-goat 488 (Jackson Immuno Research, 1:200), anti-rabbit 594 (Jackson Immuno Research, 1:200), and phalloidin (Invitrogen, 1:50). The secondary antibodies were diluted to the appropriate concentrations in PBS-TX-BSA and were added to the embryos before a one-hour incubation at room temperature. A final 30-minute PBS-TX-BSA blocking step was conducted before mounting the stained embryos on a glass slide in Moviol solution with a small amount of 1,4-Diazabicyclo2.2.2octane (Dabco, Sigma Aldrich) crystals. The immunostained, mounted embryos were stored at 4^{o}C and imaged within 1 week. Positive controls for the anti-polyADP ribose immunostaining were first exposed to 10-15 minutes of UV light using the GelDoc transilluminator to induce DNA damage before the normal (unwounded) embryo fixing procedure.

2.7 Annexin V and Sytox Staining of Live Embryos

Embryos were collected from overnight apple juice plates, dechorionated using 50% bleach and rinsed using distilled water. The dechorionated embryos were transferred to a small glass vial containing a 1:1 mixture of heptane and 1x PBS (250µL of each), 40µL/mL Annexin V 588/647 (Invitrogen) and 8µL/mL Sytox 631 (Invitrogen) and were placed on the rotor at 4 rpm for 7 minutes. The heptane was removed from the vial and the embryos were washed with 1x PBS before transfer (with as little liquid as possible) to a plastic dish containing 10S Voltalef oil to prevent dehydration during the mounting process. The stained embryos were mounted and wounded as normal and were imaged immediately.

2.8 Acridine Orange Staining of Live Embryos

A similar protocol to that used for Annexin V and Sytox staining was used (as described in section 2.3.4). The dechorionated embryos were transferred to a small glass vial containing a 1:1 mixture of heptane and 1x PBS (250µL of each) plus 1µL of Acridine Orange (AO) and were placed on the rotor at 4 rpm for 5 minutes. The heptane was removed, and embryos were washed in 1x PBS before transfer to 10S Voltalef oil followed by mounting, wounding, and imaging.

2.9 Confocal Imaging of Live and Fixed Samples

Imaging was carried out using a Leica TCS SP8 confocal microscope on the 40X and 63X oil objectives with standard settings for both fixed and live samples. Z-slices were taken every 2µm for the majority of confocal images, for results section 4.4 (*parp* knockdown in hemocytes), z-slices were taken every 1µm to ensure all hemocytes were imaged appropriately. Z-stacks were taken from the top of the epithelium (epithelium just in focus) for all movies/images. The lower maximum differed between experiments and the tissues of interest, for example when investigating wound closure, the lower maximum of the z-stack was set to just below the visible edges of the wound to account for the embryo moving slightly between planes as it underwent the healing process. If looking at hemocyte behaviour, the lower maximum is set lower to ensure all hemocyte populations of (epithelial hemocytes) are in frame throughout the movie. Maximum z-projections were then produced from the confocal images/movies using Fiji, the size of these varied between groups of experiments. For example, to quantify PARylation within the epithelium a maximum z-projection of 5 z-slices (each of 2µm) was used. However, when analysing the behaviour of individual hemocytes deeper in the embryo, a maximum projection of only two slices was used.

The confocal microscope was set up with the appropriate setting prior to imaging including of live, wounded samples. The embryos were wounded as described in methods 2.3 and were then transferred to the confocal microscope for imaging. Singular embryos could be imaged within 5

minutes of wounding, however, if multiple embryos were mounted on the same slide (on average eight embryos mounted per session) then this time frame could be increased to a maximum of 20 minutes. This time delay resulted largely from the requirement of first marking the position and then setting up individual z-stacks for each mounted embryo before any imaging could take place. The length of each movie and of the intervals between images is described in the appropriate results sections.

2.10 Data Processing

Quantification of wound size, fluorescence levels, and area were carried out using ImageJ/Fiji (NIH). To quantify wound size, either the straight line tool or the freehand line, were used to measure the diameter or area of the wound, respectively. The length/area of the line/section was then recorded appropriately. For wounded movies, the diameter/area was measured at the first time point and repeated measurements were then taken at set intervals across the length of the movie (precise timings given in results sections). To quantify fluorescence of the whole embryo/area of interest, the freehand section tool was used to measure either the mean or intensity density of the area as required. The mean intensity was utilised when looking at the overall fluorescence of the embryo, for example when analysing anti-PAR staining for unwounded and wounded embryos. Intensity density was used when patterns of fluorescence vary across a large area, for example acridine orange staining. To quantify fluorescence at the wound edge (results 3.4 and 3.4), the freehand line tool was used with a line width of two to measure mean fluorescence directly at the edge of the wound. Graphs and the statistical analysis of these were carried out in GraphPad Prism. Data presented within the graphs is shown as mean ± SEM. Appropriate statistical tests were used including the Holm-Sidak multiple comparisons and the Mann-Whitney test, details of the exact test used is listed in the figure description. Statistical significance was represented as follows: no significance (ns), $p>0.05$, *$p<0.05$, **$p<0.01$, ***$p<0.001$, and ****$p<0.00001$. All figures were produced using Adobe Illustrator.

2.11 Protein Extraction from *Drosophila* Embryos

Embryos were collected from overnight apple juice plates, dechorionated using 50% bleach and rinsed using distilled water. Embryos of the appropriate developmental stage (e.g. stage 14/15) and with the correct transgenes (e.g. fluorophores) were selected using a Leica fluorescent stereoscope, these were collected in a second mesh basket. The selected dechorionated embryos (n=50) were washed in a mixture of 0.15M sodium chloride (NaCl) and 0.05% Triton X. These embryos were then transferred to an Eppendorf with RIPA buffer containing HALT protease and phosphatase inhibitor cocktail (1:100 dilution), a plastic pestle was then used to mechanically breakdown the embryos.

The ground tissue (in RIPA buffer) was incubated at 4°C on a rotor for 30 minutes and then was centrifuged at 13,000 rpm at 4°C for a further 30 minutes. The supernatant was carefully removed from the samples and transferred to a clean Eppendorf for storage at -80°C until required. For each condition two biological replicates were taken and then two samples were taken from each extraction for use in quantification.

2.12 Quantification of Protein Concentration

Eight bovine serum albumin (BSA) samples were prepared of the following concentrations: 40 µg/ml, 20 µg/ml, 10 µg/ml, 5 µg/ml, 2.5µg/ml, 1 µg/ml, 0.5 µg/ml, and 0 µg/ml using RIPA as the diluent. The working reagent was prepared in the following ratio 25 MA : 24 MB : 1 MC, volumes were calculated according to the number of samples required. The unknown protein samples were prepared with 10µl of sample in 490µl of RIPA alongside duplicate 500µl samples of the BSA standards. Working reagent was added to the Eppendorfs in a 1:1 ratio and thoroughly mixed using a vortex before incubating all samples at 60°C for 60 minutes. Samples were allowed to cool to room temperature (no longer than 15 minutes to prevent sample degradation) and were then transferred to cuvettes for absorbance measurements. The spectrophotometer was set to 562nm and zeroed using a blank of distilled water. All absorbance measurements of the samples were taken within 10 minutes. The absorbances of the BSA samples were plotted on a standard curve, allowing for the unknown protein concentrations to be calculated. The mean absorbance was for the two samples was first calculated, followed by correction against the standard curve. The protein concentration in 1ml of liquid could then be calculated (µg/ml) using the equation of the line for the standard curve. This concentration could then be converted to the actual number of micrograms (µg) of protein present within the original sample. The final step then required calculating how much protein was left in the original sample after removing two sample replicates to give the final amount available for any proteomic experimentation. To do this, the calculated protein amounts (µg) for the genotype/condition of interest were combined to give the total amount of protein in the original extracted samples. This was then divided by two hundred to give a total concentration in the original 200 µl samples (two 100 µl samples). Finally, this concentration was multiplied by 160 to account for the 40 µl (two samples taken from both biological replicates) that was removed for quantification.

Chapter 3 (Results I): Characterising the Role of PARylation During Acute Wound Repair

3.1 Basal PARylation Levels Are Low in the Unwounded Epithelium and Hemocytes of *Drosophila* Embryos

The key aim of this study was to explore the role of Parp (and subsequent PARylation) following wounding to the epithelium of *Drosophila* embryos. Firstly, I needed to assess the basal levels of Parp activity (i.e. PARylation) in the unwounded epithelium, and to do this I performed immunostaining of fixed embryos using an antibody that specifically recognises PAR (see Materials and Methods).

PARylation was indeed visible at low levels throughout the epithelium of unwounded embryos (Figure 4A); PAR levels were then quantified by assessing the mean fluorescent intensity (see Methods for further details). A negative control was included, these embryos were treated in the same manner as the other samples, with the exception that the primary anti-PAR antibody was not added during the immunostaining procedure to enable the detection of any background levels of fluorescence (Figure 4B). The anti-PAR staining for these embryos was quantified and subtracted from the raw values of all other conditions to remove any background staining. For a positive control, unwounded embryos were exposed to UV radiation (see Methods for details) in an attempt to induce DNA damage and ultimately increase PARylation levels (Figure 4C). These embryos exhibited a significant increase in anti-PAR staining compared to wild-type control embryos (Figure 4C), confirming that radiation-induced DNA strand breaks did indeed cause an increase in PARylation. This suggests that the staining observed within the wild-type unwounded embryos is specific for PAR and PARylation is present throughout the embryo even when unwounded albeit at low levels (Figure 4E).

The *Drosophila* embryos used above for Figure 4A-D were transgenic and employed the Gal4-UAS system to label the epithelium with GFP-tagged actin. These embryos carried a ubiquitously expressed Gal4 driver (called daughterless-Gal4) which is able to facilitate genetic manipulation via the Gal4-UAS system (Elliot & Brand, 2008). Since *parp* is the gene of interest for this study, a *Drosophila* stock carrying a UAS-*parp* RNAi construct was crossed to this stock, promoting the knockdown of *parp* in all embryonic tissues; this experiment enabled us to test the efficiency of the RNAi in reducing PARylation. Anti-PAR staining was significantly decreased in these embryos following RNAi-induced *parp* knockdown compared to the wild-type control embryos (Figure 4D & E). Comparisons of mean fluorescent intensity for each of the three experimental conditions (unwounded control, UV-exposed and *parp* RNAi) confirmed that PARylation is detectable in

unwounded embryos, is increased following DNA damage, and the *parp* RNAi stock selected is efficient at reducing PARylation (Figure 4E).

I next assessed levels of PARylation in other *Drosophila* tissues, aside from the epithelium. For this, I utilised *Drosophila* embryos which had both the epithelium and the *Drosophila* innate immune cells (termed hemocytes) labelled with GFP-tagged E-cadherin (to mark adherens junctions) and serpent-Gal4 driven (hemocyte-specific) expression of cytoplasmic GFP and nuclear RFP (Figure 4F). These embryos were stained using the same anti-PAR antibody described above and were imaged using identical confocal settings (Figure 4F-H). The positive control embryos were exposed to UV radiation in the same manner described above to induce DNA damage (Figure 4G). Firstly, the levels of PARylation in the hemocytes of unwounded embryos were quantified (Figure 4I). Hemocytes within control embryos (Figure 4F) had relatively low levels of anti-PAR staining (Figure 4I) in unwounded conditions. Exposure to UV light (positive control) significantly increased the levels of anti-PAR staining (Figure 4G & I), similar to the increase observed within the unwounded epithelium. A negative control was also included for the hemocyte stain (in the same manner to above) and was subtracted from all values to assess the staining observed is above that of background fluorescence. Knocking down *parp* via RNAi also significantly decreased levels of anti-PAR staining (Figure 4H & I) compared to control embryos.

Hemocytes disperse through the embryo during embryonic development, using well-known migratory patterns (Tepass et al., 1994); this stereotypical immune cell distribution (as well as midgut morphology) could be used to carefully stage the immunostained embryos (Wood et al., 2002). The purpose of this staging was to assess whether any changes in levels of PARylation occur within the epithelium or hemocytes across different developmental stages of embryogenesis. The embryos were split into three groups according to their developmental stage: early stages (stage 13 of embryogenesis), mid (stages 14 and 15) or late (stages 16 and 17). The previously quantified hemocyte PARylation levels (Figure 4I) could then be re-plotted according to the different embryonic stages.

The first comparison to be made was hemocyte PARylation levels across embryonic development in wild-type control embryos (Figure 4J). Hemocyte PARylation increased throughout development with the most significant change between mid and late stage embryos, perhaps due to increased sources of endogenous stress. As previously mentioned, UV-exposure was utilised to (theoretically) induce DNA damage and increased PARylation, providing the positive control for these experiments. Comparisons could then be drawn between respective PARylation levels at different developmental stages for control and UV-exposed embryos (Figure 4K). The embryos were slightly younger for the UV exposure hence why there is no comparison between late-stage embryos. Interestingly, UV

exposure significantly increased hemocyte PARylation in early stage embryos, however, mid stage embryos exhibited a decrease in anti-PAR staining (Figure 4K).

The hemocytes in this *Drosophila* stock also expressed a Gal4 driver which is able to facilitate genetic manipulation via the Gal4-UAS system. Since *parp* is the gene of interest for this study, a *Drosophila* stock carrying a UAS-*parp* RNAi construct was crossed to the srp-Gal4 stock, promoting the knockdown of *parp* specifically in the hemocytes via the serpent driver. The effectiveness of this RNAi-driven *parp* knockdown could then be assessed across the various embryonic developmental stages, as described above. Anti-PAR staining was significantly decreased in hemocytes across mid and late embryonic stages when using the *parp* RNAi stock compared to the wild-type controls (Figure 4H and 3L). The early-stage embryos (stage 13) do not exhibit a significant reduction in PAR, perhaps as the serpent driver is only weakly expressed in these early stages and does not become strongly expressed until later in development. Following on from this, the *parp* knockdown appears to be most effective from the mid stage of embryogenesis onwards, once the srp-Gal4 driver is robustly active. The most significant difference is observed in the later stage embryos (stage 16/17) due to the much higher levels of PARylation in the unwounded controls (Figure 4L), likely a result of an accumulation of DNA damage over embryonic development. However, these embryos are too old for most other experimentation since they will soon hatch into larvae. As a result of these combined findings, mid stage embryos (stage 14/15) will be selected for all experiments moving forward.

In summary these data suggest that PARylation levels increase with the developmental stage of the embryo, even in unwounded conditions. As seen in humans and other mammalian species, oxidative damage often accumulates within an organism's tissues as it ages due to increased sources of ROS and the reduced capacity to handle oxidative stress (Tran et al., 2019). ROS is produced via many different mechanisms, including via mitochondrial respiration required for energy production. This could be the reasoning behind the observed increase in PARylation, as older embryos might have greater energetic requirements leading to an increase in the production of ROS and levels of oxidative stress and accumulated cellular damage. Moreover, hemocytes clear apoptotic corpses via phagocytosis and during this process the hemocytes produce ROS via the action of NADPH oxidases to help breakdown the corpses. Older embryos have greater numbers of engulfed corpses per hemocyte (Weavers et al., 2016) which would also increase the concentration of ROS and generate higher levels of oxidative stress within the embryo, perhaps driving the increased PARylation within older staged hemocytes.

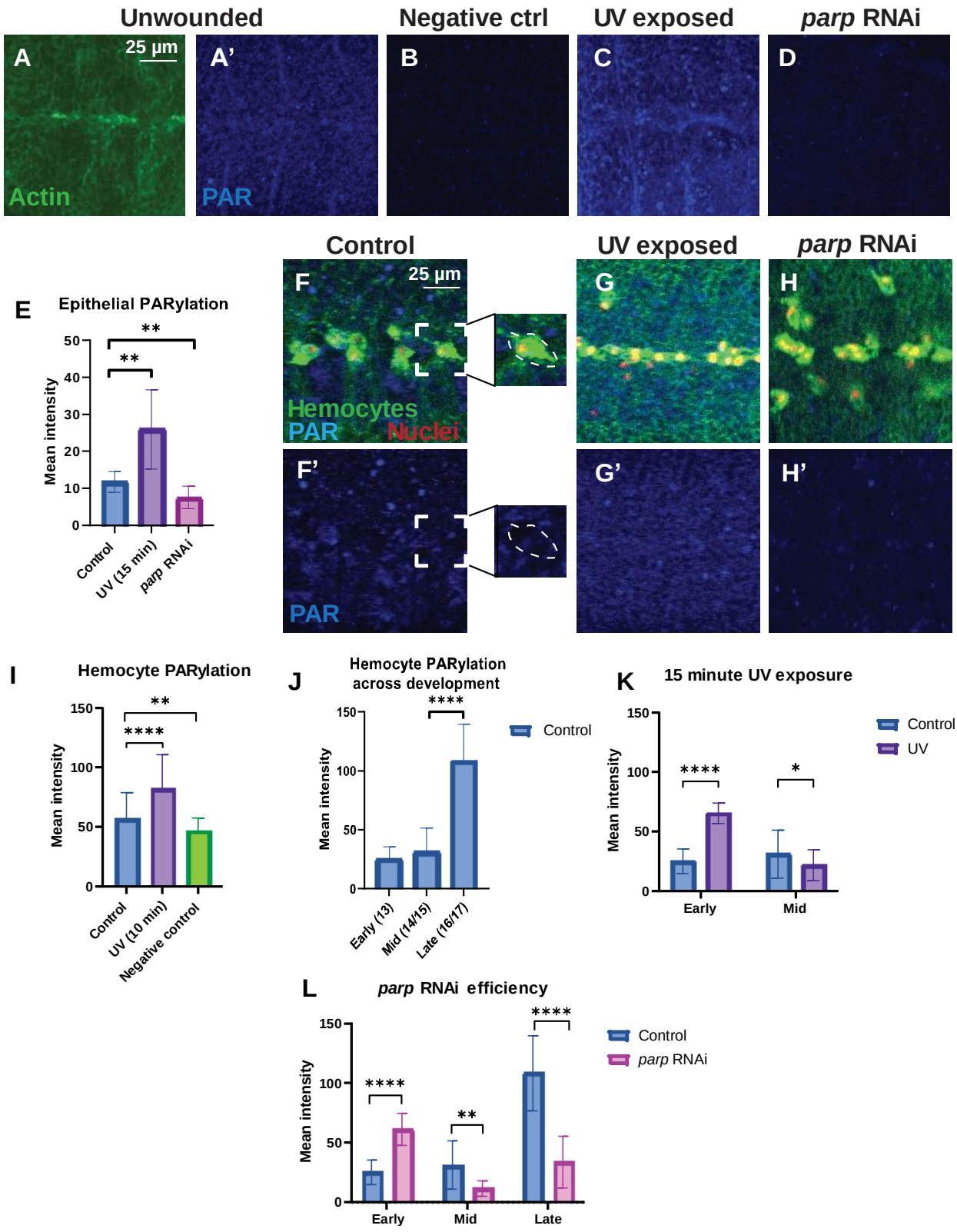

Figure 4: **PARylation is present throughout unwounded *Drosophila* embryos in both the epithelium and the hemocytes.** (A-D) Maximum z-projections of confocal images of unwounded embryos stained with anti-PAR antibody, under various conditions: control *da>GMA x w67* (A), negative control (*da>GMA x w67)* without addition of anti-PAR (B), UV-exposed controls (C), and *parp* knockdown *da>GMA x parp-RNAi* (D). Epithelium (actin) labelled in green (A) and anti-PAR staining in blue (A'). (E) Mean intensity quantified for control, UV-exposed and *parp*-RNAi knockdown embryos (following subtraction of average negative control fluorescence). (F-H') Unwounded embryos stained with anti-PAR antibody (blue), control *ECadGFP, srp>GFP x w67* (F), UV exposed controls (G), *parp* knockdown *srp>GFP/UAS>parp RNAi* (H). (I-L) Comparisons of mean intensity of anti-PAR staining; general staining for each condition, negative control embryos lack primary anti-PAR (I), changes in hemocyte PARylation with embryonic stage, background subtracted (J), changes in UV-induced PARylation with embryonic stage, background subtracted (K), efficiency of RNA-induced *parp* knockdown within hemocytes, background subtracted (L). Statistical significance measured via Holm-Sidak method using Prism (n = 6 embryos per condition).

3.2 Epithelial Levels of PARylation Increase Following Wounding in *Drosophila*

The above experiments (Results 3.1) explored the basal levels of PARylation in unwounded embryos in both the epithelium and the hemocytes. One of the key aims of this project is to understand the role of Parp (and PARylation) in epithelial wound healing and therefore the next step was to analyse any potential change in the epithelial level of PARylation following wounding. Using identical confocal settings to the previous experiments, unwounded and wounded embryos were imaged and epithelial PARylation quantified (Figure 5). Interestingly, wounding significantly increased epithelial levels of anti-PAR staining ($p<0.0001$) (Figure 5 A-B, quantified in Figure 5E) in wild-type control embryos. The strongest anti-PAR staining appeared around the wound boundaries (Figure 5B), potentially near the site at which actin accumulates for the contractile actin cable. This data suggests that *parp* is indeed active within the epithelium of *Drosophila* embryos and the significant increase of PARylation observed may indicate a key role within the wounded epithelium.

I next assessed embryos lacking *parp* and explored the impact of wounding on their epithelial PARylation levels. Results Section 3.1 confirmed the efficiency of RNAi-induced *parp* knockdown within the epithelium of unwounded embryos. Using the same *Drosophila* stock (containing a ubiquitous Gal4driver), *parp* was knocked down across the entire embryo, including the epithelium (Figure 5C-D). *Daughterless-Gal4* used for these experiments ensures gene knockdown across the entire embryo, other drivers such as *engrailed-Gal4* would cause segment-specific knockdown (FlyBase, 2019). Once again wounding significantly increased PARylation levels (Figure 5D) compared to the unwounded *parp* RNAi controls (Figure 5C), as well as the unwounded wild-type controls (Figure 5A). Despite the major increase in PARylation, levels still remained lower than those observed for the wounded controls (Figure 5E), although this reduction was not statistically significant and should ideally be repeated in the future.

Another interesting observation from the wounded immunostain images is the lack of visible actin cable at the edge of the *parp* RNAi wounds. The wild-type controls have a strong cable encompassing the wound circumference as would be expected (Figure 5B), however, this is not the case for the *parp* knockdown wounds (Figure 5D). The embryos used for these experiments were fixed 20 minutes post-wounding to allow for the healing process to begin (including actin cable formation and upregulation of transcription factors etc). This potential actin cable impairment will be explored in greater detail in the following results sections.

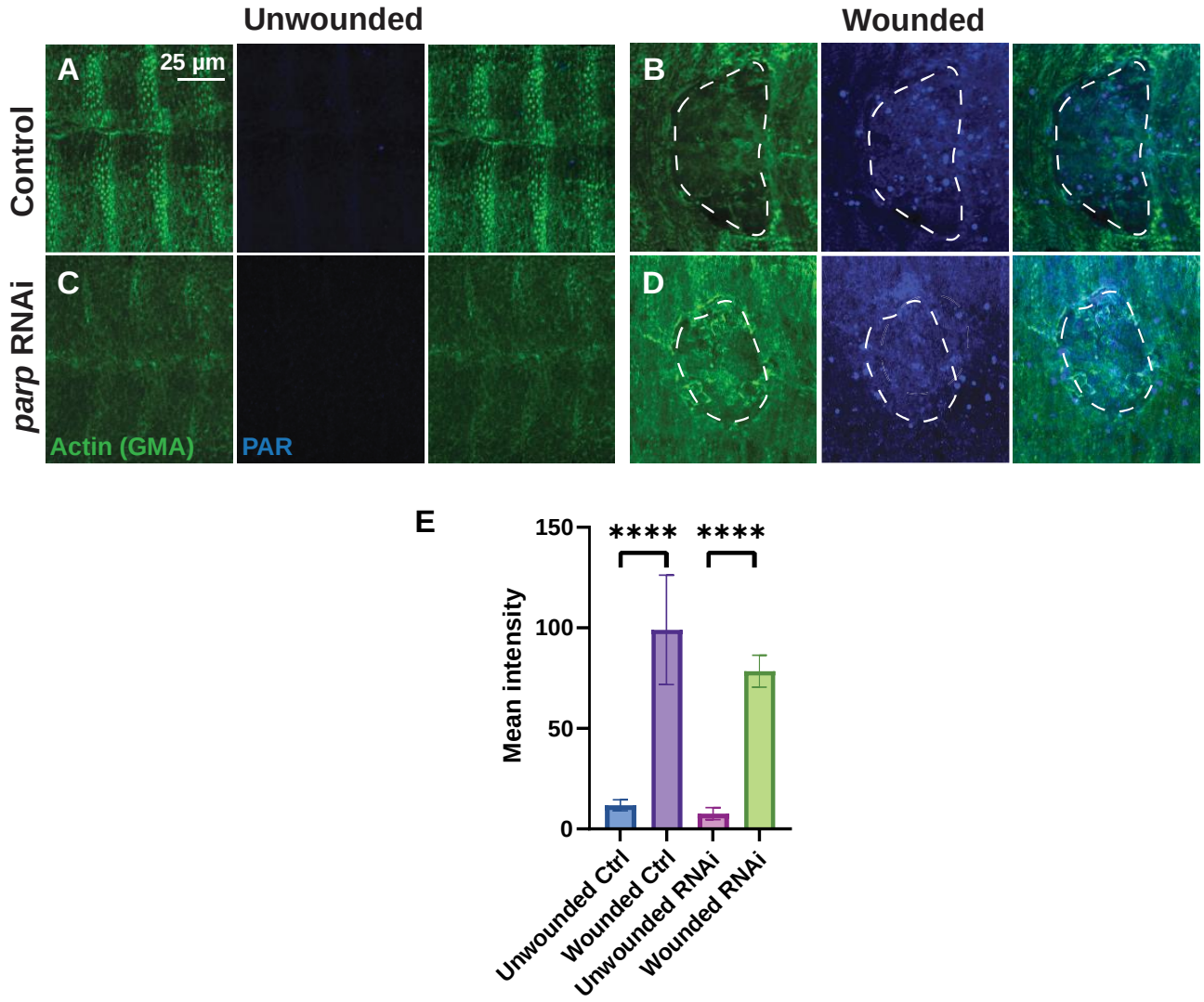

Figure 5: **Laser-induced wounding of *Drosophila* embryos triggers an increase in PARylation in the epithelium.** (A-D) Confocal images of unwounded (A & C) and wounded (B & D) embryos, both wild-type (using *daughterless* driver) *da>GMA* (A & B) and *parp* knockdown *da>GMA/UAS>parp RNAi* (C & D). Epithelium (green) labelled with GFP-tagged actin (GMA) stained with anti-GFP and PARylation (blue) stained with anti-PAR 10H, single channel images and overlay shown. White dashed line represents the wound boundary. (E) Quantification comparing mean intensity of epithelial anti-PAR fluorescence between unwounded and wounded embryos for both control and *parp*-RNAi. Wounding significantly ($p<0.00001$) increases epithelial PARylation in both wild-type and *parp* knockdown embryos. Statistical significance of fluorescence measured via Holm-Sidak method using Prism between unwounded and wounded embryos (n = 6 embryos per condition).

3.3 *Parp* Knockdown Decreases the Rate of Epithelial Wound Healing Within *Drosophila*

To investigate the role of PARylation during epithelial tissue repair, *parp* expression was inhibited within *Drosophila* embryos using a ubiquitous driver (called daughterless-Gal4) and two independent *parp* RNAi lines. Since the daughterless gene is ubiquitously expressed (Weavers et al., 2016), *parp* knockdown is effective across the whole embryo. *Drosophila* only possess one *parp* gene (with three isoforms) and both RNAi lines have been shown to target all three isoforms, as published on the TRiP RNAi collection website. Strikingly, RNAi-mediated knockdown of *parp* significantly slowed

down the rate of wound closure within *Drosophila* embryos using both independent RNAi lines (Figure 6A-C).

The wounded embryos were first imaged 20 minutes post-wounding and then every 5 minutes until 120 minutes post-wounding. Wounds with a starting diameter in the range of 60-90 µm were chosen for analysis to ensure the appropriate healing mechanisms could be analysed during the 2-hour time frame. Control wounds healed efficiently, as expected at a relatively constant rate (Figure 6C), with the smaller wounds (60-65µm) fully resolving during imaging. On the other hand, *parp* knockdown wounds healed at a significantly slower rate with the most notable differences visible at around one-hour post-wounding (Figure 6A-C).

The gradient of the line for wound closure (Figure 6C) was then quantified (Figure 6D) to compare the 'rate of wound closure' across the various time points. There was fluctuation in the wound closure rate over the course of healing for each of the three conditions, including the control that dips at 80-100 minutes. Interestingly, the RNAi wounds (using stock #57265) exhibited a negative rate of closure during the first 20-40 minutes post-wounding, confirming the initial increase in wound diameter that was previously observed by eye (Figure 6B) and during quantification (5C). Similarly, the RNAi wounds using the #34888 stock exhibited a delay in wound repair during the first 80 minutes post-injury, followed by a rapid increase in the rate of closure in the final 40 minutes, which is opposite to the trend seen for the controls.

In addition to wound diameter, the wound area was also quantified for a clearer picture of how the whole wound changes over time (Figure 6E). A similar trend to that seen for wound diameter was observed, with the wound increasing in area in the first 40 minutes post-wounding. Both *parp* RNAi lines (#57265 and #34888) exhibited very similar closure phenotypes, however #57265 had a more exaggerated increase in wound area compared to the control (Figure 6E). Since both the wound closure in terms of diameter and area were decreased for *parp* RNAi, and most significantly for stock #57265, this is the stock that is used for the remainder of *parp*-related experiments in this study.

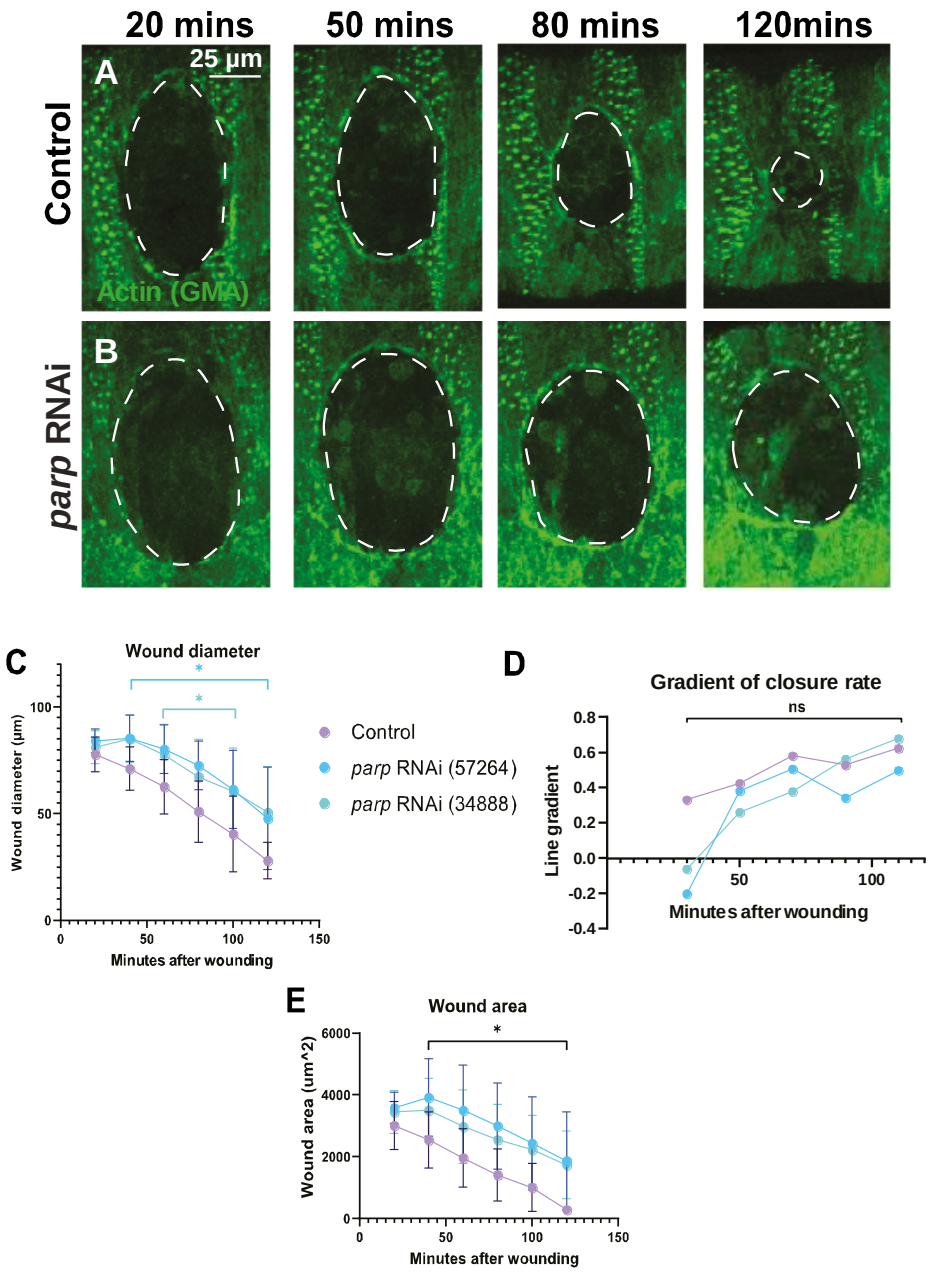

Figure 6: **Knocking down *parp* decreases the rate at which a laser-induced wound in the epithelium (green) is able to close.** (A&B) Snapshots at given time points following wound induction (20, 40, 60, 120 minutes) for wild-type control (*daughterless* driver) *da>GMA* (A) and *parp* knockdown *da>GMA/UAS>parp RNAi* (B). White dashed line outlines the wound edge. (C-E) Graphs comparing changes in wound diameter (C), line gradient of wound diameter graph (central time point denoted on x-axis) (D) and wound area (E) for each genotype. White dashed line denotes the wound boundary. Statistical significance measured via Holm-Sidak method using Prism between wound diameter of each of the three conditions at each given time point (n = 8 embryos per condition).

3.4 *Parp* is Required for Efficient Actin Cable Formation During Tissue Repair

As previously mentioned, both mammalian and *Drosophila* embryonic wounds exhibit rapid and robust actin cable formation at the leading edge of the wound (Martin & Lewis, 1992). In a healthy, acute healing wound, this process is rapid with a cable appearing within two minutes post-wound formation (Redd et al., 2004). However, in this study *parp* RNAi wounds appeared to have a delay in actin cable formation when compared to control wounds (Figure 7), as visualised through the use

of a GFP-tagged Moesin construct that labels the endogenous actin cytoskeleton (GFP-tagged actin binding domain of Moesin, 'GMA').

All previous movies have focussed on the wound healing process from 20 minutes post wound induction, however, since the actin cable formation at the wound leading edge is known to begin within the first few minutes following wounding (in a healthy acute wound) I decided to take movies starting much sooner following injury (see Material and methods). Here, laser-induced wounds were imaged singularly, allowing for movies to be taken within 5 minutes of wounding to ensure the rapid cable formation was captured. Timelapse images were then taken of wound closure progression every 2.5 minutes to provide a comprehensive analysis of wound closure and actin cable formation. Actin fluorescence directly at the wound edge was quantified at regular 5-minute intervals, until 30-minutes post-wounding. Control wounds quickly assembled an actin cable from 5-minutes post-wounding and a fully formed, thick cable was visible by 30 minutes (Figure 7A). On the other hand, *parp* RNAi wounds encountered issues throughout actin cable formation with uneven edges encompassing the wound edge (Figure 7B). Although both control and *parp* RNAi wounds increased the relative level of actin fluorescence at the wound edge over the 25-minute movie, the actin cable fluorescence within *parp* RNAi embryos was significantly lower throughout the entire timelapse movie compared to the control (Figure 7C).

Further analysis of this live-imaging data suggested some interesting differences between control and *parp* RNAi wounds. In control embryos, the wounds showed higher levels of actin at the wound edge which accumulated over time until the whole wound edge was encompassed in a solid, bright cable. However, not only did the *parp* RNAi wounds exhibit a delay in cable formation, but when the cable began to form, the behaviour was not as expected; in many cases, the actin cable began to form directly at the wound edge (as in controls), but it then moved further back so it is no longer situated at the leading edge (Figure 7B). In some cases, it appeared to correct itself and reformed back at the leading edge, whereas other times the actin accumulation (and wound contraction) both remained further back. Even when the actin cable is 'fully' formed, the *parp* RNAi wounds were dimmer (as quantified above) and appeared patchy.

Using the time-lapse imaging data (from Figure 6) I could also quantify actin cable fluorescence in the later stages of wound closure (Figure 7D-F). A similar trend was observed across these movies with *parp* RNAi wounded embryos exhibiting lower levels of actin fluorescence at the wound edge than controls (Figure 7D-F). However, these measurements were not statistically significant due to higher levels of variation quantified for the controls. When analysing these movies by eye, fewer structural impairments were visible, however, the cable itself appeared much dimmer and incomplete for *parp* RNAi embryos. This data confirms the previous observations of delayed actin cable

formation (Figure 7D-E) that *parp* knockdown significantly delays actin cable formation at the wound edge and may also alter its localisation (Figure 7).

This is not the first time that a weaker actin cable has been observed during this study, as mentioned in the previous section (Results 3.2, Figure 5). A dimmer actin cable was observed in wounded, fixed *parp* RNAi embryos compared to their control counterparts (Figure 5). These embryos were fixed approximately 20 minutes post-wounding and therefore should have in theory formed a thick, contractile actin cable. This can be seen in the wounded control embryos (Figure 5B), the cable may not appear as strongly as those visible during live imaging since the fixation process can impair staining. The *parp* RNAi embryos show the beginnings of cable formation, with minor actin accumulation visible at the top half of the wound (Figure 5D).

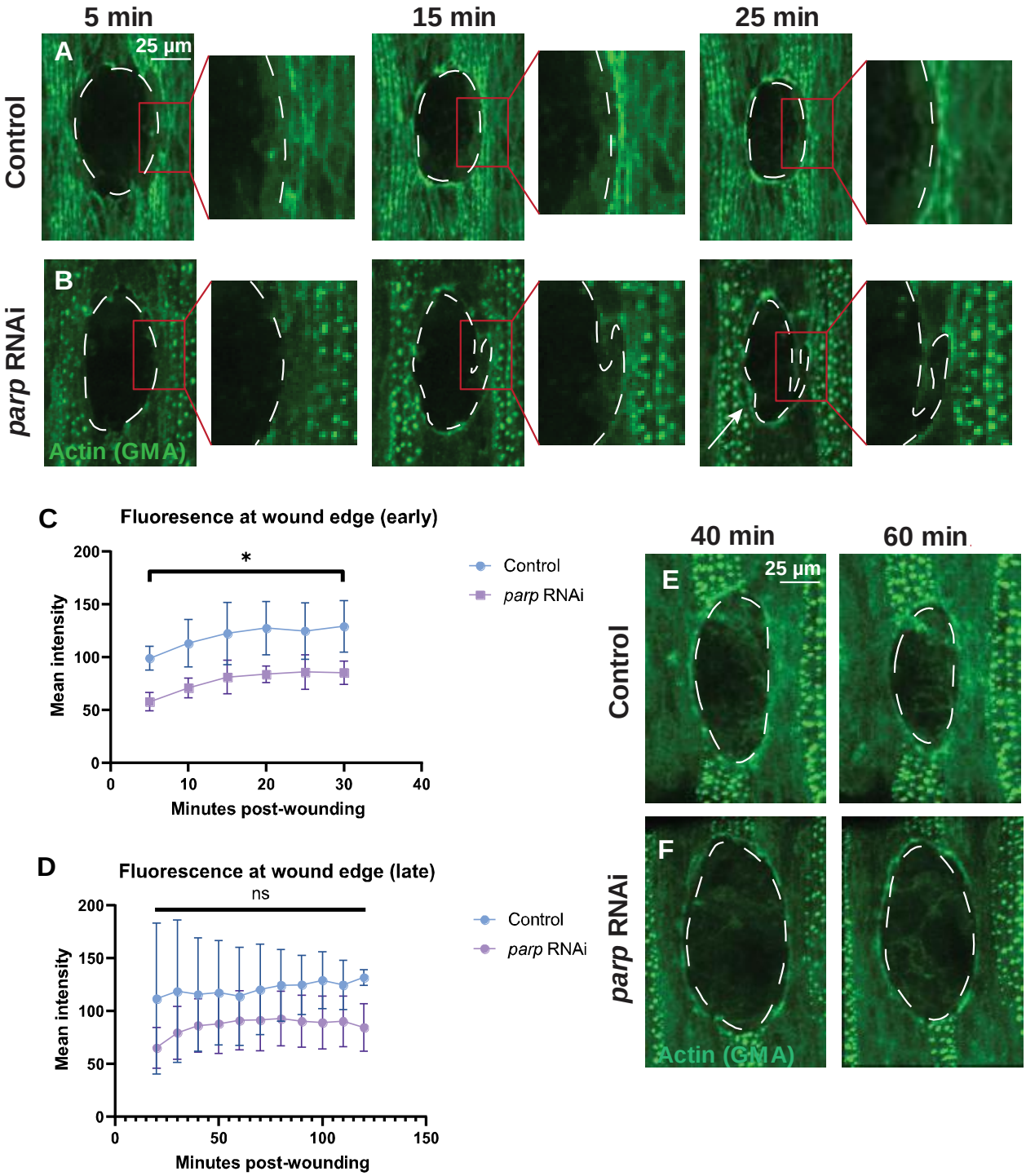

Figure 7: **Knocking down *parp* decreases the rate of actin cable formation (green) at the wound edge.** (A & B) Snapshots of wounded control *da>GMA x w67* (A) and *parp* knockdown *da>GMA/UAS>parp RNAi* (stock #57265) embryos at given time points (5, 15, 25 minutes). White dashed line outlines the wound edge/actin cable formation. White arrow highlights impaired cable. (C & D) Quantification of mean fluorescent intensity at the wound edge for 5-30 minutes (C) and 20-120 minutes post-wounding (D). (E & F) Confocal images of wounded control (E) and *parp* knockdown (F) embryos at 40 and 60 minutes post-wounding. Statistical significance measured via Holm-Sidak method using Prism between the fluorescent intensity (actin accumulation) at the wound edge for the two conditions at each given time point (n = 8 embryos per condition).

3.5 *Parg* Knockdown Also Delays Epithelial Wound Closure Rate

As previously discussed, PARG is the enzyme responsible for the removal (via hydrolysation) of PAR units from the target protein (or DNA) (Páhi et al., 2020). The main purpose of this removal is to prevent hyperactivation of the target proteins, particularly PARP1 itself. Since previous studies have shown hyperactivation of PARP1 to be detrimental to the healing process in diabetic mice models (Zhou et al., 2017), I was interested to explore the potential impact this may have on wounded *Drosophila* embryos. As with the *parp* knockdown, ubiquitously expressed daughterless-Gal4 was utilised to drive RNAi-mediated *parg* knockdown and inhibit the production of the Parg protein. To confirm the effectiveness of the knockdown, I immunostained unwounded embryos for PAR in the same manner used as for when testing *parp* RNAi efficiency (see Materials and Methods). Confocal images were taken for both control and *parg*-RNAi embryos immunostained with anti-PAR and mean fluorescent intensity of PAR staining in the epithelium was measured. Embryos were selected based on developmental stage (mid-embryogenesis, stages 14 and 15) to ensure that PARylation levels were representative of the embryos that would later be used for wound closure experiments. Appropriate orientation was also a necessity when imaging embryos to ensure the correct part of the epithelium was quantified. Both the control and *parg* knockdown embryos imaged are at stage 14 and mounted with the ventral epithelium in focus (Figure 8A &B). Using the chosen *parg* RNAi line, PAR levels were significantly higher than when compared to the control unwounded embryos (Figure 8C), once again confirming the appropriateness of this line for further knockdown experiments.

To determine whether Parg is required during embryonic wound repair, I analysed wound closure in control and *parg* RNAi embryos. Interestingly, a similar wound closure phenotype to the *parp* knockdown embryos was observed with a significant decrease in the rate of wound closure (Figure 8D-F). However, one key difference was that the *parg* knockdown did not appear to cause an initial increase in wound size that was previously observed with the *parp* RNAi embryos. Instead, the *parg* RNAi wounds very slowly began to close immediately following wounding (within 20 to 40 minutes post-wounding) and their closure rate appears significantly lower than controls. From 60 minutes onwards, the rate of closure of *parg* RNAi increased to a comparable rate to the wild-type embryos, this can be observed both in terms of the timelapse movies (Figure 8D &E) and the wound closure graph plotted (7F). To quantify wound closure rate more accurately, the gradient of the line between each timepoint was calculated (Figure 8G); the change in y-coordinates (wound diameter) was divided by the change in x-coordinates (minutes post-wounding). This suggested that the control wounds healed at a much more consistent rate with only minor fluctuations in the general trend. However, the rate of wound closure exhibited by *parg* knockdown wounds was initially much lower than that of controls, although this increases to more wild-type levels across the two-hour healing period (Figure 8G).

As described in Results 3.3, *parp* knockdown appeared to delay wound closure and negatively impacted the ability of the embryo to form an actin cable at the edge of the wound. Since *parg* knockdown also delayed wound closure at a similar rate to that of *parp*, I analysed actin cable formation in the first 30-minutes following laser-induced wound formation (Figure 8H-J). Embryos of both genotypes were wounded and imaged separately to facilitate movies within the first 5-minutes following wounding. Control embryos exhibited strong actin cable formation (as would be expected), with the entire wound encompassed by 15-minutes post-wounding (Figure 8H). Knocking down *parg* did not appear to have a major impact on actin cable accumulation at the wound edge (Figure 8I). Following quantification of integrated density, the *parg* RNAi embryos had comparable levels of wound edge actin fluorescence (labelled with GFP-tagged actin) to the control embryos immediately following wounding (within the first 10-minutes post-wounding) (Figure 8J). However, despite no significant differences early on in actin cable formation, there was a significant decline in actin cable fluorescent intensity 15-20 minutes post-wounding in *parg* RNAi wounds which was observed in all knockdown embryos (taken across multiple imaging sessions).

The two wounds depicted in Figure 8 are of very similar starting diameter (~60µm) to ensure accurate comparisons can be drawn between the control and *parg* RNAi embryos. Within these 25-minute snapshots of the initial stages of wound closure, the wild-type wound (Figure 8H) began to heal efficiently with a stereotypical oval shape. Although actin accumulation is partially visible in the first 5 minutes, by 15 minutes post-wounding, a solid actin cable is visible around the entirety of the wound edge perimeter. Another key observation from control wounds is that even though the wound begins with jagged edges (caused by laser-induced wounding), as the cable forms to draw the wound closed, the wound edges become smooth. Conversely, the *parg* knockdown wound (Figure 8I) forms the initial actin cable at the same rate as the control wound but it appears to exhibit much weaker fluorescence. By 15 minutes post-wounding, actin is visible around the whole wound edge perimeter but is significantly dimmer than the control counterpart ($p=0.00146$) (Figure 8J). This trend continues later on at 25 minutes post-wounding, where the actin cable accumulation (and mean fluorescent intensity) remains lower in the *parg* knockdown embryo.

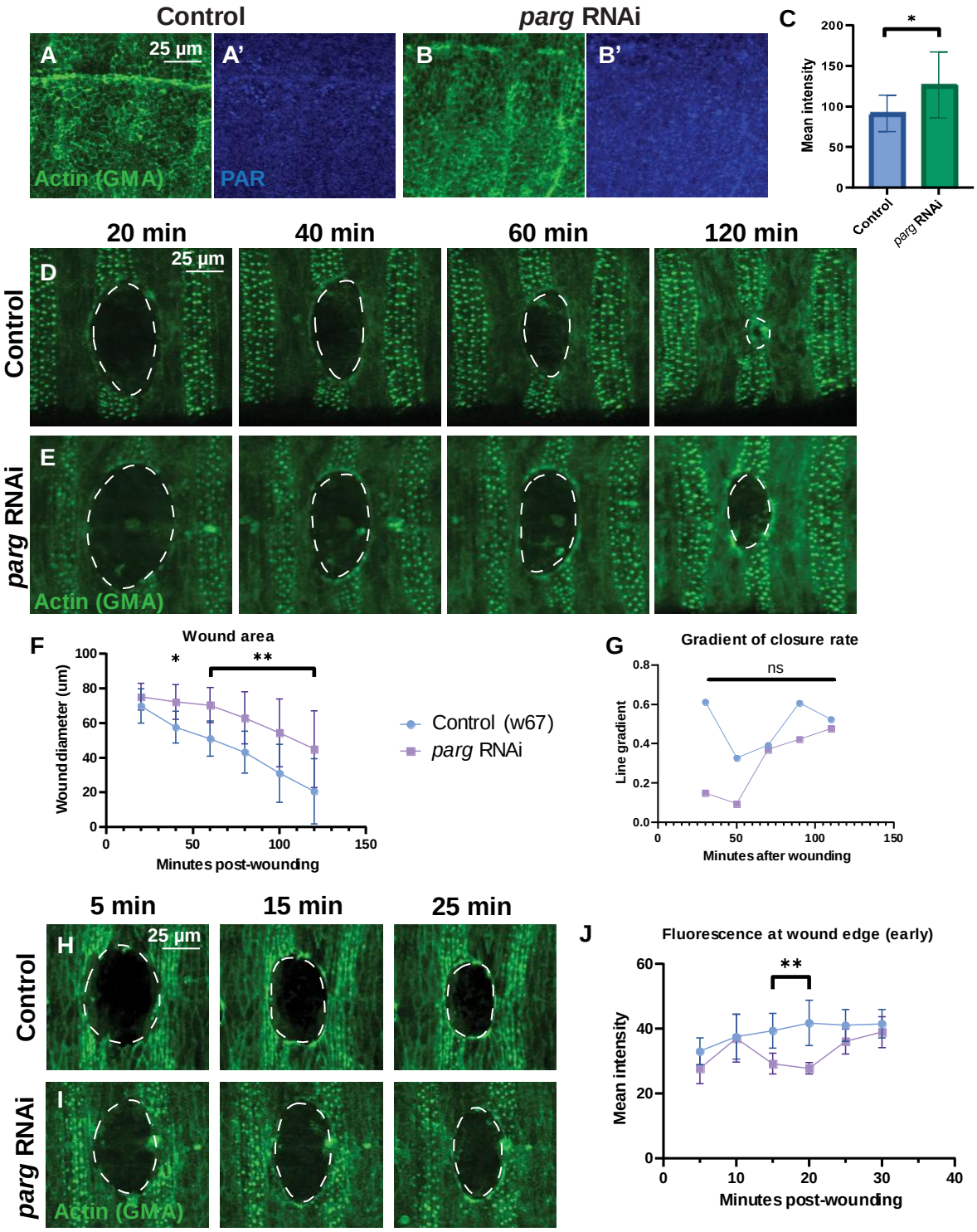

Figure 8: **Knocking down *parg* significantly increases PARylation levels and decreases the rate at which a laser-induced wound in the epithelium (green) is able to close.** (A-C) Anti-PAR staining (blue) on unwounded wild-type *da>GMA* (A) and *da>GMA/UAS>parg* RNAi (B), bar chart comparing PAR levels/mean fluorescent intensity (blue channel) between wild-type and *parg* RNAi unwounded embryos. (D-F) Wound closure comparisons between wild-type and *parg* RNAi embryos; snapshots of wound closure in wild-type (D) and *parg* RNAi (E) embryos at 20, 40, 60 and 120 minutes post-wounding, quantified and plotted on graph (F). (G) Table of calculated line gradients for each listed time point. (H-J) Actin cable formation of wounded wild-type and *parg* RNAi embryos; snapshots taken at 5, 15 and 25 minutes post-wounding (H & I), quantified and plotted on graph (J). Wound edge indicated by white dashed line. Statistical significance measured via Holm-Sidak method using Prism between the two conditions at each given time point (n = 8 embryos per condition).

3.6 Results I Summary

So far, this study has revealed a potential role for *parp* within the repairing epithelium. PARylation is present at low levels throughout the epithelium and within hemocytes even in unwounded embryos but levels can be experimentally reduced by Gal4-mediated expression of UAS-*parp* RNAi. Not only does wounding significantly increase the level of PARylation, but levels of PARylation might be important for wound repair as knocking down *parp* (or *parg,* individually) impairs the healing capacity of the embryo (decreasing the rate of closure). *Parp* knockdown also appears to affect the formation of the actomyosin cable that is involved in the first steps of wound closure in *Drosophila* embryos. Interestingly, these results indicate that both too much and too little PARylation might be detrimental to the repair process, and that a fine balance of the pathway might be required for optimal healing.

Chapter 4 (Results II): The Molecular and Cellular Mechanisms of Parp Function During Tissue Repair

Our data have so far demonstrated that levels of the post-translational modification PARylation significantly increase following wounding. Furthermore, knocking down the enzymes responsible for the synthesis or degradation of PAR, (*parp* or *parg,* respectively*)* within *Drosophila* embryos via RNAi causes a significant decrease in the rate of wound closure. Upon further investigation, the wounds lacking *parp* appeared to initially get larger before beginning the healing process as well as exhibiting defects with actin cable formation at the wound edge. These data suggest that Parp and Parg-dependent regulation of wound-induced PARylation appears to play a key role in the repairing epithelium of the *Drosophila* embryo. The aim of this Results chapter is to better understand the underlying cellular and molecular mechanisms by which *parp*-driven PARylation promotes wound closure and that may explain the impaired closure of wounds lacking *parp*.

4.1 Parp is Required for Efficient DNA Damage Repair Following Wounding

Given that PARP1 is known to be activated in response to DNA damage, I next assessed whether DNA damage increases following wounding and whether this is affected by *parp* knockdown. Immunostaining against the phosphorylated histone H2AvD(using anti-pH2AvD) was utilised for this experiment to detect levels of DNA damage repair. pH2AvD is the fly equivalent of phosphorylated histone H2AX, an extremely sensitive marker for DNA damage, particularly that of double strand breaks (DSBs) (Mah et al., 2010). A rapid response to DSBs in mammalian cells is the phosphorylation of H2AX at Serine-139 to produce γH2AX, which is then able to act as a signalling molecule to initiate repair (Mah et al., 2010).

It is assumed that the more pH2AvD staining that is visible, the higher levels of ongoing DNA repair, and thus the higher the original levels of DNA damage. DNA damage repair staining is detectable in the unwounded embryo at very low levels (Figures 8A), perhaps due to low endogenous sources of DNA damage (such as mitochondrial respiration inducing oxidative stress). However, pH2AvD staining was significantly higher in wounded embryos (Figures 8B and E), most notably at the wound edges. The difference between unwounded and wounded embryos is striking, even by eye, especially when looking at the single anti-pH2AvD channel (red) (Figures 8A and B). Interestingly, much higher levels of anti-pH2AvD staining can be seen at the wound edge of wild-type embryos (Figure 9B), suggesting that the cells at the wound edge suffer the most damage (and perhaps that this is normally repaired in wild-type wounds).

However, the pH2AvD staining is less intense at the wound edge of the wounded *parp* knockdown embryos (Figure 9D). Moreover, the pH2AvD staining appears to be generally lower in the *parp* knockdown embryos, both unwounded (Figure 9C) and wounded (Figure 9D) - indeed, there is a significant decrease in the mean intensity for pH2AvD staining for the unwounded *parp* RNAi compared to control (Figure 9F). This trend is observed also in the wounded embryos with *parp* RNAi embryos exhibiting a lower level of staining, but this difference is not statistically significant (Figure 9E). The N-number for the wounded embryos is also relatively low (n=5) and therefore significance may have been detected had more embryos been imaged and quantified; this will be an important focus of future research. As noted in previous results, embryos experience different levels of PARylation, and likely DNA damage, throughout embryonic development (Figure 4). Due to this observation, all embryos used in these DNA damage repair experiments were of the same stage (stage 15, mid stage development). Wound diameter and positioning were also kept constant for the results analysis since a particularly large wound is likely to have significantly higher levels of DNA damage compared to one of a smaller diameter.

Nevertheless, despite overall lower levels of pH2AvD staining within the epithelium of *parp* knockdown embryos, bright red pH2AvD punctate are visible in the centre of the RNAi wound (Figure 9D, see arrow). These bright punctate are reminiscent of apoptotic cells that have been engulfed by patrolling macrophages. Some are visible in the wild-type embryos (Figure 9B); however, these are much less bright and are visible in macrophages in a pattern that most likely reflects the normal developmental uptake of apoptotic corpses by macrophages during tissue sculpting.

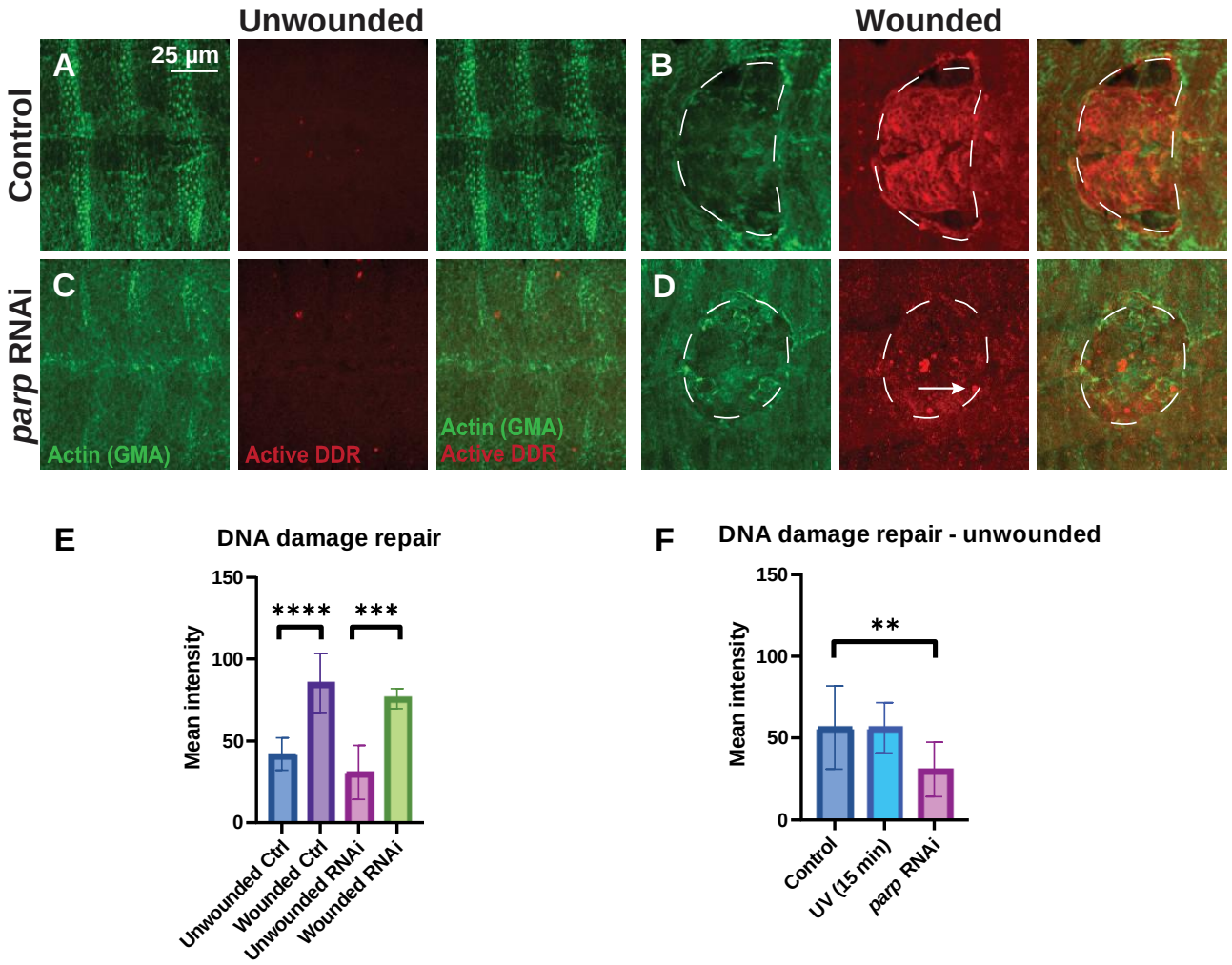

Figure 9: **Laser-induced wounding triggers an increase in DNA damage repair staining with anti-pH2AvD (active DNA damage repair) (red) in the epithelium (green) of *Drosophila* embryos.** (A-D) Confocal images of unwounded (A & C) and wounded (B & D) embryos, both wild-type *da>GMA* (A & B) and *parp* knockdown *da>GMA/UAS>parp RNAi* (C & D). White dashed line denotes the wound boundary and white arrows highlight cells of interest. (E) Wounding significantly increases staining for DNA damage repair ($p<0.0001$). (F) Knocking down *parp* via RNAi significantly decreases staining for DNA damage repair ($p<0.01$). Statistical significance measured via Holm-Sidak method using Prism between unwounded and wounded embryos (E) and across the three unwounded conditions, control, UV-exposed positive control, and *parp*-RNAi knockdown embryos (F) (n = 6 embryos per condition).

4.2 Wound-Induced PARylation Might Regulate Wound Edge Cell Death

The observed defects in wound closure, particularly the initial expansion in wound size, along with the reduction in DNA damage repair following *parp* knockdown led me to suspect that there may be an increase in apoptosis (or another form of cell death) occurring at the wound edge in the absence of *parp*. The two key types of cell death that I will be testing for are apoptosis and necrosis. Apoptosis is a controlled, active form of cell death that is carefully regulated at the cellular level by caspases in order to avoid initiating inflammation (Zhou et al., 2021). Necrosis on the other hand is an uncontrolled, passive, and less specific form of cell death.

I attempted to analyse these different types of cell death using a variety of methods in both live and fixed *Drosophila* embryos. Annexin V detects apoptotic cells via the abnormal expression of phosphatidylserine (PS) within the plasma membrane (Figure 10A). Normal, healthy cells express PS residues on the inner cytoplasmic membrane; however, apoptosis induces structural changes within the plasma membrane and the PS residues translocate to the outer, extracellular membrane (Demchenko, 2013). Annexin V specifically stains for external PS residues with the help of calcium ions. As PS residues are phospholipids, translocation to the outer leaflet causes exposure of the negative charge that can then be bound by positively-charged calcium ions and annexin V (Demchenko, 2013) (Figure 10A). Another cell death marker called Sytox, a nucleic acid stain, was also used within these experiments to reveal any potential cell death. Unlike annexin V that binds the outer membrane of cells, Sytox is able to permeate compromised cellular plasma membranes, i.e., of a dead cell, but is impermeable to living cells (McKenzie et al., 2016). Finally, acridine orange (AO) is another dye that has previously been used to stain for dead cells; AO is a nuclear dye that accumulates in highly acidic organelles such as lysosomes which commonly assemble at sites of cell death (with AO lysosomes fluoresce bright red under blue light excitation) (Lin et al., 2017).

Firstly, levels of apoptosis were analysed through the use of annexin V staining of live wounded embryos (Figure 10B & C). Staining became concentrated at the centre of the wound, visible from 20 minutes but intensified around one hour. Levels of staining were quantified around the wound site at three time points post-wounding (20, 60 and 90 minutes) to analyse any potential changes that may occur between control and *parp* RNAi embryos (Figure 10D & E). The raw integrated density was used for these data to ensure all signals were appropriately detected. At 20 minutes there is very little difference in the staining pattern between control and *parp* RNAi embryos, with a minor decrease for *parp* RNAi (Figure 10D). Interestingly, control embryos exhibited a decrease in annexin V staining intensity with time progression, as evident in the raw data (Figure 10D). There is a strong decrease observed between 20 and 60 minutes for the control ($p=0.0706$). This decrease was not seen in the *parp* RNAi embryos and instead levels of staining appeared to remain relatively constant (Figure 10D).

The raw integrated density was then normalised to the appropriate control to better understand how levels of staining changed in *parp* knockdown embryos at each time point compared to the controls (Figure 10E). At 20 minutes post-wounding, levels of staining appeared slightly lower for *parp* RNAi embryos, however, as time progressed staining increased for the *parp* RNAi embryos with the greatest change visible at 90 minutes post-wounding (Figure 10E). This was also visible by eye (Figure 10C-D), uniform staining was visible across the centre of the wounds for both *parp* RNAi and the control embryos, but this increased across the movie duration. At 20 minutes there was little contrast between the general background staining and that within the wound (for both conditions).

However, as time progressed the signal increased with visibly higher levels of annexin staining for *parp* RNAi embryos 90 minutes post-wounding (Figure 10D). Despite these slight trends in annexin V staining, the differences between control and *parp* RNAi wounds were not statistically significant. Nevertheless, as expected, the control wound (Figure 10B) healed efficiently, whereas the *parp* RNAi wound (Figure 10C) started with an irregular shape which appeared to resolve in shape by 60 minutes but did not heal. Another observation between the two conditions was that all control data is similar in value (Figure 10B) whereas *parp* RNAi embryos had a large spread of data despite all embryos being imaged and quantified in an identical manner.

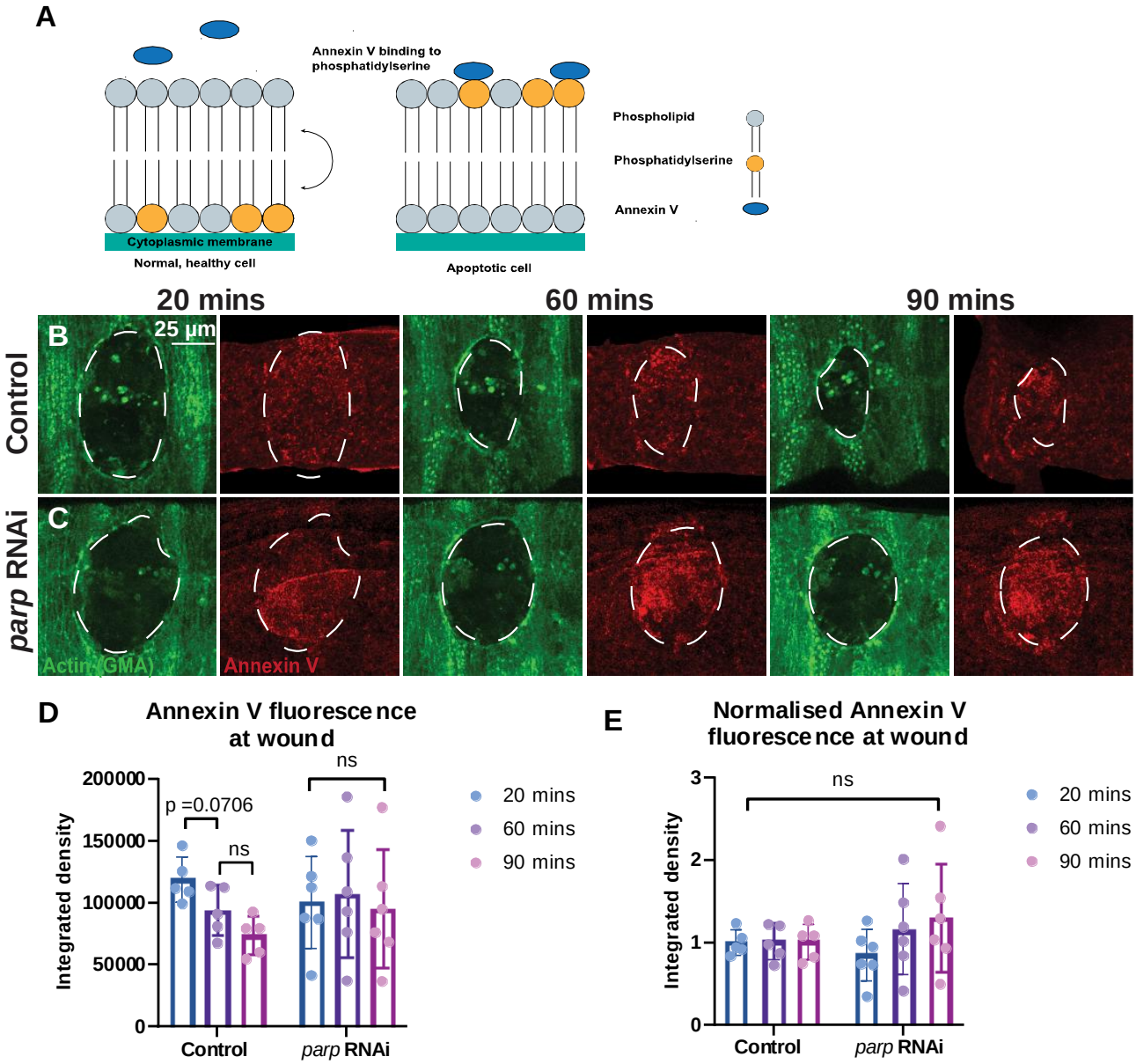

Figure 10: **Analysis of cell death through Annexin V staining following wounding.** (A) Simple schematic of Annexin V mechanism. (B & C) Confocal images of wounded *Drosophila* embryos stained with Annexin V, both wild-type *da>GMA* (B) and *parp* knockdown *da>GMA/UAS>parp* RNAi (C) at given time points (20, 60 and 90 minutes). (D & E) Quantification of integrated density at the wound edge at each of the given time points, raw (D) and normalised to the mean of the control embryos (E). Wound edge indicated by white dashed line. Statistical significance measured via Holm-Sidak method using Prism.

The next stain to analyse cell death was AO (Figure 11), this staining was challenging since AO is highly photo-sensitive meaning the stained embryos experienced high levels of bleaching when exposed to any light source. Laser power and gain were set extremely low for these experiments to help counter this, hence why the usual actin fluorescence throughout the epithelium was not visible. Images were also taken every 20 minutes rather than every 5 minutes to further limit photo-bleaching. Even with these considerations, significant bleaching occurred during the movies making it difficult to draw any direct comparisons between different time points. All quantification was normalised to the appropriate control (the unwounded wild-type embryos) to provide more reliable data; for example, quantification of AO intensity for images taken 20 minutes post-wounding were normalised to the mean value obtained for the control at 20 minutes. The data showed a modest increase in both green and red AO staining for unwounded *parp* RNAi embryos compared to the unwounded wild-type control (Figure 11E). This increase was also visible by eye when analysing the confocal images (Figure 11A-D), perhaps suggesting that there is elevated cell death in the absence of Parp.

A similar trend was observed for the wounded embryos (Figure 11F); however the overall level of staining was decreased (likely due to bleaching) and was not statistically significant. Interestingly, the wounded control embryo had visibly high levels of green AO staining immediately surrounding the wound (Figure 11B), potentially reflecting the amount of damage induced by the wound formation. Elevated AO staining has previously been linked to cell damage and death, however the exact mechanism underlying increased AO fluorescence upon cell death remains unclear. In these data, it appears that 3-5 rows of cells have a brighter green AO fluorescence surrounding the wound, suggesting that these cells might have undergone some form of cell death following wounding. In relation to the red AO fluorescence, neither distribution nor mean fluorescence, appeared to change between control and *parp* RNAi following wounding (Figure 11A-F).

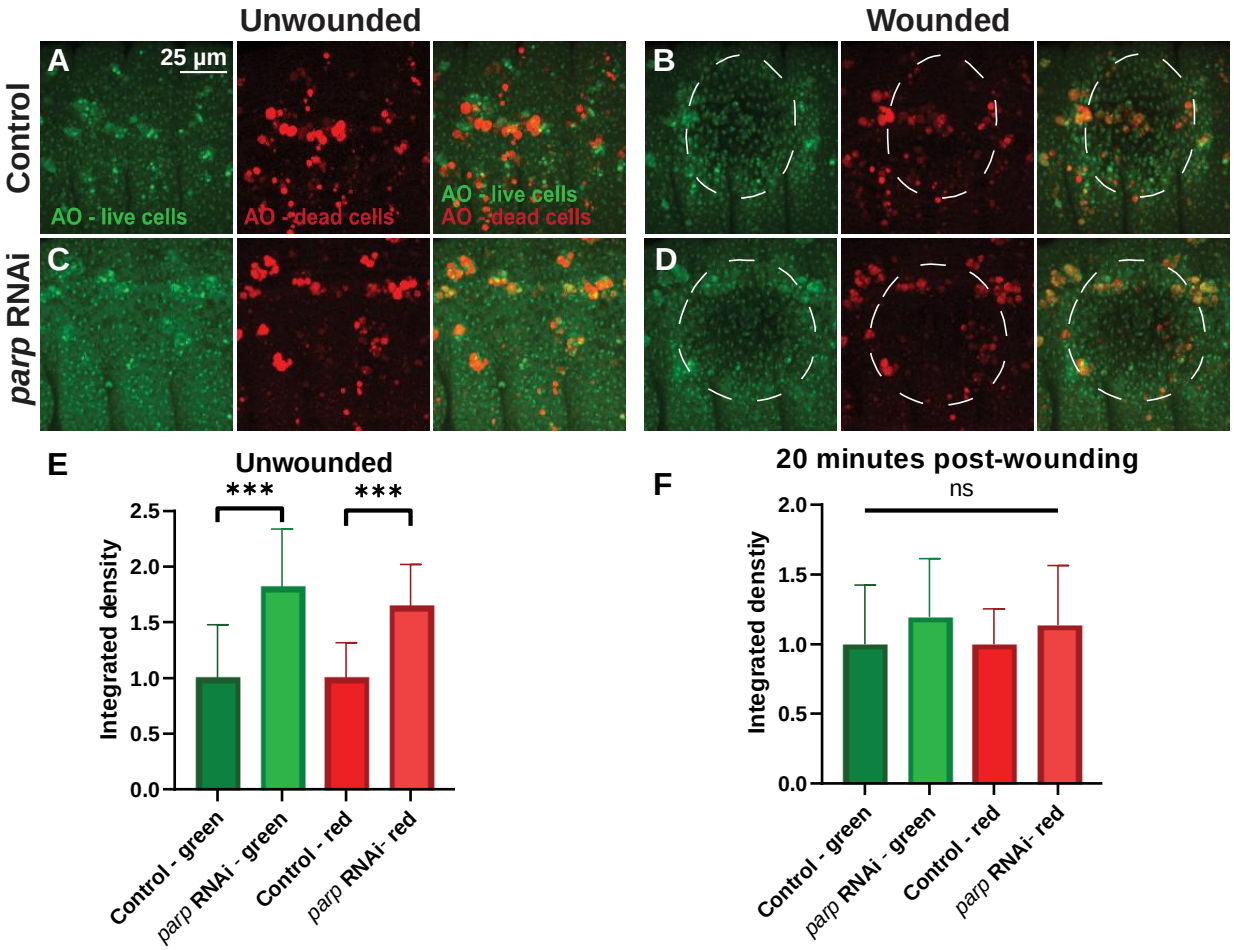

Figure 11: **Analysis of cell death through Acridine Orange staining following wounding. (A-D)** Confocal images of unwounded (A & C) and wounded (B & D) *Drosophila* embryos for both wild-type *da>GMA* (A & B) and *parp* knockdown *da>GMA/UAS>parp* RNAi (C &D). Panels left to right: green showing stained live cells, red showing stained dead cells and an overlay (E & F) Quantification of integrated density of AO staining for unwounded embryos (E) and at 20 minutes post-wounding (F). Statistical significance measured via Holm-Sidak method using Prism (n = 5 embryos per condition).

The final stain that was attempted to examine cell death was Sytox, which is traditionally used to detect cells with compromised cell membranes (Figure 12). Firstly, unwounded embryos were imaged, interestingly no staining was observed across any of the control embryos (Figure 12A). These embryos were then wounded and imaged for 120 minutes during which time high levels of Sytox staining became apparent (Figure 12B). Sytox staining was brightest at the centre of the wound, indicating a high presence of dead cells, and levels of intense Sytox staining peaked at 80 minutes post-wounding (Figure 12C) as shown by quantification of integrated density for the area within the wound. Unfortunately, due to time constraints, the Sytox staining could not be repeated for the *parp* RNAi wounds; this will be an interesting avenue to explore in the future.

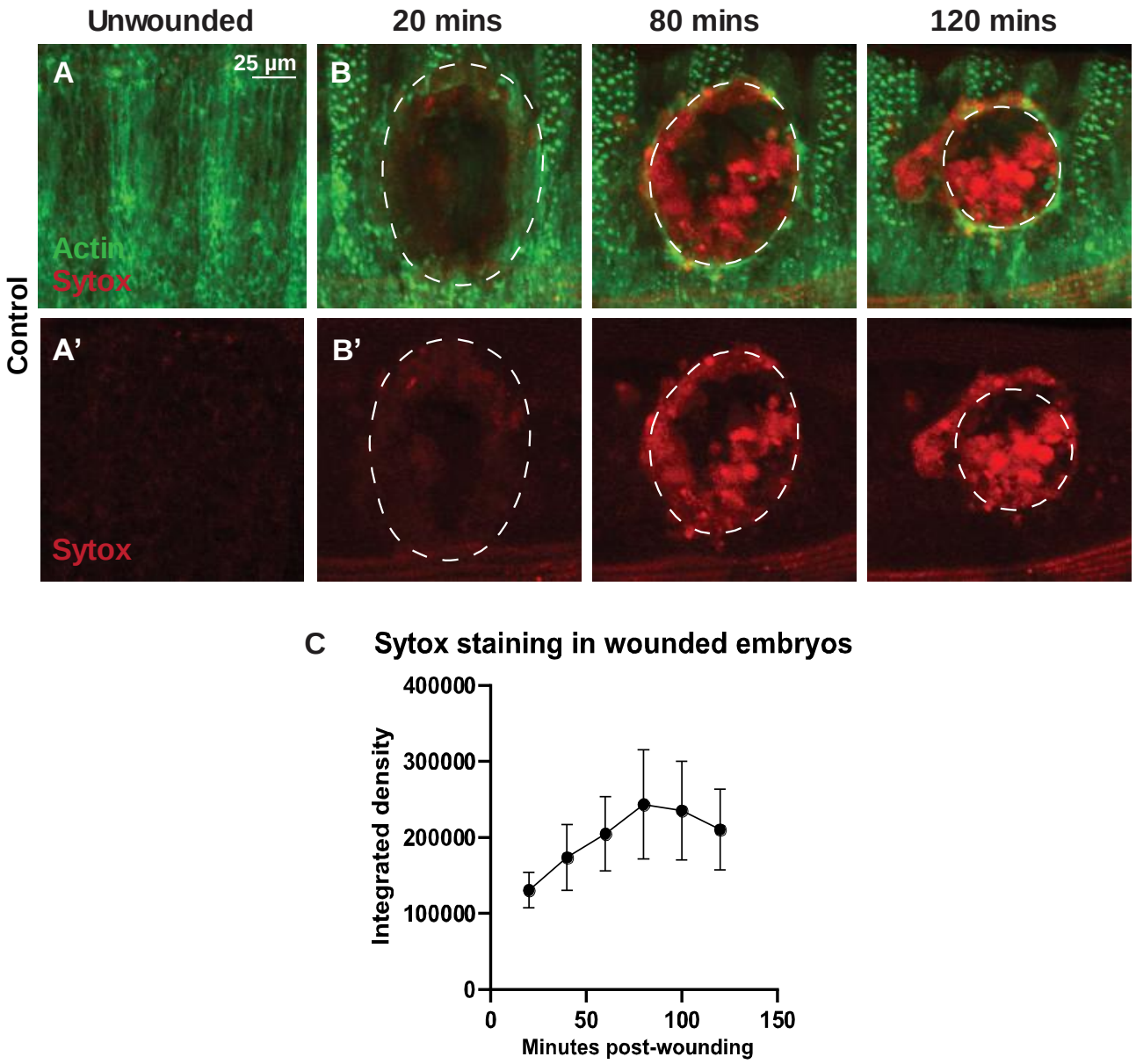

***Figure 12*: Wounding induces Sytox staining of control embryos.** (A&B) Confocal images of unwounded (A) and wounded (B) *Drosophila* embryos, control *da>GMA x w67*, stained with Sytox (red) at 20, minutes post wounding. (C) Integrated density of staining of control embryos. Statistical significance measured via Holm-Sidak method using Prism (n = 5 embryos per condition).

4.3 Investigating the Link Between PARylation and Wound-Induced JNK Signalling

Previous studies have indicated that the JNK signalling cascade is activated following cellular stress, including wounding (Bosch et al., 2005), and is required for efficient wound closure (Rämet et al., 2002). The cascade involves a series of phosphorylation and dimerisation events and culminates in the assembly of a dimer of activated protein-1 (AP-1), a transcription factor capable of recognising TPA (tetradecanoyl phorbol acetate) Response Elements (Chatterjee & Bohmann, 2012), known as TRE sites. Given that the PARylation stress response has previously been linked to JNK signalling (Weaver & Yang, 2013) and that *parp* RNAi wounds appear to close significantly slower than controls, I analysed whether wound-induced JNK signalling is affected following Parp knockdown.

To explore this phenomenon, a transgenic *Drosophila* JNK reporter stock (known as TRE-GFP) was used to report live JNK signalling activity (Figure 13). This fly stock contains TRE sites upstream of the GFP coding sequence meaning that AP-1 produced following activation of the JNK signalling cascade will bind the TRE site resulting in GFP fluorescence. This stock also has a daughterless-Gal4 construct driving the expression of a mCherry tagged Moesin protein, meaning the actin within embryonic epithelium will be labelled for easy wound visualisation, and *parp* can also be knocked down using UAS-driven *parp* RNAi. The aim of these experiments is to explore how JNK signalling behaves following RNAi-induced *parp* knockdown. Since JNK activation will result in GFP fluorescence, the area and intensity of this will be quantified to understand any potential changes.

In control wild-type wounds, JNK activity remained low immediately following wounding with very little fluorescence visible at 20 minutes post-wounding (Figure 13A), however, there was a striking increase in TRE-GFP fluorescence around 80 minutes post-wounding. Conversely, at 20 minutes post-wounding, the *parp* RNAi embryo had minor 'dashes' of fluorescence across the embryo (Figure 13B) which were not present in the control embryos. This trend was observed for all of the *parp* RNAi embryos examined, with a surprisingly random distribution of localised GFP fluorescence that was not limited to the epithelium at the site of the wound (unlike the stereotypical wound-induced TRE-GFP fluorescence observed later in the movie). Since the amount of ectopic fluorescence following *parp* RNAi relative to the total area of the embryo was rather small, measuring mean fluorescence intensity was not sensitive enough to capture the potential changes. Hence for these measurements, fluorescent integrated density was used to measure the total fluorescence of each pixel in the selected area rather than just the overall mean of all selected pixels. Using this method, the *parp* RNAi embryos had significantly higher JNK activity measurements at 20 minutes post-wounding for the whole embryo compared to the wild-type controls (Figure 13C).

The next stages of quantification involved characterising the timing of the activation of the JNK cascade between control and *parp* RNAi embryos. The timing of JNK activation was classified as the time point at which wound-induced green fluorescence was first visible. The dashes of GFP fluorescence (as described above) were still visible across the *parp* RNAi epithelium throughout the 2-hour imaging session. Interestingly, there was a trend towards more rapid JNK activation in the *parp* RNAi embryos, but due to limited n numbers this was not statistically significant (Figure 13D). For the control embryos, the mean time at which visible TRE-GFP fluorescence (and therefore JNK activation) was observed was 105 minutes post-wounding, whereas the *parp* RNAi embryos exhibited a mean JNK activation time of 100 minutes.

The mean fluorescent intensity was then measured for the whole embryo once the wound-induced JNK cascade had been activated. This measurement was taken at 120 minutes post-wounding to ensure that all embryos had an opportunity to activate the JNK cascade (Figure 13E). This revealed that *parp* knockdown significantly increased the levels of wound-associated TRE-GFP fluorescence, similar to the trend seen at 20 minutes with intensity density. Finally, the area of wound-induced TRE-GFP fluorescence was quantified, and this revealed that there was a trend towards an increase in JNK activation for wounded *parp* RNAi embryos compared to the controls (Figure 13F), however this was not statistically significant. Since many of the *parp* RNAi wounds had not closed by 120 minutes post-wounding and remained relatively large, adjustments were made during the quantification of JNK area (only measuring the actual area of GFP fluorescence surrounding the wound rather than the wound itself). Despite the lack of statistical significance for this last set of data (Figures 12F), overall these data provide an interesting overview of the impact of a *parp* knockdown on the JNK cascade and its activation. Taken together, there is a nod towards faster activation as well as a greater intensity and area of JNK activation (Figure 13C-F). It would be interesting to repeat these experiments in the future with higher n-numbers to get a clearer picture of any potential Parp impact.

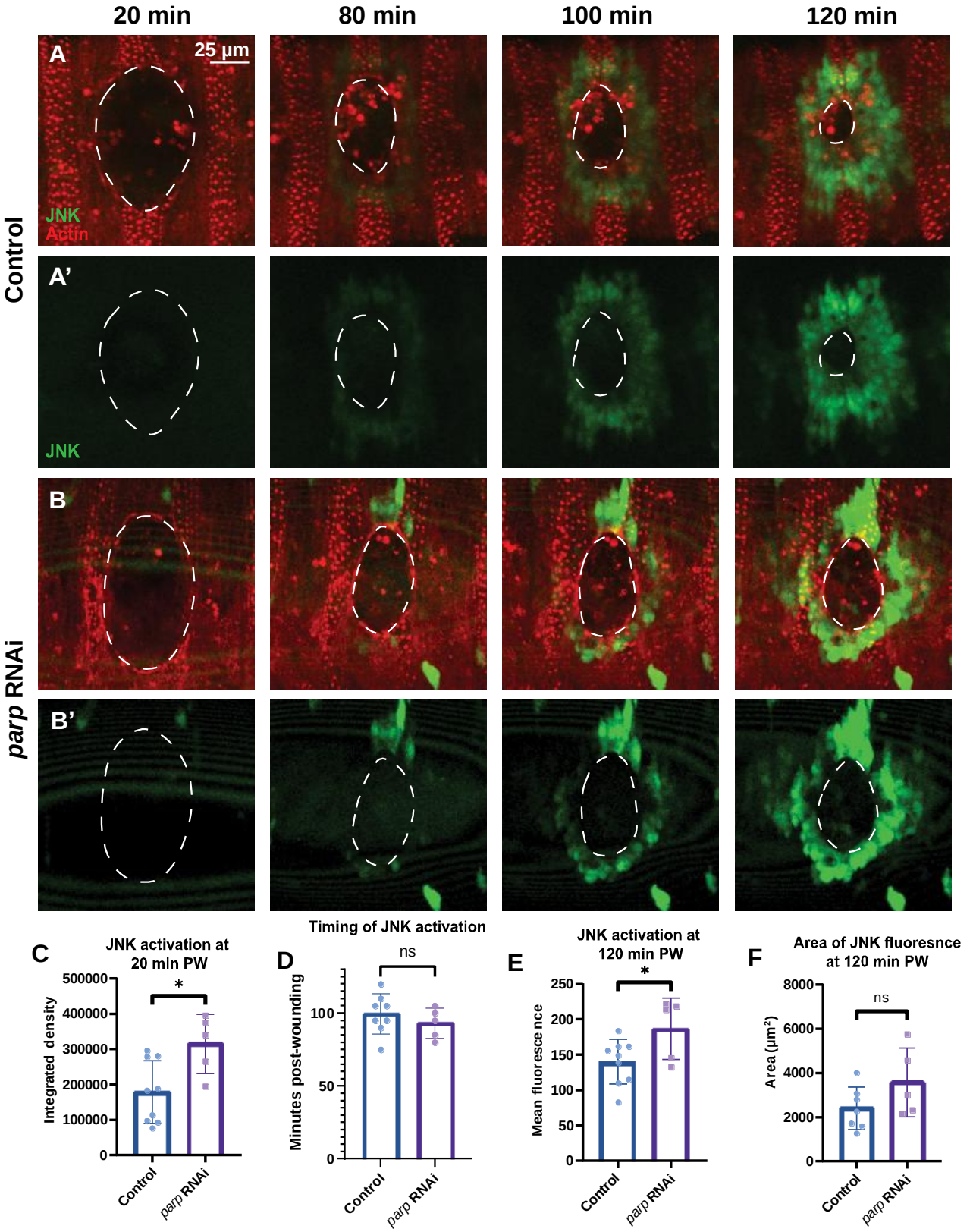

Figure 13: **Comparison of JNK signalling in wounded *Drosophila* embryos between control and *parp* RNAi genotypes.** (A&B) Confocal images of wounded wild-type control Tre-GFP/CyO; da>mch-moe/TM6 *x w67* (A) and *parp* Tre-GFP/CyO; da>mch-moe/TM6 x *parp RNAi* (B) taken over the course of 2 hours post-wounding, snapshots taken at 20 minutes, 80 minutes, 100 minutes, and 120 minutes. Actin (GMA) labelled in red with JNK activity labelled in green with TreGFP. White dashed line denotes the wound edge. (C-F) Quantification of JNK activated via integrated density at 20 minutes post-wounding (C), the time at which JNK was first activated (D), integrated density at 120 minutes post-wounding (E) and the area of visible JNK activity at 120 minutes post-wounding (F). Statistical significance measured via Holm-Sidak method using Prism.

4.4 Investigating the Role of Parp and PARylation on Immune Cell Behaviour

Thus far, the majority of this study has focused on the impact of *parp* knockdown in the epithelium and the downstream effects of this on wound closure. Another aim of this study was to explore the effect of *parp* knockdown on the behaviour of the innate immune cells (known as hemocytes) within *Drosophila.* The *Drosophila* embryos used for the aforementioned *parp* RNAi experiments (described above) do in fact possess *parp* knockdown throughout the embryo, in both the epithelium and the hemocytes (Results Section 3.1). However, previously only the epithelium (using GFP-tagged actin) was labelled when analysing wound closure so the effect on hemocyte behaviour was not directly examined. To more specifically address the role of *parp* within hemocytes, a different *Drosophila* transgenic line was used to directly knockdown *parp* in the hemocytes (but not the epithelium) using a serpent-Gal4 driver; these flies also carried a UAS-GFP construct to label the hemocyte cytoplasm and a GFP-tagged E-cadherin construct to allow visualisation of the overlying epithelium. This combination of markers allowed us to assess not only hemocyte behaviour following hemocyte-specific *parp* knockdown, but also the rate of epithelial wound closure.

The two key areas of interest to explore were the behaviour of hemocytes during their regular homeostatic patrolling and the ability of hemocytes to migrate to a laser-induced wound (Moreira et al., 2010) when *parp* is knocked down specifically in the hemocytes (using a serpent-Gal4 driver). The first point to address was whether the RNAi-induced *parp* knockdown had any effect on the overall number of hemocytes within the unwounded embryo. Our results indicated that in fact the *parp* RNAi embryos did have significantly less visible hemocytes than the wild-type control embryos (Figure 14A-C) before wounding. On average unwounded control embryos had 38 hemocytes visible beneath the ventral epithelium whereas for *parp* RNAi embryos this reduced to only 25 (Figure 14C). Following wounding this trend continued, wounded *parp* RNAi embryos appeared to have less visible hemocytes than the wounded control (Figure 14D) although this was not statistically significant.

I next explored the hemocytes ability to migrate to a wound (Figure 14E-J). Using a combination of both the green channel (hemocyte cytoplasm) and the red channel (hemocyte nuclei), I counted the number of hemocytes at the wound edge at each given time-point (Figure 14I). The first image was taken at 10 minutes post-wounding and then images were taken every 5 minutes until 2 hours post-wounding. The Z-projections taken were relatively deep to account for embryo movement and hemocyte migration, however when counting small maximum projections of 3 slices were produced to ensure the correct populations of hemocytes were analysed. The number of visible nuclei (red spots) were counted at the wound edge since especially later in the movies with high levels of hemocyte migration it became difficult to distinguish between separate hemocytes. As expected, hemocytes accumulated at the wound edge over the two-hour timeframe, with the highest levels visible around 70 minutes post-wounding for control and 80 minutes for *parp* RNAi (Figure 14I).

There was a slight difference between the number of hemocytes at the wound edge for both conditions with slightly fewer hemocytes present within *parp* RNAi embryos, however this difference was not statistically significant. Control hemocytes appeared to reach their peak quicker and disperse away from the wound more rapidly than those of *parp* RNAi embryos (Figure 14I). To confirm any potential differences in hemocyte dispersal, it would have been interesting to take longer wounded timelapse movies that surpass the regular two-hour interval.

To further analyse the homeostatic patrolling mechanism of the hemocytes, the Manual Tracking Plug-In within Fiji was utilised to quantify the velocity at which hemocytes migrated underneath the epithelium (in unwounded and wounded embryos). The migration velocity was measured from the first frame (10 minutes post-wounding) to the point at which the hemocyte reached the wound edge. No significant changes were observed from these experiments (Figure 14J), for either genotype when unwounded or wounded. Wounding induced a minor increase in migration velocity compared to that of unwounded embryos, perhaps due to inflammatory cues produced by the wounded tissue. However, knocking down *parp* via RNAi did not alter hemocyte velocity for either unwounded or wounded embryos.

Hemocytes perform important roles during embryogenesis as they patrol the embryo, engulfing dead/dying cells (particularly apoptotic cells) during developmental tissue sculpting (Weavers & Wood, 2016); these engulfed apoptotic corpses are visible within the hemocytes even in unwounded embryos when imaged on a confocal microscope (Figure 14A & B). Knocking down *parp* trends towards an increase in the number of vacuoles (phagocytosed corpses) visible per hemocyte (Figure 14K), this increase was not statistically significant however the p-value (0.0917) indicates that an increase in n-number may confirm this trend. As is to be expected, wounding causes a severe amount of damage to the tissue, in turn increasing the amount of cell death. This was confirmed as the number of visible vacuoles per hemocyte significantly increased following wounding for both control and *parp* RNAi embryos (Figure 14K). Following the trend previously observed in unwounded embryos there was also a minor (but not statistically significant) increase in the number of vacuoles within wounded *parp* RNAi embryos compared to controls, potentially suggesting higher levels of cell death (e.g. apoptosis) within these embryos.

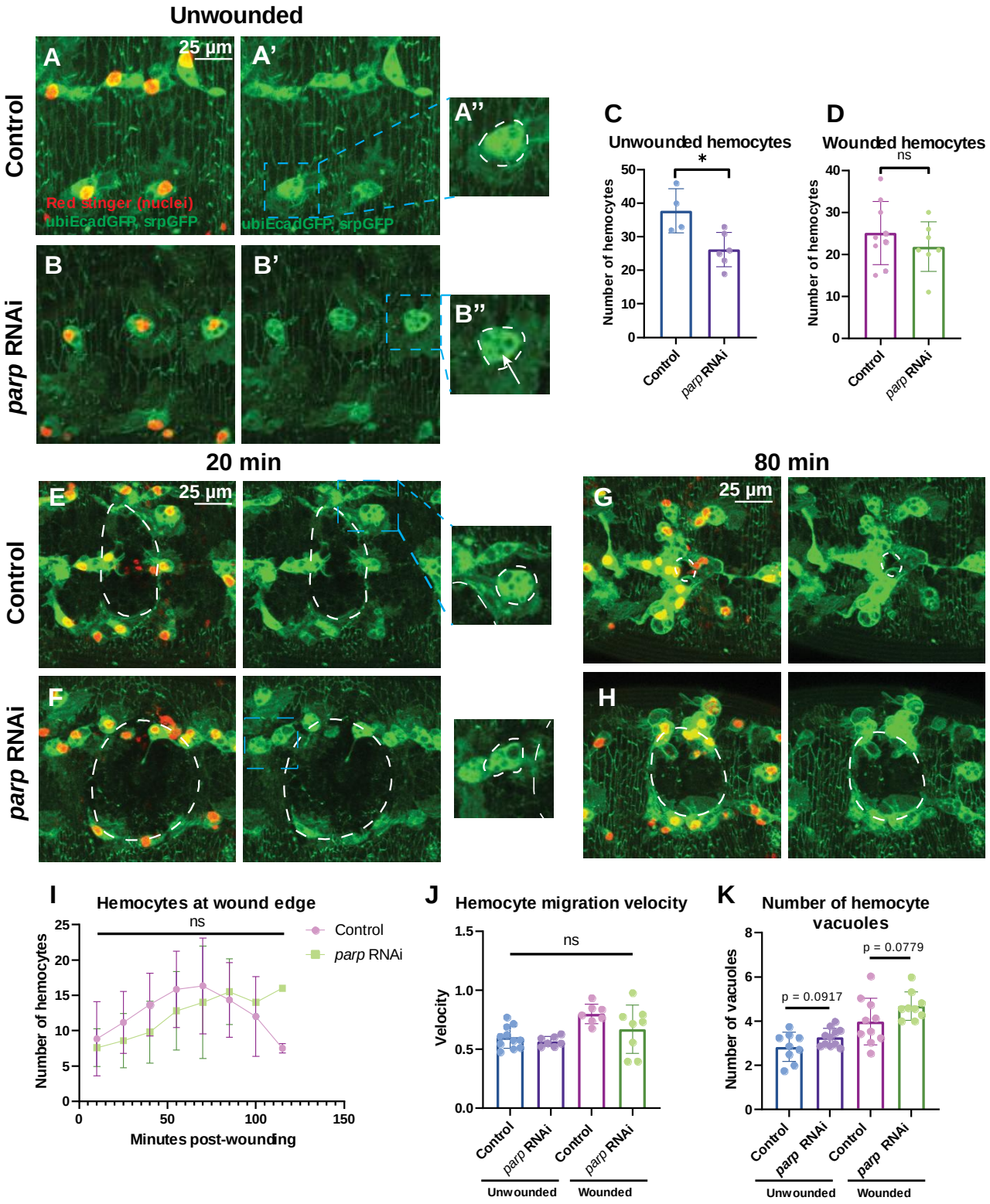

Figure 14: **Specific *parp* knockdown in hemocytes (only) has no significant impact on recruitment or engulfment ability.** (A&B) Confocal images of unwounded embryos, both control *ubiEcadGFP, srp>GFP; srpH2A3mch x w67* (A) and *parp* knockdown *ubiEcadGFP, srp>GFP/UAS>parpRNAi; srpH2A3mch* (B). White arrow denotes hemocyte vacuole. (C&D) Number of hemocytes visible throughout the embryo when unwounded (C) and at 20 minutes post-wounding (D). (E-H) Confocal images of wounded embryos; at 20 minutes post-wounding control (E) and *parp* RNAi (F), and at 80 minutes post-wounding control (G) and *parp* RNAi (H). (I) Hemocyte recruitment to wound edge. (J) Mean velocity of hemocytes for each condition. (K) Number of vacuoles (corpses) within hemocytes for each condition. White dashed line denotes wound edge and hemocyte outline. Statistical significance calculated using an unpaired t-test with Welch's correction on Prism.

4.5 Optimising Embryo Protein Extraction for Future Proteomics-Based Experiments

In order to determine the underlying molecular mechanisms responsible for the defective wound closure following *parp* RNAi, it would be beneficial to compare the proteome of wild-type and *parp* RNAi embryos. To perform quantitative proteomic experiments, it is necessary to determine how much protein can be extracted from *Drosophila* embryos. Although I did not have sufficient time during my project to complete the entire proteomic experiment, I generated pilot data to identify the number of embryos that would be required for future Tandem Mass Tagging (TMT)-based phospho-quantitative proteomics. This protein extraction data will be helpful for other researchers when continuing this project in the future with *Drosophila* embryos.

To determine how much protein can be extracted from *Drosophila* embryos, unwounded wild-type control embryos and unwounded *parp* knockdown embryos were collected, and protein was extracted (as described in Materials and Methods, Section 2.10). Two different methods of protein extraction were tested to compare efficiency/protein concentration: firstly, using direct mechanical breakdown with a plastic pestle, and secondly, breakdown via sonication. To do this RIPA-based standards were used to plot a standard curve for absorbance which could then be used to calculate the absorbances and subsequently the protein concentrations of the unknown samples (for details see Materials and Methods Section 2.12). For the first run-through, thirty embryos of each genotype were collected and processed (Table 1), however this only generated low levels of protein (average = 1.358 µg/ml), meaning multiple collections would be required to generate sufficient protein for further quantitative proteomics experiments. As shown in Table 2, the mechanical and sonication breakdown methods produced comparable protein levels. Since there was little difference in the levels of extracted protein, I decided to pursue the mechanical (pestle) method, as this was a more streamlined process with less margins for introductions of error.

The next stage was to increase the number of collected embryos (from thirty to fifty) and determine how much this affected the total amount of protein that was able to be extracted. Using fifty embryos raised the total protein extracted (from control unwounded embryos) from a mean of 32.15 µg (with thirty embryos) to 76.12 µg (see Table 1), which is a more suitable concentration when collecting for proteomics. Protein extractions were also performed again using fifty *parp* RNAi embryos (two biological replicates); the total amount of protein extracted from *parp* RNAi embryos was slightly lower than the amount extracted from the control (mean of 61.69 µg), however, this was still much higher than the first attempt. For my experiments, fifty embryos w decided to be the ideal number for collection to ensure that all embryos were of the correct genotype and stage. Increasing the number of adults in the laying pots appeared to correlate with an increased number of viable embryos up until a certain point; after which the addition of more adults had no major impact and instead resulted in overcrowding and more adults dying prematurely.

Table 1: Table representing the raw absorbance readings (duplicate) for each of the samples, control (w67) and *parp* RNAi embryos following either sonication or mechanical breakdown (thirty or fifty embryos). Protein quantification measurements made using micro-BCA kit. The mean and corrected mean (calculated via standard curve) are also given for each sample.

Sample	Absorbance 1	Absorbance 2	Mean Absorbance	Corrected Mean
Thirty embryos				
Control (sonicated)_1	0.235	0.281	0.258	0.037
Control (mechanical)_1	0.272	0.253	0.263	0.041
Control (mechanical)_2	0.243	0.243	0.243	0.022
Fifty embryos				
Control (mechanical)_3	0.680	0.672	0.676	0.488
Control (mechanical)_4	0.601	0.585	0.593	0.362
parp RNAi (mechanical)_1	0.651	0.639	0.645	0.351
parp RNAi (mechanical)_2	0.643	0.622	0.633	0.338

Table 2: Protein concentration of the sample, concentration before RIPA dilution and amount of protein extracted in the original sample (thirty or fifty embryos).

Sample	Protein Concentration (µg/ml)	Protein Concentration Pre-Dilution (µg/ml)	Actual Amount of Protein Extracted (µg)
Thirty embryos			
Control (sonicated)_1	1.502	75.103	37.551
Control (mechanical)_1	1.687	84.362	42.181
Control (mechanical)_2	0.885	44.239	22.119
Fifty embryos			
Control (mechanical)_3	17.491	874.552	87.455
Control (mechanical)_4	12.957	647.850	64.785
parp RNAi (mechanical)_1	12.581	629.032	62.903
parp RNAi (mechanical)_2	12.097	604.839	60.484

The final stage of the protein quantification was the calculation of the concentration of the remaining sample (in -80°C storage) after the two replicate samples used in the quantification had been removed (equivalent to one hundred embryos). This was an important step as this is the amount of protein available for any proteomics experiments that may be carried out and gives a clear picture of how many embryo collections will be required before quantitative proteomics can begin. The method used for these calculations is described in detail in the Material and Methods (Section 2.11); this method was used for both unwounded control and *parp* RNAi experiments, using fifty embryos for each. As shown in Table 3, the final concentration of protein remaining in the two collected control

samples (combined total of one hundred embryos) was 121.79 µg/ml. The final, total concentration for the *parp* RNAi embryos was 98.71 µg/ml. For the planned proteomic experiments (see Discussion), a minimum of 110 µg would be required for each biological replicate. This means that three extractions of fifty embryos each, would likely be required to ensure there was enough protein to run the desired experiments. There would be a total of six samples, including the two biological replicates (minimum of two) that would be required to ensure experimental accuracy for each of the three sets of extractions.

Table 3: Combining amount of protein extracted from the second duplicate samples (control and *parp* RNAi) that underwent mechanical breakdown. Calculations for the concentration of protein in the remaining samples in -80ºC storage that would be available for proteomic experimentation.

Sample	**Total Protein Extracted (µg)**	**Total Concentration (µg/ml)**	**Remaining Concentration (µg/ml)**
Control	152.240	0.761	121.792
parp RNAi	123.387	0.6169	98.710

4.6 Results II Summary

Data presented in Results II has suggested the requirement of *parp* in efficient wound closure could be related to maintaining DNA damage repair processes and ensuring that stress signalling (e.g. JNK activity) are controlled following wounding. RNAi-induced knockdown of *parp* resulted in lower levels of DNA damage repair post-wounding, as well as mature and expand the activation of the JNK signalling cascade. There is also some suggestion that cell death might increase in *parp* RNAi embryos (as indicated by the Annexin V and AO stains) and this may be reflected by an increase in corpse uptake by hemocytes. Protein extraction methods have also now been optimised for use in future proteomic experimentation to further explore the mechanisms by which *parp* influences wound repair.

Chapter 5 Discussion

5.1 Parp1 Plays a Key Role in Epithelial Wound Closure in *Drosophila* Embryos

PARP1 has been known for many years to be involved in the cellular stress response, particularly the DNA damage repair response. Despite its known activation in human acute wounds, the exact role of PARylation has remained largely unexplored. Rather the handful of mammalian PARP-related wound healing studies thus far have focused on the link between hyperactivated PARP and chronic non-healing wounds (Banerjee et al., 2019). This study instead focuses on exploring the role of Parp in normal, healing, acute wounds using *Drosophila melanogaster* as a model organism. Our results have demonstrated that levels of PARylation significantly increase following wounding in the injured epithelium. Knocking down *parp* via RNAi (using multiple independent RNAi constructs) produced interesting phenotypes in relation to re-epithelialisation of wounded *Drosophila* embryos, suggesting a potential role for Parp in the efficient closure of acute epithelial wounds in *Drosophila*.

ROS play important roles in the wound healing process by destroying any pathogens and preventing infection at the site of the wound. However, ROS are highly reactive and can cause excessive indiscriminate damage to the surrounding healthy, host tissue via oxidative stress, inducing DNA strand breaks, as well as damage to proteins and lipids. To counter this, tissues have developed a variety of resilience mechanisms to help limit any unnecessary damage (Weavers et al., 2019). These 'cytoprotective networks' encompass many different signalling pathways and are activated in multiple cell types. PARylation is a well-known cellular stress response and we speculated that it might be involved, at least in part, in the cytoprotective mechanisms activated following wounding. Studies in mammalian models have shown that PARylation of PARP1 initiates DNA repair mechanisms by aiding in the recruitment of the necessary proteins and co-factors and acting as a scaffold for the repair process to begin (Zhen & Yu, 2019). Here I find that PARylation is indeed significantly increased in the wounded epithelium compared to unwounded controls, as confirmed via immunostains. These PAR immunostains also allowed us to confirm the effectiveness of the *parp* RNAi *Drosophila* stocks that would be used for these experiments to knockdown PARP1.

Knocking down *parp* in the epithelium of *Drosophila* embryos via RNAi caused a striking wound closure phenotype in which the rate of wound closure was significantly decreased compared to wild-type control embryos of a similar wound diameter. Interestingly, the *parp* RNAi wounds even appeared to get larger before eventually healing. Previous studies in *Drosophila* have shown epithelial wound repair to take place across four stages based on the visible morphological changes, the first of these is an expansion phase (Abreu-Blanco et al., 2012). During this phase the leading edge of the wound is established and any irreparable cells are removed (likely via fly's innate immune cells called hemocytes) from the area (Abreu-Blanco et al., 2012). However, this process is observed

in all *Drosophila* epithelial wounds, including the controls, and does not alone explain the large difference that was quantified between the control and *parp* RNAi wounds. Also the expansion phase previously characterised in wild-type control wounds takes place in the first 10-15 minutes post-wounding, although there is potential for variations in the time scale, the expansion I observed in the *parp* RNAi movies occurs for 30-40 minutes post-wounding, suggesting that there may be another force at play. Previous studies have shown that in wild-type wounds the next 10 minutes of the healing process following expansion, actin accumulation begins to start the repair process (Abreu-Blanco et al., 2012). As previously mentioned, wounds induced in the epithelium of both mammalian and *Drosophila* embryos exhibit an increase in actin and myosin concentration in the cells at the leading edge to form a thick actomyosin cable (Wood et al., 2002). This cable then acts as a 'purse string' to draw the wound closed, ensuring efficient closure (Wood et al., 2002). It is therefore highly likely that actin cable formation plays a central role in halting the previously described expansion phase (Abreu-Blanco et al., 2012) from developing further.

Robust actin cable formation at the leading edge was observed following wounding of control embryos, however, issues appeared to arise following RNAi-induced *parp* knockdown. When analysing the confocal movies of *parp* knockdown embryos (over a two-hour time frame) it became clear that there were impairments in this process. Rather than a thick cable forming rapidly, *parp* RNAi knockdown wounds formed thin, patchy actin cables that were not always located directly at the leading edge and instead visible several rows of cells further back (Figure 7). These observations were made around 40-60 minutes post-wounding which correlated with the timepoint at which the *parp* RNAi wounds then began to heal at a more comparable rate to the control wounds, likely due to the cable forming later on and now being able to aid in drawing the wound closed.

Detailed analysis of actin cable formation in the first 30 minutes following wounding revealed that the actin cable took longer to form for *parp* RNAi wounded embryos compared to that observed for wild-type controls. Moreover, the cables that did form at *parp* RNAi wounds were dimmer, patchy and much thinner than the robust, thick cable that normally encompasses control wounds. In the *parp* RNAi movies it became clear that the actin cable was forming several rows of cells back from the visible wound edge, around 3-5 rows. In some cases, the cable was able to correct itself, moving forward to the original leading edge, in front of the cable that had already formed. Perhaps in these cases damaged cells near the wound edge may have undergone some form of repair (e.g. DDR), and therefore are able to upregulate and accumulate actin at the wound edge. For the majority of *parp* knockdown embryos this is not the case and instead the cable remains away from the original laser-induced wound edge and the healing process continues from this point. Published data shows that during the coalescence phase (second phase of *Drosophila* embryonic wound healing) at around 15 minutes post-wounding, all cellular repair machinery has been assembled and the actin cable

should appear thick with no visible patches (Abreu-Blanco et al., 2012). By this stage the wound should no longer have jagged, irregular edges and instead should have formed a clean, oval/circular wound. The control wounds in this study exhibited this expected behaviour, however, a number of the *parp* RNAi wounds did not and remained irregularly shaped for the entirety of the healing process.

These results suggested that knocking down *parp* impairs the ability of an embryonic wound to assemble a proper actin cable. Other studies have shown that loss of an actin cable (in *Drosophila*) does not prevent wound closure but does delay the process (Rothenberg & Fernandez-Gonzalez, 2019). This correlates with our findings as control wounds capable of forming a robust cable heal as expected at a constant rate whereas *parp* knockdown wounds have impaired cable formation and a decreased rate of closure. We speculated that in the absence of *parp* there may be reduced DNA damage repair, and this may increase cell death, which would lead to wound expansion and the actin cable weakly forming further back from the leading edge resulting in a larger wound with irregular edges. It is likely that each cell is able to gauge the levels of damage and determine whether it is viable to repair both the physical and genetic damage experienced. DNA repair is essential to maintain the genome integrity of the cell and if this is not feasible then the cell is likely to undergo some form of cell death, likely apoptosis. This may explain why the actin cable forms further back as cells at the wound edge are excessively damaged and are marked for apoptosis, therefore it is not worthwhile for these cells to produce an actin cable.

5.2 Impact of *parp* Knockdown on DNA Damage Repair and Cell Death

For many years PARP1 has been well understood to be involved in DNA damage repair pathways in both mammals and *Drosophila*, therefore it follows that knocking down *parp* throughout the developing embryo would likely cause issues in the repair mechanisms. Other proteins and biochemical pathways also play central roles in the recruitment of DNA damage repair machinery such as XRCC1. However, some of these too will be affected downstream as a result of *parp* knockdown since PARP1 aids in the recruitment of (and provides a scaffold for) XRCC1 (Pleschke et al., 2000).

In this study, the efficiency of DDR was lower in the *parp* RNAi knockdown embryos compared to the controls as confirmed by anti-pH2AvD stains (for active DDR). This trend was observed in both unwounded and wounded *parp* RNAi embryos since unwounded embryos still experience basal levels of DNA damage, mainly from endogenous sources of ROS such as mitochondrial respiration (Niethammer et al., 2009). Wounding significantly increased the levels of DDR for both controls and *parp* knockdown embryos as was expected. Previous work has shown that laser-induced wounding increases levels of oxidative stress by increasing the levels of exogenous ROS that the embryo is

exposed to, which perhaps in turn increases DNA damage and the requirement for active DNA repair (Weavers et al., 2019).

As described above, active DNA damage repair within the repairing epithelium appeared lower in *parp* knockdown embryos with some large punctate near the wound edge but within the wound lumen, potentially indicating dead cells that had been cleared by immune cells. The wounded embryos used for this anti-pH2AvD staining were fixed around 20 minutes post-wound formation; ideally multiple time points would have been imaged to get a clearer overall picture of DNA repair alongside the time points that showed major actin cable impairments. However, due to the technically challenging nature of fixing wounded embryos, the 20 minute time point was chosen to be the most practical in terms of maximising the number of embryos per collection. Fixation of earlier time-points would have reduced the number of embryos that could be appropriately mounted and wounded per session, and later stage embryos became fragile to work with.

As previously mentioned, some *parp* RNAi wounds appeared to begin accumulating an actin-rich cable a few rows back from the leading edge of the wound, but the cable appeared to move forward at a later point in the movie. In these cases, we speculate that other cellular repair mechanisms may have worked together to repair the DNA damage induced by the wound formation meaning that the damaged cells can remain viable and minimal cell death takes place, allowing the wound to heal in a more controlled manner.

Future experiments could explore the importance of the DNA damage repair response in the wound healing process. For example, since we suspect that knocking down *parp* increases cell death through the lack of an efficient repair response, an interesting experiment could involve increasing the normal levels of DDR to see if this can rescue the *parp* RNAi phenotype; for example, through the use of the drug Enoxacin, which has previously been shown to increase DICER-dependent DDR (Gioia et al., 2019). The purpose of this would be to see if this increase is able to counter the issues caused by *parp* knockdown and rescue the cells at the wound edge from cell death. Another option could be to inhibit DDR in wounded embryos using genetic manipulation, for example RNAi-induced knockdown of ATM, a DSB repair-related protein found in *Drosophila* (Joyce et al., 2011), and examine the (potential) phenotype to see if it is comparable to that induced by *parp* knockdown.

As mentioned above, our data indicates that there may be some form of cell death taking place at the wound edge following RNAi-induced *parp* knockdown since the wounds appear to get larger and the actin cable forms further back from the wound edge. To investigate this hypothesis, I carried out a number of stains (alongside the anti-pH2AvD immunostain for DDR) on live, wounded *Drosophila* embryos to explore any potential cell death. Annexin V, Sytox and Acridine Orange (AO) stains were

employed to study different aspects of cell death within the embryo. A number of challenges were faced during this section of the project in relation to staining of the embryos and finding the optimal confocal settings for imaging to prevent bleaching but ensure all staining was appropriately detected. Nevertheless, some interesting trends were observed for control and *parp* RNAi embryos; annexin V staining at the wound edge in controls was the highest early on during wound closure and annexin V levels decreased as wound closure progressed. However, annexin V levels remained high throughout wound closure for *parp* RNAi wounded embryos. Although levels of annexin V were not statistically significant between controls and *parp* RNAi, the largest differences were observed around 90 minutes post-wounding with higher levels of apoptosis staining visible in *parp* RNAi embryos. The *parp* RNAi wounds in the annexin V experiments exhibited similar closure defects (as described above) with irregular edges and minimal actin cable formation. The increased annexin V staining for *parp* RNAi at 60 and 90 minutes post-wounding may suggest a higher level of apoptosis compared to the controls. In the future, it will be important to increase the n-number for these experiments to reveal whether any significant trends are present.

We envision that damage to the epithelial barrier, for example via the laser-induced wounds, might inflict major damage to cells in the area of impact, most notably to those immediately surrounding the wound (and those that will go on to form the leading edge during the wound healing process). These damaged cells could be repaired via a number of pathways, however, if the damage is too severe to be repaired then the damaged cells might undergo some form of cell death, such as apoptosis or necrosis. This wound damage is suggested in the Sytox stain carried out for this study. Sytox is membrane impermeable and so normally labels dead cells with compromised membranes. In controls, the most intense Sytox staining was observed in the wound lumen, but Sytox staining could also be observed in some epithelial cells at the wound edge, suggesting that these cells had suffered membrane damage. Time limitations prevented Sytox stain analysis of wounded *parp* RNAi embryos to confirm if levels of cell death (or membrane damage) are indeed higher in these knockdown embryos compared to the wounded controls. I also used AO to explore levels of cell damage and death. AO permeates cells and stains the nuclei green, but dead cells are more brightly stained with AO than the surrounding live ones, giving an indication of the number of dead versus live cells. Interestingly, staining intensity for unwounded *parp* RNAi embryos increased compared to the controls, suggesting a potentially higher level of cell death, this trend (not statistically significant) was also observed between unwounded and wounded embryos.

There are other options for analysing cell death which could be utilised had there been more time within this project or for any future work. The first of these would be a cleaved caspase-3 antibody stain that would require fixation of wounded and unwounded embryos of both genotypes. Caspases are activated upon cleavage by other caspases (Bardet et al., 2008) in the caspase cascade, and

are the key proteins involved in apoptosis. Caspase-3 is central to this process and is known to cleave PARP1 at the NLS to give two fragments of 24 and 89kDa (Gobeil et al., 2001), a hallmark of apoptosis. The fixing and staining procedure would closely follow that used for the anti-pH2AvD immunostain (see Methods sections 2.4 - 2.6). Anti-cleaved caspase-3 antibody is only able to bind caspase-3 in the cleaved, activated form and therefore any staining should indicate that apoptosis is taking place. For a better understanding of the specific time points at which cell death might be occurring in control and *parp* RNAi wounds it would be interesting to collect and fix embryos (for staining) at various times after wounding.

Another potential experiment for exploring cell death would be through the use of a specific *Drosophila* stock that employs UAS to drive the expression Apoliner, a fluorescent reporter for caspase activity (Bardet et al., 2008). The Apoliner sequence contains two fluorescent proteins joined via a caspase-sensitive sequence. Living cells will retain both fluorescent proteins at the membrane (Apoliner-negative). Caspase activation results in cleavage and changes in subcellular location for each half, giving two separate fluorescent signals. Apoliner is a sensitive tool for detecting early apoptosis and for tracking immune cell engulfment of apoptotic cells (Bardet et al., 2008). To use UAS-Apoliner in future experiments a specific *Drosophila* stock would need to be produced, expressing Apoliner in the epithelium alongside either a wild-type control or *parp* RNAi stock. This generated stock could then be utilised for live imaging at the various time points of interest following wounding to observe any potential Apoliner-positive cells that may be formed at the wound edge and whether there is an increase in cell death following *parp* knockdown.

5.3 Parp Affects Wound-Associated JNK Signaling

The JNK cascade has long been known to be involved in many cellular functions from apoptosis to tumour development. The JNK cascade has also been found to be activated following wounding in both mammals (Okada et al., 2009) and *Drosophila melanogaster* (Rämet et al., 2002). The JNK signalling cascade has also been implicated in the process of dorsal closure during *Drosophila* embryonic development (Bosch et al., 2005). JNK signalling is required for efficient embryonic wound closure where it activates the expression of various genes required for wound re-epithelialisation and promotes changes to the physical characteristics of the cells (Rämet et al., 2002).

JNK is sensitive to the cellular redox balance and can therefore be activated following the production of ROS, and the subsequent oxidative stress. One enzyme involved in ROS production is Duox, an NADPH oxidase capable of producing H_2O_2; knocking down Duox via RNAi has previously been shown to decrease levels of JNK caused by wounding (Weavers et al., 2019). Here in this current study, we revealed that *parp* knockdown led to increased JNK activity following wounding compared to controls. RNAi-induced *parp* knockdown triggered flashes of JNK across the embryo even in

unwounded embryos (data not shown) and this was also visible after wounding, as shown by a significant increase in fluorescent integrated density for the JNK TRE-GFP reporter across the embryo. TRE-GFP fluorescence remained significantly higher throughout the healing process in *parp* RNAi embryos, suggesting loss of *parp* caused elevated levels of JNK activity post-wounding. This may suggest that *parp* RNAi embryos experience higher levels of oxidative stress throughout the healing process (Weavers et al., 2019). JNK activation is also known to be an early response to cell death (Santabárbara-Ruiz et al., 2015) and may be consistent with our working hypothesis that there is increased cell death at the wound edge in the absence of *parp*.

5.4 *Parg* Knockdown Delays Wound Closure Rate

PARylation is a reversible modification that is carefully regulated to prevent energy depletion since both PAR and ATP production require large concentrations of NAD^+. PARG reverses the action of PARP by removing PAR units from the target protein, such as from PARP1 itself, DNA polymerases, or histones (Páhi et al., 2020). Auto-PARylation of PARP1 can be thought of as a positive feedback loop promoting further PARylation of itself; however, the major risk of this process is hyperactivation of PARP1 which has the potential to deplete the NAD^+ pool by up to 80% (Zhou et al., 2021), leaving little available for ATP production and other metabolic functions such as the Krebs cycle. PARG works to prevent this by cleaving the glycosidic bond and removing PAR units from activated PARP1 (Páhi et al., 2020), allowing NAD^+ to be recycled by the cell for other uses.

This study has highlighted a potential key role for *parp* in the repairing epithelium of *Drosophila* embryos since knocking down *parp* impairs healing capacity. This was an interesting phenotype since other *in vivo* studies (with mammalian models) have noted that PARP overexpression also negatively affects wound healing (Banerjee et al., 2019; Bodnár et al., 2018). Combining these findings with those obtained from this investigation suggests that there is a fine balance between levels of Parp (and PARylation) and optimal wound healing, too much or perhaps too little impairs the ability of proper epithelial repair. In studies that investigated the overactivation of PARP1, one of the key factors impacting wound repair was the high levels of sustained inflammation as seen in non-healing chronic wounds, as well as impaired vasculature repair (Zhou et al., 2017). However, during this present study inflammation does not appear to be significantly affected following knockdown of *parp* and is not likely the main process disrupting the healing process. Since PARG is the enzyme responsible for preventing overactivation of PARP1, we decided to knockdown *parg* using the same RNAi method used for the previous *parp* experiments.

The *parg* RNAi stock was efficient at inducing PAR elevation, as determined by the anti-PAR immunostain on unwounded embryos for levels of epithelial PARylation. Time constraints prevented

wounded immunostain experiments which I would have liked to carry out, however, the unwounded stains provided promising data that confirmed the RNAi was likely functional. Without *parg,* the embryonic wounds closed slower than the controls, at a comparable speed to those seen following the original *parp* knockdown. Despite the similarity in the overall trend/phenotype of delayed closure, *parg* knockdown wounds did not exhibit the same wound expansion or actin cable impairment that was previously observed in *parp* knockdown wounds. Actin accumulation at the wound edge was measured via mean fluorescent intensity of actin-bound GFP, but minimal variation was observed between the control and *parg* knockdown embryos with the exception of 15-25 minutes post-wounding. During these specific time points, fluorescent intensity significantly decreased, but it is not clear what may have caused this drop.

Had more time been available for this project it would have been interesting to repeat some of the same experiments that were conducted using *parp* RNAi but instead using the *parg* RNAi *Drosophila* stock. For example, analysing hemocyte behaviour and levels of cell death; parthanatos is a PARP-dependent form of cell death that occurs independently of caspase activation and is triggered by excessive oxidative damage to DNA (Zhou et al., 2021). The key reason for focusing on this form of cell death in *parg* knockdown experiments is due to parthanatos being triggered by PARP1 overactivation, as would be caused by the RNAi-induced knockdown of *parg*. Parthanatos is characterised by PAR accumulation, AIF release and DNA fragmentation (Zhou et al., 2021). In the future, wounded embryos could be collected, fixed (20-40 minutes post-wounding), and stained to detect the presence of parthanatos using anti-PAR to detect PAR accumulation over and above levels normally observed.

There are also *Drosophila* stocks available that drive the overexpression of *parg* by employing enhancer promoter (EP)-induced overexpression combined with the Gal4-UAS system to target specific cells/tissues of interest. As mentioned above, PARG breaks down PAR chains to prevent hyperactivation, and the previous experiments explore the impact on the repairing epithelium if *parg* is absent. An overexpression of *parg* should therefore cause an excessive breakdown of PAR chains, resulting in minimal Parp activity. Anti-PAR immunostains would be required to quantify the effect and overall efficiency of the overexpression on epithelial PAR levels. It would be interesting to compare PAR levels caused by RNAi-induced *parp* knockdown with those caused by EP-induced *parg* overexpression, as well as any potential impact on wound closure. In theory, *parg* overexpression should cause comparable PAR levels and subsequently a similar wounded phenotype to the *parp* knockdown.

5.5 Impact of *parp* Knockdown on Innate Immune Cell Behaviour

Hemocytes (*Drosophila* macrophages) are present throughout the *Drosophila* lifecycle, all the way through embryonic development to the adult fly (Weavers et al., 2016). These innate immune cells play many different roles across development but the main focus for this project was corpse uptake (via phagocytosis) of dead cells generated either during normal embryonic development (during tissue sculpting) or of dead cells generated following wounding. As to be expected, there was an increase in corpse uptake by macrophages following wounding, likely due to the major damage induced during wound formation. I next tested whether *parp* was required within hemocytes for their normal behaviour. For this *parp* was only knocked down in the hemocytes using the hemocyte specific driver serpent-Gal4. In these *parp* knockdown embryos, I observed a trend towards increased corpse uptake compared to controls for both unwounded and wounded embryos, suggesting the presence of more dead cells (either apoptotic or necrotic). Interestingly, fewer total hemocytes were observed in the *parp* RNAi embryos even in unwounded conditions, which may also explain the increase in the number of corpses present per hemocyte as there are less hemocytes available for phagocytic uptake. It could be that Parp is required for the survival of hemocytes and that *parp* knockdown causes hemocyte cell death, leading to less total hemocytes present and more dead cells to be cleared by phagocytosis.

There was also a trend towards slower hemocyte accumulation at the wound edge for hemocytes expressing *parp* RNAi, as well as slower dispersal away from the wound, although these differences were not statistically significant. In the future it will be important to increase the n-number for these experiments to help to identify any statistically significant trends. Hemocyte migration during both homeostatic patrolling and migration to the wound edge was also analysed, however, little variation was apparent across each of the conditions. Wounded embryos saw a slight increase in migration velocity compared to unwounded embryos, particularly in the controls, likely due to inflammatory chemotactic cues upregulated following wound induction.

The *Drosophila* embryos used for these *parp* RNAi experiments analysing hemocyte behaviour do not express an epithelial (Gal4) driver meaning that *parp* is only knocked down in the hemocytes by the serpent>Gal4. Since our earlier experiments knocking down *parp* everywhere in the embryo (including the epithelium) caused a delay in the rate of wound closure, one interesting experiment in the future would be to repeat this ubiquitous *parp* knockdown but using a line with fluorescently labelled hemocytes. Another potential phenotype that might be associated with the wound closure defects observed following epithelial knockdown of *parp* could be elevated inflammation e.g. excessive hemocyte accumulation at the wound edge or excessive corpse uptake. If the cells lacking *parp* are unable to repair themselves, then they may undergo cell death (e.g. apoptosis) and trigger recruitment of (and clearance by) hemocytes; this increased inflammation in turn could contribute to

unresolved healing, as is seen in chronic non-healing wounds in patients in the clinic (Bodnár et al., 2018).

5.6 Future Directions

The key aim of this study was to characterise the role of *parp* during wound healing using *Drosophila* embryos. This was achieved through RNAi-mediated genetic manipulation and live confocal imaging and revealed an important role for *parp* and *parg* in the repairing epithelium. However, we do not yet fully understand the downstream effects that knocking-down *parp* (or *parg)* has on other proteins, including those involved in cellular repair processes.

Repair of the epithelial barrier, following wounding, is paramount to ensure the organisms survival and to protect against infection from the external environment. On a much smaller scale, individual cell membranes must also undergo repair to prevent cell death and damage. Our experiments in this study have suggested that in the absence of *parp,* cells near to the wound edge may become irreversibly damaged and undergo cell death, contributing to reduced wound healing rate. Interestingly, PARP1 is not only involved in DNA damage repair but has recently been linked to the repair of compromised cell membranes (Mashimo et al., 2022). In this recent study, inhibition of PARP1 via PJ-34 in cell culture prevented membrane repair, resulting in NAD leakage into the cytoplasm and increasing detectable levels of cell death (Mashimo et al., 2022). It is possible that after wounding, cellular membrane integrity is damaged resulting in leakage of ions across the barrier and altering the concentrations of various intracellular ions such as calcium (Ca^{2+}) (Mashimo et al., 2022). An increase of Ca^{2+} ions could in turn promote the production of ROS leading to DNA damage and PARP1 activation. Indeed, it is already known that wounding triggers an increase in calcium levels in the damaged epithelium (Weavers et al., 2019). It is possible that *Drosophila* embryos lacking *parp* experience issues in membrane repair following RNAi-induced knockdown. In order to test this theory, membrane repair of wounded embryos could be analysed using high-magnification, high-resolution imaging with a confocal microscope using fluorescent dyes that only enter cells when their membrane is compromised.

Quantitative proteomics, the study of the proteome, could also be employed to better understand and characterise the role of *parp*. During this project I carried out pilot experiments to optimise the protein extraction methods that would be required to begin an ambitious proteomics study. Our results indicated a minimum of six protein extractions of fifty embryos, per condition, would be necessary to obtain the quantity of protein that is required (this value also took into consideration running two biological replicates for each condition). In the future, a proteomics study would ideally compare the proteome of four different conditions: unwounded control embryos, unwounded *parp*

RNAi embryos, wounded control embryos, and wounded *parp* RNAi embryos. From this pilot work, approximately fifty embryos (of the appropriate developmental stage) would be required to obtain enough protein for each experimental condition.

The first stage of any proteomic experiments would be to characterise the unwounded proteome for control and *parp* RNAi knockdown embryos and any potential differences in protein levels between the two conditions. The next stage would then be to analyse any changes induced by wounding. This quantitative proteomics approach on protein extracted from whole embryos would enable us to detect significant changes in protein levels, regardless of whether the protein was directly PARylated by PARP or not. In order to more specifically detect which proteins are directly PARylated by Parp in *Drosophila*, we would need to employ a more refined proteomics approach. Mass spectrometry (MS)-based proteomics are commonly used to identify post-translational modifications (like PARylation) and the relative target location of their effect (Jungmichel et al., 2013) and could be used for these characterisation experiments. To analyse these changes, we could use PAR pulldown assays (Aguilera-Gomez et al., 2016) using the anti-PAR 10H antibody followed by mass spectrometry to isolate and identify which proteins become PARylated following wounding. Data obtained from these proteomic experiments could then be used to better our understanding of the role of *parp* following wounding. For example, any detected PARylated proteins could be knocked down via RNAi in a similar way to other proteins in this study. This would be an ideal, non-biased approach of protein identification. Alternatively, other potential protein targets of Parp may be identified using a candidate approach through literature searches. For example, Charon, a protein involved in the NF-κB pathway, has been identified to be associated with Parp1 expression in *Drosophila* (Ji et al., 2017).

5.7 Contribution to Knowledge

In summary, this study has a highlighted a key role for *parp* (and downstream PARylation) in the repairing epithelium of *Drosophila melanogaster* embryos. Without *parp,* wounds close at a significantly slower rate and formation of the actin cable purse string is impaired, resulting in irregular shaped wounds encompassed by a patchy cable. Knocking down *parg* (and inducing an upregulation of PARylation) also resulted in decreased rate of closure but without any apparent actin defects. Taken together these findings indicate that optimal wound closure requires a fine balance between PAR formation and catabolism controlled by *parp* and *parg* activities.

Bibliography

Abreu-Blanco, M. T., Verboon, J. M., Liu, R., Watts, J. J., & Parkhurst, S. M. (2012). *Drosophila* embryos close epithelial wounds using a combination of cellular protrusions and an actomyosin purse string. *Journal of cell science*, *125*(24), 5984-5997. https://doi.org/10.1242/jcs.109066

Aguilera-Gomez, A., van Oorschot, M. M., Veenendaal, T., & Rabouille, C. (2016). In vivo vizualisation of mono-ADP-ribosylation by dPARP16 upon amino-acid starvation. *eLife*. https://doi.org/10.7554/eLife.21475

Ahmed, A., Olah, G., Herndon, D. N., & Szabo, C. (2018). The clinically used PARP inhibitor olaparib improves organ function, suppresses inflammatory responses and accelerates wound healing in a murine model of third-degree burn injury. *British journal of pharmacology*, *175*(2), 232-245. https://doi.org/10.1111/bph.13735

Alvarez-Gonzalez, R., & Althaus, F. R. (1989). Poly(ADP-ribose) catabolism in mammalian cells exposed to DNA-damaging agents. *Mutation research*, *218*(2), 67-74. https://doi.org/10.1016/0921-8777(89)90012-8

Aragona, M., Dekoninck, S., Rulands, S., Lenglez, S., Mascre, G., Simons, B. D., & Blanpain, C. (2017). Defining stem cell dynamics and migration during wound healing in mouse skin epidermis. *Nature Communications*, *8*, 14684. https://doi.org/10.1038/ncomms14684

auf dem Keller, U., Kumin, A., Braun, S., & Werner, S. (2006). Reactive Oxygen Species and Their Detoxification in Healing Skin Wounds. *Journal of Investigative Dermatology Symposium Proceedings*, *11*(1), 106-111. https://doi.org/10.1038/sj.jidsymp.5650001

Azarm, K., & Smith, S. (2020). Nuclear PARPs and genome integrity. *Genes & development*, *34*(6), 285-301. https://doi.org/10.1101/gad.334730.119

Banerjee, J., Lodhi, N., & Nguyen, B. O. (2019). The role of poly(ADP-ribose) polymerase-1 in cutaneous wound healing. *Advances in Wound Care*, *8*(12), 634-643. https://doi.org/10.1089/wound.2018.0821

Bardet, P.-L., Kolahgar, G., Mynett, A., Miguel-Aliaga, I., Briscoe, J., Meier, P., & Vincent, J.-P. (2008). A fluorescent reporter of caspase activity for live imaging. *PNAS*, *105*(37), 13901-13905. https://doi.org/10.1073/pnas.0806983105

Bodnár , E., Bakondi, E., Kovács , K., Hegedűs , C., Lakatos, P., Robaszkiewicz, A., . . . Szabó, E. (2018). Redox Profiling Reveals Clear Differences between Molecular Patterns of Wound Fluids from Acute and Chronic Wounds. *Oxidative Medicine and Cellular Longevity*, *2018*, 5286785. https://doi.org/10.1155/2018/5286785

Bosch, M., Serras, F., Martin-Blanco, E., & Baguna, J. (2005). JNK signalling pathway required for wound healing in regenerating *Drosophila* wing imaginal discs. *Developmental Biology*, *280*(1), 73-86. https://doi.org/10.1016/j.ydbio.2005.01.002

Brady, P. N., Goel, A., & Johnson, M. A. (2018). Poly(ADP-ribose) polymerases in host-pathogen interactions, inflammation and immunity. *Microbiology and Molecular Biology Reviews*, *83*(1). https://doi.org/10.1128/MMBR.00038-18

Brand, A. H., & Perrimon, N. (1993). Targeted gene expression as a means of altering cell fates and generating dominant phenotypes. *Development*, *118*(2), 401-415.

Braun, S., Hanselann, C., Gassmann, M. G., auf dem Keller, U., Born-Berclaz, C., Chan, K., . . . Werner, S. (2002). Nrf2 Transcription Factor, a Novel Target of Keratinocyte Growth Factor Action Which Regulates Gene Expression and Inflammation in the Healing Skin Wound. *Molecular and Cellular Biology*, *22*(15), 5492-5505. https://doi.org/10.1128/MCB.22.15.5492-5505.2002

Brückner, K., Kockel, L., Ducheck, P., Luque, C. M., Rørth, P., & Perrimon, N. (2004). The PDGF/VEGf receptor controls blood cell survival in Drosophila. *Developmental Cell*, *7*(1), 73-84. https://doi.org/10.1016/j.devcel.2004.06.007

Busson, D., & Pret, A. M. (2007). *GAL4/UAS Targeted Gene Expression for Studying Drosophila Hedgehog Signalling* (Vol. 397). Humana Press. https://doi.org/10.1007/978-1-59745-516-9_13

Chambon, P., Weill, J. D., & Mandel, P. (1963). Nicotinamide mononucleotide activation of a new DNA-dependent polyadenylic acid synthesizing nuclear enzyme. *Biochemical and Biophysical Research Communications*, *11*(1), 39-43. https://doi.org/10.1016/0006-291X(63)90024-X

Chatterjee, N., & Bohmann, N. (2012). A Versatile WC31 Based Reporter System for Measuring AP-1 and Nrf2 Signaling in Drosophila and in Tissue Culture. *PLoS ONE*, *7*(4), e34063. https://doi.org/10.1371/journal.pone.0034063.g003

Ciccarone, F., Zampieri, M., & Caiafa, P. (2017). PARP1 orchestrates epigenetic events setting up chromatin domains. *Seminars in Cell & Developmental Biology*, *63*, 123 -134. https://doi.org/10.1016/j.semcdb.2016.11.010

Demchenko, A. P. (2013). Beyond annexin V: fluorescence response of cellular membranes to apoptosis. *Cytotechnology*, *65*(2), 157-172. https://doi.org/10.1007/s10616-012-9481-y

Ducuing, A., & Vincent, S. (2016). The actin cable is dispensable in directing dorsal closure dynamics but neutralizes mechanical stress to prevent scarring the in Drosophila embryo. *Nature cell biology*, *18*(11), 1149-1160. https://doi.org/10.1038/ncb3421

Dunnill, C., Patton, T., Brennan, J., Barrett, J., Dryden, M., Cooke, J., . . . Georgopoulos, N. T. (2017). Reactive oxygen species (ROS) and wound healing: the functional role of ROS and emerging ROS-modulating technologies for augmentation of the healing process. *International Wound Journal*, *14*(1), 89-96. https://doi.org/10.1111/iwj.12557

El-Hamoly, T., Hegedűs, C., Lakatos, P., Kovács, K., Bai, P., El-Ghazaly, M. A., . . . Virág, L. (2014). Activation of poly(ADP-ribose) polymerase-1 delays wound healing by regulating keratinocyte migration and production of inflammatory mediators. *Molecular medicine (Cambridge, Mass.)*, *20*(1), 363-371. https://doi.org/10.2119/molmed.2014.00130

Elliot, D. A., & Brand, A. H. (2008). The GAL4 System: A Versatile System for the Expression of Genes. In C. Dahmann (Ed.), *Drosophila: Methods and Protocols* (1 ed., pp. 79-96). Humana Press.

Eming, S. A., Martin, P., & Tomic-Canic, M. (2014). Wound repair and regeneration: mechanisms, signalling, and translation. *Science Translation Medicine*, *6*(265), 265sr266. https://doi.org/10.1126/scitranslmed.3009337

Erener, S., Petrilli, V., Kassner, I., Minotti, R., Castillo, R., Santoro, R., . . . Hottiger, M. O. (2012). Inflammasome-activated caspase 7 cleaves PARP1 to enhance the expression of a subset of NF-kB target genes. *Molecular cell*, *46*(2), 200-211. https://doi.org/10.1016/j.molcel.2012.02.016

FlyBase (2019). Engrailed. https://flybase.org/reports/FBgn0000577

Galko, M. J., & Krasnow, M. A. (2004). Cellular and genetic analysis of wound healing in *Drosophila* larvae. *PLoS biology*, *2*(8). https://doi.org/10.1371/journal.pbio.0020239

Germain, M., Affar, E. B., D'Amours, D., Dixit, V. M., Salvasen, G. S., & Poirier, G. G. (1999). Cleavage of automodified poly(ADP-ribose) polymerase during apoptosis: evidence for involvement of caspase-7. *Cell biology and metabolism*, *274*(40), 28379-28384. https://doi.org/10.1074/jbc.274.40.28379

Ghosh, S. G., Becker, K., Huang, H., Dixon-Salazar, T., Chai, G., Salpietro, V., . . . Gleeson, J. G. (2018). Biallelic Mutations in ADPRHL2, Encoding ADP-Ribosylhydrolase 3, Lead to a Degenerative Pediatric Stress-Induced Epileptic Ataxia Syndrome. *American journal of human genetics*, *103*(3), 431-439. https://doi.org/10.1016/j.ajhg.2018.07.010

Gioia, U., Francia, S., Cabrini, M., Brambilliasca, S., Michelini, F., Jones-Winert, C. W., & Fagagna, F. A. (2019). Pharmacological boost of DNA damage response and repair by enhanced biogenesis of DNA damage response RNAs. *Scientific Reports*, *9*(1), 6460. https://doi.org/10.1038/s41598-019-42892-6

Gobeil, S., Boucher, C. C., Nadeau, D., & Poirier, G. G. (2001). Characterization of the necrotic cleavage of poly(ADP-ribose) polymerase (PARP-1): implication of lysosomal proteases. *Cell Death and Differentiation*, *8*(6), 588-594. https://doi.org/10.1038/sj.cdd.4400851

Greenspan, R. J. (1997). *Fly Pushing: The Theory and Practice of Drosophila Genetics 2nd Revision*. Cold Spring Harbor Press.

Guest, J. F., Fuller, G. W., & Vowden, P. (2020). Cohort study evaluating the burden of wounds to the UK's National Health Service in 2017/2018: update from 2012/2013. *BMJ open*, *10*(12). https://doi.org/10.1136/bmjopen-2020-045253

Hanai, S., Kanai, M., Ohashi, S., Okamoto, K., Yamada, M., Takahashi, H., & Masanao, M. (2004). Loss of poly(ADP-ribose) glycohydrolase causes progressive neurodegeneration in *Drosophila melanogaster*. *PNAS*, *101*(1), 82-86. https://doi.org/10.1073/pnas.2237114100

Hiebert, P., & Werner, S. (2019). Regulation of Wound Healing by the NRF2 Transcription Factor - More Than Cytoprotection. *International Journal of Molecular Sciences*, *20*(16), 3856. https://doi.org/10.3390/ijms20163856

Hiebert, P., Wietecha, M. S., Cangkrama, M., Haertel, E., Mavrogonatou, E., Stumpe, M., . . . Werner, S. (2018). Nrf2-Mediated Fibroblast Reprogramming Drives Cellular Senescence by Targeting the Matrisome. *Developmental cell*, *46*(2), 145-161. https://doi.org/10.1016/j.devcel.2018.06.012

Irrera, N., Cucinotta, M., Pallio, G., Mannino, F., Arcoraci, V., Squadrito, F., . . . Bitto, A. (2017). Oxidative Stress: Harms and Benefits for Human Health. *Oxidative Medicine and Cellular Longevity*. https://doi.org/10.1155/2017/8416763

Ishak, L., Moretton, A., Garreau-Balandier, I., Lefebvre, M., Alziari, S., Lachaume, P., . . . Dubessay, P. (2016). DNA maintenance following bleomycin-induced strand breaks does not require poly(ADP-ribsoyl)ation activation in *Drosophila* S2 cells. *DNA repair*, *48*, 8-16. https://doi.org/10.1016/j.dnarep.2016.10.002

Ji, Y., Thomas, C., Tulin, N., Boamah, E., Kolenko, V., & Tulin, A. (2017). Charon mediates IMD-driven PARP-1-dependent immune responses in Drosophila. *Journal of Immunology*, *196*(6), 2382-2389. https://doi.org/10.4049/jimmunol.1600994

Joyce, E. F., Pedersen, M., Tiong, S., White-Brown, S. K., Paul, A., Campbell, S. D., & McKim, K. S. (2011). *Drosophila* ATM and ATR have distinct activities in the regulation of meiotic DNA damage and repair. *Journal of Cell Biology*, *195*(3), 359-367. https://doi.org/10.1083/jcb.201104121

Jungmichel, S., Rosenthal, F., Altmeyer, M., Lukas, J., Hottiger, M. O., & Nielsen, M. L. (2013). Proteome-wide Identification of Poly(ADP-Ribosyl)ation Targets in Different Genotoxic Stress Responses. *Molecular Cell*, *52*(2), 272-285. https://doi.org/10.1016/j.molcel.2013.08.026

Ke, Y., Lv, X., Fu, X., Zhang, J., Bohio, A. A., Zeng, X., . . . Ba, X. (2021). Poly(ADP-ribosyl)ation enhances HuR oligomerization and contributes to pro-inflammatory gene mRNA stabilization. *Cellular and Molecular Life Sciences*, *83*, 1817-1835. https://doi.org/10.1007/s00018-020-03618-4

Ke, Y., Zhang, J., Lv, X., Zeng, X., & Ba, X. (2019). Novel insights into PARPs in gene expression: regulation of RNA metabolism. *Cellular and molecular life sciences*, *76*(17), 3283-3299. https://doi.org/10.1007/s00018-019-03120-6

Kraus, W. L. (2008). Transcriptional control by PARP-1: chromatin modulation, enhancer-binding, coregulation, and insulation. *Current Opinion in Cell Biology*, *20*(3), 294-302. https://doi.org/10.1016/j.ceb.2008.03.006

Krüger, A., Bürkle, A., Hauser, K., & Mangerich, A. (2020). Real-time monitoring of PARP1-dependent PARylation by ATR-FTIR spectroscopy. *Nature Communications*, *11*(1), 2174. https://doi.org/10.1038/s41467-020-15858-w

Kuchino, Y., Mori, F., Kasai, H., Inoue, H., Iwai, S., Miura, K., . . . Nishimura, S. (1987). Misreading of DNA templates containing 8-hydroxydeoxyguanosine at the modified base and at adjacent residues. *Letters to Nature*, *327*, 77-79. https://doi.org/10.1038/327077a0

Langelier, M.-F., Eisemann, T., Riccio, A. A., & Pascal, J. M. (2019). PARP family enzymes: regulation and catalysis of the poly(ADP-ribose) posttranslational modification. *Current opinion in structural biology*, *53*, 187-198. https://doi.org/10.1016/j.sbi.2018.11.002

Langelier, M.-F., Planck, J. L., Roy, S., & Pascal, J. M. (2012). Structural basis for DNA damage-dependent poly(ADP-ribosyl)ation by human PARP-1. *Science*, *336*(6082), 728-732. https://doi.org/10.1126/science.1216338

Langelier, M.-F., Zandarashvili, L., Aguiar, P. M., Black, B. E., & Pascal, J. M. (2018). NAD^+ analog reveals PARP-1 substrate-blocking mechanism and allosteric communication from catalytic center to DNA-binding domains. *Nature Communications*, *9*(1), 844. https://doi.org/10.1038/s41467-018-03234-8

Laurens, N., Koolwijk, P., & de Maat, M. P. M. (2006). Fibrin structure and wound healing. *Journal of Thrombosis and Haemostasis*, *4*(5), 932-939. https://doi.org/10.1111/j.1538-7836.2006.01861.x

Letsou, A., & Bohmann, D. (2005). Small flies - big discoveries: Nearly a century of *Drosophila* genetics and development. *Developmental Dynamics*, *232*(3), 526-528. https://doi.org/10.1002/dvdy.20307

Li, H., Zhou, X., Huang, Y., Liao, B., Cheng, L., & Ren, B. (2021). Reactive Oxygen Species in Pathogen Clearance: The Killing Mechanisms, the Adaption Response, and the Side Effects. *Frontiers in Microbiology*, *11*. https://doi.org/10.3389/fmicb.2020.622534

Lin, Y.-C., Lin, J.-F., Tsai, T.-F., Chen, K.-Y., Yang, S.-C., Tang, Y.-M., & -S., H. T. I. (2017). Acridine orange exhibits photodamage in human bladder cancer cells under blue light exposure. *Scientific Reports*, *7*, 14103. https://doi.org/10.1038/s41598-017-13904-0

Luo, X., & Kraus, W. L. (2012). On PAR with PARP: cellular stress signalling through poly(ADP-ribose) and PARP-1. *Genes & Development*, *26*(5), 417-432. https://doi.org/10.1101/gad.183509.111

Mah, L.-J., El-Osta, A., & Karagiannis, T. C. (2010). γH2AX: a sensitive molecular marker of DNA damage and repair. *Leukemia*, *24*, 679-686. https://doi.org/10.1038/leu.2010.6

Martin, P., & Lewis, J. (1992). Actin cables and epidermal movement in embryonic wound healing. *Nature*, *360*(6400), 179-183. https://doi.org/10.1038/360179a0

Mashimo, M., Kita, M., Nobeyama, A., Nomura, A., & Fuji, T. (2022). PARP1 is activated by membrane damage and is involved in membrane repair through poly(ADP-ribosyl)ation. *Genes to Cells*. https://doi.org/10.1111/gtc.12926

McKenzie, K., Maclean, M., Grant, M. H., Ramakrishnan, P., MacGregor, S. J., & Anderson, J. G. (2016). The effects of 405 nm light on bacterial membrane integrity determined by salt and bile tolerance assays, leakage of UV-absorbing material and SYTOX green labelling. *Microbiology*, *162*(9), 1680-1688. https://doi.org/10.1099/mic.0.000350

Mehta, J., Rayalam, S., & Xinyu, W. (2018). Cytoprotective Effects of Natural Compounds against Oxidative Stress. *Antioxidants*, *7*(10). https://doi.org/10.3390/antiox7100147

Miwa, M., Hanai, S., Yamashita, S., Tanaka, M., & Uchida, K. (2020). *Drosophila melanogaster* as a model for understanding polyADP-ribosylation. *Frontiers in Bioscience (Landmark edition)*, *25*, 118-133.

Moreira, S., Stramer, B., Evans, I., Wood, W., & Martin, P. (2010). Prioritisation of competing damage and developmental signals by migrating macrophages in the Drosophila embryo. *Current Biology*, *20*(5), 464-470. https://doi.org/10.1016/j.cub.2010.01.047

Nguyen, G. T., Green, E. R., & Mecsas, J. (2017). Neutrophils to the ROScue: Mechanisms of NADPH Oxidase Activation and Bacterial Resistance. *Frontiers in Cellular and Infection Microbiology*, *7*, 373. https://doi.org/10.3389/fcimb.2017.00373

Nguyen, T. T., Ding, D., Wolter, W. R., Perez, R. L., Champion, M. M., Mahasenan, K. V., . . . Chang, M. (2018). Validation of Matrix Metalloproteinase-9 (MMP-9) as a Novel Target for Treatment of Diabetic Foot Ulcers in Humans and Discovery of a Potent and Selective Small-Molecule MMP-9 Inhibitor That Accelerates Healing. *Journal of Medicinal Chemistry*, *61*(19), 8825-8837. https://doi.org/10.1021/acs.jmedchem.8b01005

Niethammer, P., Grabher, C., Look, A. T., & Mitchison, T. J. (2009). A tissue-scale gradient of hydrogen peroxide mediates rapid wound detection in zebrafish. *Nature*, *459*(7249), 996-999. https://doi.org/10.1038/nature08119

Oda, H., Tsukita, S., & Takeichi, M. (1998). Dynamic Behaviour of the Cadherin-Based Cell-Cell Adhesion System during *Drosophila* Gastrulation. *Developmental Biology*, *203*(2), 435-450. https://doi.org/10.1006/dbio.1998.9047

Okada, Y., Saika, S., Shirai, K., Yamanaka, O., Kitano, A., Wang, Z., . . . Reinach, P. (2009). JNK MAPK signalling contributes in vivo to injury-induced corneal epithelial migration. *Ophthalmic Research*, *42*(4), 185-192. https://doi.org/10.1159/000232401

Park, S., Gonzalez, D. G., Guirao, B., Boucher, J. D., Cockburn, K., Marsh, E. D., . . . Greco, V. (2017). Tissue-scale coordination of cellular behaviour promotes epidermal wound repair in live mice. *Nature Cell Biology*, *19*, 155-163. https://doi.org/10.1038/ncb3472

Pizzino, G., Irrera, N., Cucinotta, M., Pallio, G., Mannino, F., Arcoraci, V., . . . Bitto, A. (2017). Oxidative Stress: Harms and Benefits for Human Health. *Oxidative Medicine and Cellular Longevity*, *2017*. https://doi.org/10.1155/2017/8416763

Pleschke, J. M., Kleczkowska, H. E., Strohm, M., & Althaus, F. R. (2000). Poly(ADP-ribose) Binds to Specific Domains in DNA Damage Checkpoint Proteins. *The Journal of biological chemistry*, *275*(52), 40974-40980. https://doi.org/10.1074/jbc.M006520200

Páhi, Z. G., Borsos, B. N., Pantazi, V., Ujfaludi, Z., & Pankotai, T. (2020). PARylation during transcription: Insights into the fine-tuning mechanism and regulation. *Cancers*, *12*(1). https://doi.org/10.3390/cancers12010183

Radice, G. P. (1980). The spreading of epithelial cells during wound closure in *Xenopus* larvae. *Developmental Biology*, *76*(1), 26-46. https://doi.org/10.1016/0012-1606(80)90360-7

Rajiah, I. R., & Skepper, J. (2014). Differential localisation of PARP-1 N-terminal fragment in PARP-1(+/+) and PARP-1(-/-) murine cells. *Molecules and Cells*, *37*(7), 526-531. https://doi.org/10.14348/molcells.2014.0077

Raziyeva, K., Kim, Y., Zharkinbekov, Z., Kassymbek, K., Jimi, S., & Saparov, A. (2021). Immunology of Acute and Chronic Wound Healing. *Biomolecules*, *11*(5), 700. https://doi.org/10.3390/biom11050700

Redd, M. J., Cooper, L., Wood, W., Stramer, B., & Martin, P. (2004). Wound healing and inflammation reveal the way to perfect repair. *Philosophical Transactions of the Royal Society of London. Series B, Biological Sciences*, *359*(1445), 777-784. https://doi.org/10.1098/rstb.2004.1466

Richardson, R., Metzger, M., Knyphausen, P., Ramezani, T., Slanchev, K., Kraus, C., . . . Hammerschmidt, M. (2016). Re-epithelialization of cutaneous wounds in adult zebrafish combines mechanisms of wound closure in embryonic and adult mammals. *Development 143*(12), 2077-2088. https://doi.org/10.1242/dev.130492

Rothenberg, K. E., & Fernandez-Gonzalez, R. (2019). Forceful closure: cytoskeletal networks in embryonic wound repair. *Molecular Biology of the Cell*, *30*(12). https://doi.org/10.1091/mbc.E18-04-0248

Rudolph, J., Roberts, G., Muthurajan, U. M., & Luger, K. (2021). HPF1 and nucleosomes mediate a dramatic switch in activity of PARP1 from polymerase to hydrolase. *eLife*, *10*, e65773. https://doi.org/10.7554/eLife.65773

Rämet, M., Lanot, R., Zachary, D., & Manfruelli, P. (2002). JNK Signalling Pathway Is Required for Efficient Wound Healing in *Drosophila*. *Developmental Biology*, *241*(1), 145-146. https://doi.org/10.1006/dbio.2001.0502

Santabárbara-Ruiz, P., López-Santillán, M., Martínez-Rodríguez, I., Binagui-Casas, A., Pérez , L., Milán , M., . . . Serras, F. (2015). ROS-Induced JNK and p38 Signaling Is Required for Unpaired Cytokine Activation during *Drosophila* Regeneration. *PLoS genetics*, *11*(10). https://doi.org/10.1371/journal.pgen.1005595

Satoh, M. S., & Lindahl, T. (1992). Role of poly(ADP-ribose) formation in DNA repair. *Nature*, *356*(6367). https://doi.org/10.1038/356356a0.

Schäfer, M., Farwanah, H., Willrodt, A.-H., Huebner, A. J., Sandhoff, K., Roop, D., . . . Werner, S. (2012). Nrf2 links epidermal barrier function with antioxidant defense. *EMBO Molecular Medicine*, *4*(5), 364-379. https://doi.org/10.1002/emmm.201200219

Seger, R. A. (2008). Modern management of chronic granulomatous disease. *British Journal of Haematology*, *140*(3), 255-266. https://doi.org/10.1111/j.1365-2141.2007.06880.x

Soares, M., & Ribeiro, A. M. (2015). Nrf2 as a master regulator of tissue damage control and disease tolerance to infection. *Biochemical Society transactions*, *43*(4), 663-668. https://doi.org/10.1042/BST20150054

Stramer, B., Wood, W., Galko, M. J., Redd, M. J., Jacinto, A., Parkhurst, S. M., & Martin, P. (2005). Live imaging of wound inflammation in *Drosophila* embryos reveals key roles for small GTPases during in vivo cell migration. *The Journal of cell biology*, *168*(4), 567-573. https://doi.org/10.1083/jcb.200405120

Sumioka, T., Iwanishi, H., Okada, Y., Miyajima, M., Ichikawa, K., Reinach, P. S., . . . Saika, S. (2021). Impairment of corneal epithelial wound healing is association with increased neutrophil infiltration and reactive oxygen species activation in tenascin X-deficient mice. *Laboratory Investigation; A Journal of Technical Methods and Pathology*, *101*(6), 690-700. https://doi.org/10.1038/s41374-021-00576-8

Tao, Z., Gao, P., & Liu, H.-w. (2009). Identification of the ADP-ribosylation sites in the PARP-1 automodification domain: analysis and implications. *Journal of the American Chemical Society*, *131*(40), 14258-14260. https://doi.org/10.1021/ja906135d

Telorack, M., Meyer, M., Ingold, I., Conrad, M., Bloch, W., & Werner, S. (2016). A Glutathione-Nrf2-Thioredoxin Cross-Talk Ensures Keratinocyte Survival and Efficient Wound Repair. *PLoS genetics*, *12*(1), e1005800. https://doi.org/10.1371/journal.pgen.1005800

Tepass, U., Fessler, L. I., Aziz, A., & Hartenstein, V. (1994). Embryonic origin of hemocytes and their relationship to cell death in Drosophila. *Development*, *120*(7), 1829-1837. https://doi.org/10.1242/dev.120.7.1829

Tetley, R. J., Staddon, M. F., Heller, D., Hoppe, A., Banerjee, S., & Mao, Y. (2019). Tissue fluidity promotes epithelial wound healing. *Nature Physics*, *15*, 1195-1203. https://doi.org/10.1038/s41567-019-0618-1

Thorpe, G. W., Fong, C. S., Alic, N., Higgins, V. J., & Dawes, I. W. (2004). Cells have distinct mechanisms to maintain protection against different reactive oxygen species: oxidative-stress-response genes. *Proceedings of the National Academy of Sciences of the United States of America*, *101*(17), 6564-6569. https://doi.org/10.1073/pnas.0305888101

Tran, V., Geraci, K., Midili, G., Satterwhite, W., Wright, R., & Bonilla, C. Y. (2019). Resilience to oxidative and nitrosative stress is mediated by the stressosome, RsbP and SigB in *Bacillus subtilis*. *Journal of Basic Microbiology*, *59*(8), 834-845. https://doi.org/10.1002/jobm.201900076

Tsai, C.-R., Anderson, A. E., Burra, S., Jo, J., & Galko, M. J. (2017). Yorkie regulates epidermal wound healing in *Drosophila* larvae independently of cell proliferation and apoptosis. *Developmental Biology*, *427*(1), 61-71.

Tulin, A., & Spradling, A. (2003). Chromatin loosening by poly(ADP-ribose) polymerase (PARP) at *Drosophila* puff loci. *Science*, *299*(5606), 560-562. https://doi.org/10.1126/science.1078764

Vilar, R., Fish, R. J., Casini, A., & Neerman-Arbez, M. (2020). Fibrin(ogen) in human disease: both friend and foe. *Haematologica*, *105*(2). https://doi.org/10.3324/haematol.2019.236901

Weaver, A., & Yang, E. (2013). Beyond DNA Repair: Additional Functions of PARP-1 in Cancer [Review]. *Frontiers in Oncology*, *3*(290). https://doi.org/10.3389/fonc.2013.00290

Weavers, H., Evans, I. R., Martin, P., & Wood, W. (2016). Corpse engulfment generates a molecular memory that primes the macrophage inflammatory response. *Cell*, *165*(7), 1658-1671. https://doi.org/10.1016/j.cell.2016.04.049

Weavers, H., & Martin, P. (2020). The cell biology of inflammation: From common traits to remarkable immunological adaptions. *Journal of Cell Biology*, *219*(7), e202004003. https://doi.org/10.1083/jcb.202004003

Weavers, H., & Wood, W. (2016). Creating a Buzz about Macrophages: The Fly as an In Vivo Model for Studying Immune Cell Behaviour. *Developmental Cell*, *38*(2), 129-132. https://doi.org/10.1016/j.devcel.2016.07.002

Weavers, H., Wood, W., & Martin, P. (2019). Injury activates a dynamic cytoprotective network to confer stress resilience and drive repair. *Current Biology*, *29*(22), 3851-3862. https://doi.org/10.1016/j.cub.2019.09.035

Wood, W., Jacinto, A., Grose, R., Woolner, S., Gale, J., Wilson, C., & Martin, P. (2002). Wound healing recapitulates morphogenesis in *Drosophila* embryos. *Nature Cell Biology*(4), 907-912. https://doi.org/10.1038/ncb875

Zaja, R., Mikoc, A., Barkauskaite, E., & Ahel, I. (2013). Molecular Insights into Poly(ADP-ribose) Recognition and Processing. *Biomolecules*, *3*(1), 1-17. https://doi.org/10.3390/biom3010001

Zhang, D., Hu, X., Li, J., Liu, J., Baks-te Bulte, L., Wiersma, M., . . . Brundel, B. J. J. M. (2019). DNA damage-induced PARP1 activation confers cardiomyocyte dysfunction through NAD+ depletion in experimental atrial fibrillation. *Nature Communications*, *10*(1), 1307. https://doi.org/10.1038/s41467-019-09014-2

Zhen, Y., & Yu, Y. (2019). Proteomic analysis of the downstream signaling network of PARP1 *Biochemistry*, *57*(7), 429-440. https://doi.org/10.1021/acs.biochem.7b01022

Zhou, X., Patel, D., Sen, S., Shanmugam, V., Sidawy, A., Mishra, L., & Ngugen, B. N. (2017). Poly-ADP-ribose polymerase inhibition enhances ischemic and diabetic wound closure by promoting angiogenesis. *Journal of Vascular Surgery*, *65*(4), 1161-1169. https://doi.org/10.1016/j.jvs.2016.03.407

Zhou, Y., Liu, L., Tao, S., Yao, Y., Wang, Y., Wei, Q., . . . Deng, Y. (2021). Parthantos and its associated components: Promising therapeutic targets for cancer. *Pharmacological Research*, *163*. https://doi.org/10.1016/j.phrs.2020.105299